

https://dspace.org/

The development of aluminium-zinc-magnesium alloys for superior stress corrosion resistance

Dauskardt, Reinhold Horst

2015-04-30
http://hdl.handle.net/10539/17595

Downloaded from a DSpace repository. https://dspace.org/

THE DEVELOPMENT OF ALUMINIUM-ZINC-MAGNESIUM ALLOYS FOR SUPERIOR STRESS CORROSION RESISTANCE

REINHOLD HORST DAUSKARDT

A Dissertation submitted to the Faculty of Engineering, University of the Witwatersrand Johannesburg in fulfilment of the requirements for the Degree of Master of Science.

Department of Metallurgy
University of the Witwatersrand
March 1983

DECLARATION

I declare that this dissertation is my own unaided work except where due acknowledgement is made to others. It is being submitted for the Degree of Master of Science to the University of the Witwatersrand, Johannesburg. It has not been submitted before for any degree or examination to any other university.

Reinhold Horst Dauskardt

29 th day May 1983

ABSTRACT

A thorough literature survey has been undertaken to provide the necessary understanding of:

i) the general metallurgy and microstructure of Al-Zn-Mg alloys,
ii) the stress corrosion cracking (SCC) of Al-Zn-Mg alloys (including accelerated SCC test methods), and
iii) the influence of composition, microstructure and heat treatment on SCC properties.

Three accelerated SCC test methods were evaluated using existing commercial alloys in different temper conditions. These were the notched rod load relaxation, the electrochemical acceleration and the slow strain rate SCC tests. The slow strain rate method gave the most reliable and reproducible results. This was therefore chosen for all subsequent testing. Baseline SCC test data was obtained from existing alloys in order to facilitate comparison of new alloy compositions.

The microstructure of a representative Al-Zn-Mg alloy was examined using optical, scanning and transmission electron microscopy. The effects of quench rate from solution heat treatment, and ageing time and temperature on both the microstructure and SCC properties were investigated. Decreasing quench rate produced a moderate increase in resistance to SCC. The characteristic increase in resistance to SCC found by overageing was, however, associated with an unacceptable loss of mechanical properties.

ABSTRACT

A thorough literature survey has been undertaken to provide the necessary understanding of:

i) the general metallurgy and microstructure of Al-Zn-Mg alloys,
ii) the stress corrosion cracking (SCC) of Al-Zn-Mg alloys (including accelerated SCC test methods), and
iii) the influence of composition, microstructure and heat treatment on SCC properties.

Three accelerated SCC test methods were evaluated using existing commercial alloys in different temper conditions. These were the notched rod load relaxation, the electrochemical acceleration and the slow strain rate SCC tests. The slow strain rate method gave the most reliable and reproducible results. This was therefore chosen for all subsequent testing. Baseline SCC test data was obtained from existing alloys in order to facilitate comparison of new alloy compositions.

The microstructure of a representative Al-Zn-Mg alloy was examined using optical, scanning and transmission electron microscopy. The effects of quench rate from solution heat treatment, and ageing time and temperature on both the microstructure and SCC properties were investigated. Decreasing quench rate produced a moderate increase in resistance to SCC. The characteristic increase in resistance to SCC found by overageing was, however, associated with an unacceptable loss of mechanical properties.

Melting, casting and hot working techniques were developed in order to fabricate defect-free small scale experimental alloy compositions.

Seven experimental casts were made to cover a wide compositional variation (Zn:4-6 wt.%, and Mg:0.8-2.5 wt.%). Slow strain rate SCC testing revealed the beneficial effects of having a Zn:Mg ratio of 3:1 (wt.%).

ACKNOWLEDGEMENTS

My gratitude is due to a number of people whose comments, criticisms and advice has proved invaluable in the completion of this work. In particular, I would like to thank the following persons.

My supervisor, Dr John Bee, for his continued support and encouragement, and particularly for his patience in reviewing this dissertation.

Professor Geoff Garrett for his constant support after persuading me to embark on this project.

Tony Nutton whose technical expertise was indispensable in the preparation of the experimental alloys.

Members of staff of Hulett Aluminium, particularly Brian Dennis, Peter Raymond, Abe de Beer and Brian Drew without whose advice and technical support this project would not have been possible.

Colleagues of the Alloy Development Group for stimulating discussions.

John Moore and Mr James (Raftopoulos) for their assistance in the workshop and stores.

Finally, I would like to thank Hulett Aluminium Ltd; the University Bursary Fund and the Council for Scientific and Industrial Research (C.S.I.R.) for their financial support.

CONTENTS

DECLARATION	i.
ABSTRACT	ii.
ACKNOWLEDGEMENTS	iv.
CONTENTS	v.
ABBREVIATIONS	ix.
ALUMINIUM ALLOY AND TEMPER DESIGNATIONS	x.
CHAPTER 1: INTRODUCTION	1.
1.1 The Mechanistic Approach to Alloy Development.	2.
1.2 Project Formulation.	3.
CHAPTER 2: THE METALLURGY OF ALUMINIUM-ZINC-MAGNESIUM ALLOYS	5.
2.1 Introduction.	5.
2.2 The Influence of Alloying Additions in the Al-Zn-Mg System.	6.
2.2.1 Major Alloying Additions.	6.
i) (Zn + Mg) level.	11.
ii) Zn : Mg ratio	14.
2.2.2 Transition Element Additions.	16.
i) Chromium.	17.
ii) Manganese.	22.
iii) Zirconium.	23.
iv) Copper.	27.
v) Titanium and Boron.	29.
vi) Combined Transition Additions.	31.

	2.2.3	Impurity Effects.	34.
	2.2.4	Experimental Confirmation of some of the Major Factors.	35.
		i) (Zn + Mg) Content.	35.
		ii) Effect of Cr, Zr and Mn on Recrystallisation.	37.
		iii) Metallographic Investigation of a Representative Al-Zn-Mg Alloy.	38.
	2.2.5	Experimental Results and Discussions.	39.
	2.2.6	Conclusions.	51.
2.3		Precipitation Sequences and Microstructure of Al-Zn-Mg Alloys.	52.
	2.3.1	Decomposition of Al-Zn-Mg Supersaturated Solid Solutions.	52.
	2.3.2	Microstructural Aspects of Wrought Al-Zn-Mg Alloys.	59.
		i) Grain Boundary Structure.	61.
		ii) Precipitate Free Zones.	63.
		iii) Solute Distribution in the PFZ.	66.
	2.3.3	Experimental Procedure.	70.
	2.3.4	Experimental Results.	71.
	2.3.5	Summary and Conclusions.	74.
2.4		Heat Treatment of Al-Zn-Mg Alloys.	84.
	2.4.1	Homogenisation and Hot Working.	84.
	2.4.2	Solution Heat Treatment.	87.
	2.4.3	Quench Rate.	91.
	2.4.4	Natural and Artificial Ageing.	95.
	2.4.5	Experimental Aim and Procedure.	102.
	2.4.6	Experimental Results and Discussions.	105.
	2.4.7	Conclusions.	117,

CHAPTER 3: STRESS CORROSION CRACKING OF Al-Zn-Mg ALLOYS. 118.

3.1 Introduction. 118

3.2 Mechanisms of SCC in Al-Zn-Mg Alloys. 119

3.2.1 Hydrogen Embrittlement. 121.

3.2.2 Anodic Dissolution. 125.

3.2.3 Stress Relaxation Mechanisms. 128.

3.3 Accelerated SCC Test Methods. 131.

3.3.1 Notched Rod Load - Relaxation. 133.

i) Experimental Procedure. 135.

ii) Results and Discussions. 137.

3.3.2 Electrochemical Acceleration Technique. 137.

i) Experimental Procedure. 138.

ii) Results and Discussions. 139.

3.3.3 Slow Strain Rate Testing. 140.

i) Experimental Procedure. 141.

ii) Results and Discussions. 146.

3.3.4 Conclusions. 153.

3.4 The Effect of Heat Treatment Variables on SCC. 155.

3.4.1 Experimental Procedure. 155.

3.4.2 Results. 156.

3.4.3 Discussion. 160.

3.4.4 Conclusions. 167.

CHAPTER 4 FABRICATION, MECHANICAL AND PHYSICAL PROPERTY TESTING OF EXPERIMENTAL ALLOY COMPOSITIONS. 169.

4.1 Introduction. 169.

4.2 Casting, Fabrication and Heat Treatment. 171.

4.3	Mechanical Property and SCC Testing.	178.
4.3.1	Experimental Procedure.	178.
4.3.2	Experimental Results.	179.
4.4	Discussion.	186.
4.5	Conclusions.	189.
CHAPTER 5:	SUMMARY AND FUTURE WORK.	191.
REFERENCES.		195.
APPENDIX.		205.

ABBREVIATIONS

SCC	- Stress corrosion cracking
SSSS	- Supersaturated solid solution
G.P.zone	- Guinier - Preston zone
η', η	- (Mg, Zn) phases/particles
PFZ	- Precipitate free zone
SHT	- Solution heat treatment
RT	- Room temperature
WQ	- Water quench
OQ	- Oil quench
AC	- Air cool
SEM	- Scanning electron microscopy
CTEM	- Conventional transmission electron microscopy
STEM	- Scanning transmission electron microscopy
EDS	- Energy dispersive spectrometer
BF	- Bright field
CDF	- Centred dar . field

ALUMINIUM ALLOY AND TEMPER DESIGNATIONS

5000 series : Al-Mg alloys

6000 series : Al-Mg-Si alloys

7000 series : Al-Zn alloys

F condition : As fabricated - no heat treatment

T6 temper : solution heat treated and peak aged

T7 temper : solution heat treated and overaged

RR temper : retrogressive and reageing heat treatment

CHAPTER 1: INTRODUCTION

Four classes of aluminium alloys exhibit moderate to high strength: the 5000 series (Al-Mg binary alloys);
the 6000 series (Al-Mg-Si ternaries);
the 2000 series (Al-Cu or Al-Cu-Mg); and
the 7000 series (Al-Zn-Mg alloys, which generally also contain copper).

The two latter series are generally the strongest, with the Al-Zn-Mg alloys offering the greatest potential of all aluminium alloys for age-hardening capacity. This property lends increased versatility to the 7000 series, which as a result has received much attention. These alloys now offer a wide range of mechanical and physical properties. At present, a major constraint on this attractive system is its susceptibility to stress corrosion cracking (SCC).

Al-Zn-Mg alloys are in the process of being revolutionised. Modern high resolution electron microscopy and improved laboratory SCC testing techniques have led to an advance in the theoretical understanding of the mechanisms of SCC. Previous strength limitations to maintain SCC resistance have been rendered somewhat redundant, with the imminent possibility of establishing peak mechanical properties independent of SCC susceptibility. This statement is amply verified by recent trends in the optimisation of composition and microstructure, and the thermal and thermo-mechanical treatments used in the production of these alloys.

The purpose of this project is to provide a sound metallurgical basis to facilitate the development of Al-Zn-Mg alloys with superior combinations of mechanical properties and SCC resistance.

1.1 The Mechanistic Approach to Alloy Development

In the past, many successful alloys were developed using an "empirical" approach. This procedure is necessarily vague and has been applied in many cases with a very limited understanding of the metallurgical mechanisms which influence the desired physical properties. In fact, there are many existing compositions in which the beneficial effects of alloying additions are not fully understood.

In order to optimise properties (such as strength : weight ratio, and SCC resistance) in aluminium alloys, a fundamental understanding of their physical metallurgy is necessary. A recent trend in alloy development is "microstructural design". Using this concept, improvements in specific properties are sought through a study of the mechanisms involved and hence the determination of the ideal microstructure. An attempt is then made to develop such a structure by careful control of composition, fabrication processes and heat treatment.

In modern technology, there are ever-increasing demands for improved material performance (at reasonable cost) in increasingly severe service environments. For such applications, a mechanistic understanding is considered

imperative. This applies both to the factors which promote superior properties, and to the mechanisms by which these properties may degrade. This knowledge can then be used not only in the development of new alloys; but also in the modification of service conditions, or the accurate determination of service lives, to avoid catastrophic materials failure.

One problem associated with alloy development is the determination or prediction of long-term properties. However, this is facilitated by the use of accelerated test methods, devised on the basis of a mechanistic understanding of in-service property degradation. Many accelerated tests are inaccurate due to their inability to reproduce and monitor the complex in-service environmental variables. In addition, the results obtained are usually dependant on the test method employed. However, once the mechanism of degradation is known, a modified test can be devised which includes only those parameters relevant to that process.

1.2 Project Formulation

The eventual aim of the aluminium alloy development programme is to replace Hulett's alloys B51S (Al-Mg-Si) and D54S (Al-Mg) and improve D74S (Al-Zn-Mg). New compositions will therefore be based on the more versatile 7000 series.

The initial aim of this project was to obtain detailed information in the general metallurgy of Al-Zn-Mg alloys, stress corrosion cracking and SCC testing. This has been achieved through a comprehensive literature review, the experimental examination of the microstructure and properties of the representative alloy D74S, and the evaluation of three potentially most useful accelerated test procedures.

Subsequently, the most promising existing SCC test method was modified and a suitable apparatus constructed. The work was then further developed to investigate the influence of different heat treatments on the structure and SCC characteristics of D74S.

The final stage of this study was the production of seven experimental alloys. These were designed to provide a wide compositional variation. The alloys were melted, cast and fabricated to provide suitable material for mechanical property and SCC testing. In this way, the influence of one major variable in SCC susceptibility (the Zn:Mg ratio) could be readily assessed. Based on this work it should be possible to further modify the most promising compositions to achieve the goal of a high-strength, SCC - resistant aluminium alloy.

CHAPTER 2: THE METALLURGY OF ALUMINIUM - ZINC - MAGNESIUM ALLOYS

2.1 Introduction

The Al-Zn-Mg alloy system (designated the 7000 series by the Aluminium Association) is one of the most interesting aluminium alloy systems in terms of physical metallurgy. It provides a class of heat treatable alloys, some of which develop the highest strengths presently known for commercial aluminium-based alloys. This is a result of a combination of elements that have a high mutual solid solubility in aluminium and also exhibit unusually high precipitation hardening characteristics.

This chapter is concerned with the internal structure, composition and metallurgical treatment of Al-Zn-Mg alloys. Variations in composition, fabrication processes and thermal treatment all lead to changes in structure. The final microstructure of the alloy is therefore determined by the composition and the metallurgical treatments used in its production. Thus the structural features are of prime importance because they not only reflect the origin and history of the metal, but also can often be used to predict or explain characteristics and performance.

2.2 The Influence of Alloying Additions in the Al-Zn-Mg System

2.2.1 Major Alloying Additions

Although most metals will alloy with aluminium, comparatively few have sufficient solid solubility to serve as major alloying additions. The solid solubilities of some elements (taken from ref. 1) are shown in Table I.

Table I: Solid Solubilities of Elements in Aluminium

Element	Temperature (°C)	Maximum solid solubility (wt.%)*	(at.%)
Copper	548	5.65	2.40
Chromium	661	0.77	0.40
Iron	655	0.05	0.025
Lithium	600	4.2	16.3
Magnesium	450	17.4	18.5
Manganese	658	1.82	0.90
Silicon	577	1.65	1.59
Silver	566	55.6	13.8
Tin	228	0.06	0.01
Titanium	665	1.3	0.74
Zinc	443	70	28.8
Zirconium	660.5	0.28	0.08

* Unless stated otherwise, alloy compositions are quoted in weight percentages.

The values quoted in Table I are for binary systems, and the presence of other elements will usually affect the solubility. However, it is clear from the Table that of the more commonly used elements, only zinc, magnesium, copper and silicon have significant solubilities.

In the Al-Zn-Mg ternary system, aluminium solutions can be in equilibrium with the binary phases Mg_2Al_3, zinc in solid solution, Mg_2Zn_{11}, and $MgZn_2$, and also with the ternary phase $Mg_3Zn_3Al_2$. As far as precipitation hardening is concerned, the most important binary phase is $MgZn_2$. This forms a quasi-binary system with aluminium, in which a eutectic alloy containing approximately 11.5% Mg and 61% Zn solidifies at 475°C. The aluminium solid solution formed in this reaction contains 2.65% Mg and 14.25% Zn [2]. The aluminium-rich corner of the Al-Zn-Mg phase diagram at 200°C is shown in Figure 2.1. The solid solubility curves at 350, 400 and 440°C give the Mg and Zn content capable of going into solution in α - Al [3].

The determining criterion in the choice of a (Zn + Mg) level is the optimisation between the required strength level and the basic susceptibility to stress corrosion cracking (SCC). Regarding the major elements in the alloy composition, the generalisation can be made that increasing the amount of solute, which can be retained in supersaturated solid solution, increases both the strength level and the susceptibility to SCC[4,5,6,7,8]. The results of numerous investigations have been summarised by Scamans[9] in Figure 2.2.

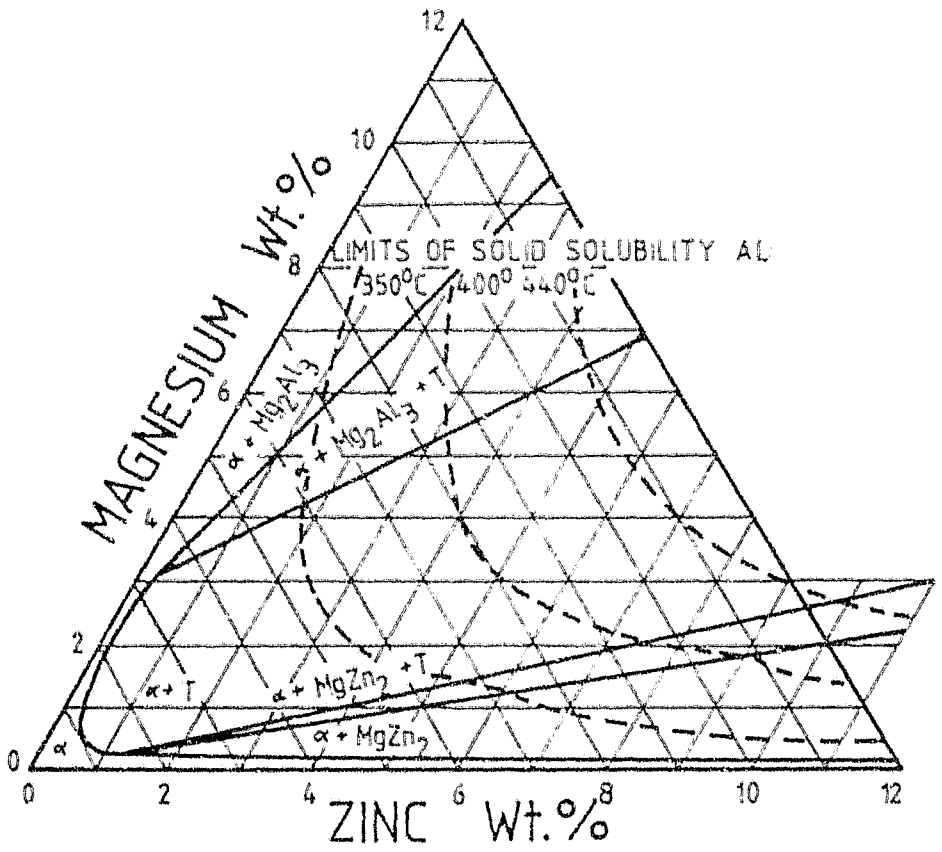


Figure 2.1 The Al-Zn-Mg phase diagram at 200°C showing the thermodynamically stable phases (T = $Al_2Mg_3Zn_3$ and α = Al solid solution)

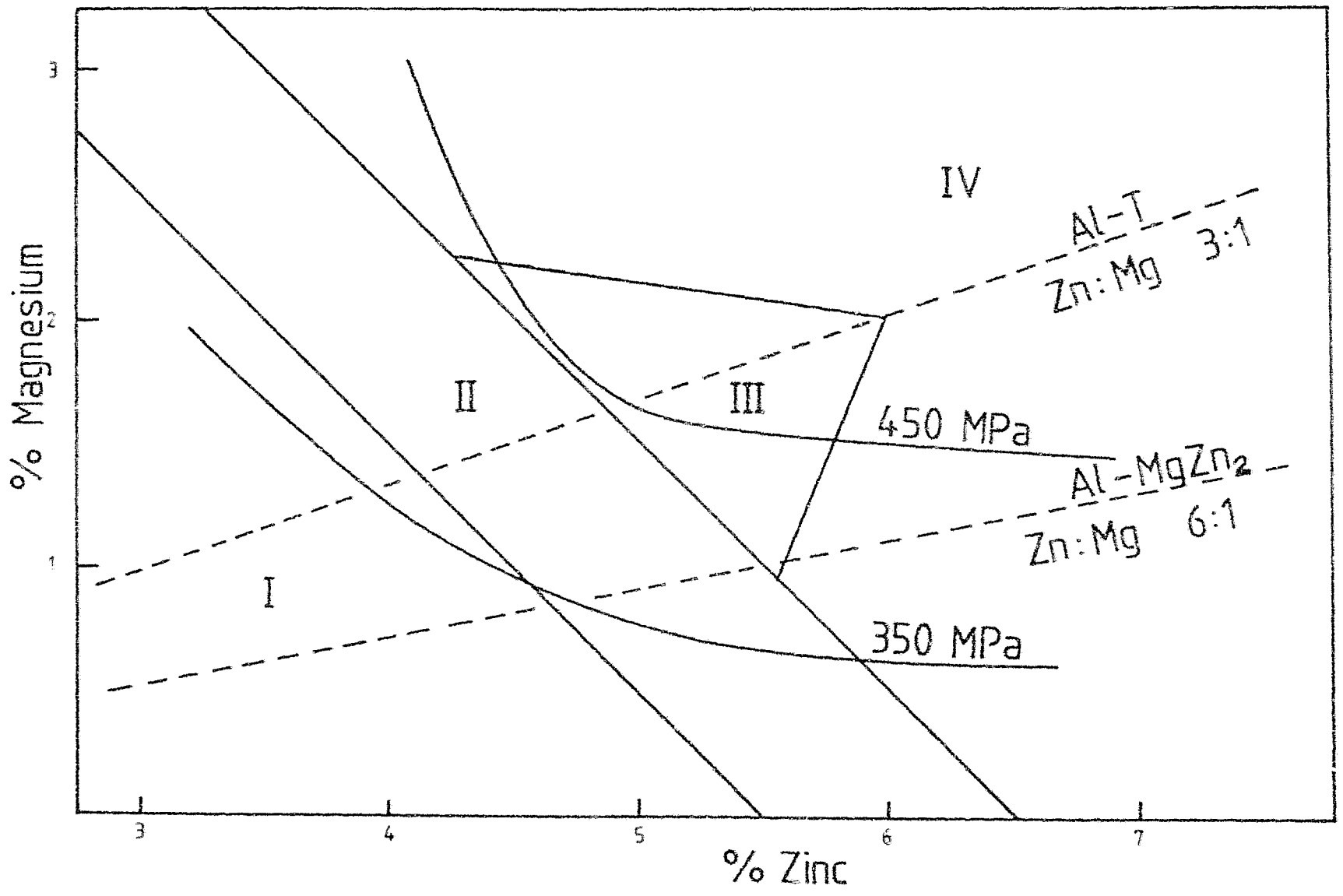


Figure 2.2 Effect of (Zn + Mg) level on stress corrosion susceptibility. The tensile strength contours of air cooled alloys are shown at 350 and 450 MPa.

This diagram has been divided into four distinct regions. The characteristics of each are described below.

I. Acceptable stress corrosion resistance can be obtained with (Zn + Mg) contents less than 5.5%. This may be achieved in recrystallized microstructures provided that controlled heat treatments involving low quench rates and artificial ageing are employed. For most applications, however, the strength levels in this region would be low. The effects of heat treatments on SCC properties will be discussed in depth in later sections.

II. In the region 5.5 to 6.5% (Zn + Mg), in addition to the metallurgical treatments mentioned in I, structure control is also required to obtain acceptable SCC properties. This is usually achieved by minor additions of Mn, Zr and Cr. The effects of these elements will be treated in the following sections.

III. In addition to the requirements of I and II, the Zn : Mg ratio must be optimised in this region.

IV. Outside of region III a further requirement is a Cu addition greater than 1.2%, together with an overageing treatment. Unlike alloys in regions I - III, the high Cu - content renders high (Zn + Mg) alloys non-weldable.

As the control of both the (Zn + Mg) level and the Zn : Mg ratio are of separate importance, they will be dealt with individually.

i) (Zn + Mg) level

The marked increase in tensile strength on increasing the (Zn + Mg) content from 4.5 to 6.5% can be seen in Figure 2.3 (from ref. 11). The observed scatter arises from the use of alloys with different Zn : Mg ratios and in different heat-treated conditions. It should also be noted that these alloys contained 0.3% Mn and 0.1% Cr for structural control.

However, there are limitations on the absolute amounts of each element which can be added. For extruded alloys, experience has shown that due to SCC problems and increasing extrusion pressures the Mg content should be limited to the lowest practical level.

As the Zn content is increased, recrystallisation on solution heat treatment is decreased. Cordier and co-workers[10] found that with an initial 33% cold reduction, an alloy containing 1.5% Mg and 4% Zn achieved complete recrystallisation at 480°C. With 5% Zn the recrystallised zone was confined to the rolled surface; and with 6% Zn the recrystallisation was completely suppressed in favour of a fibrous structure.

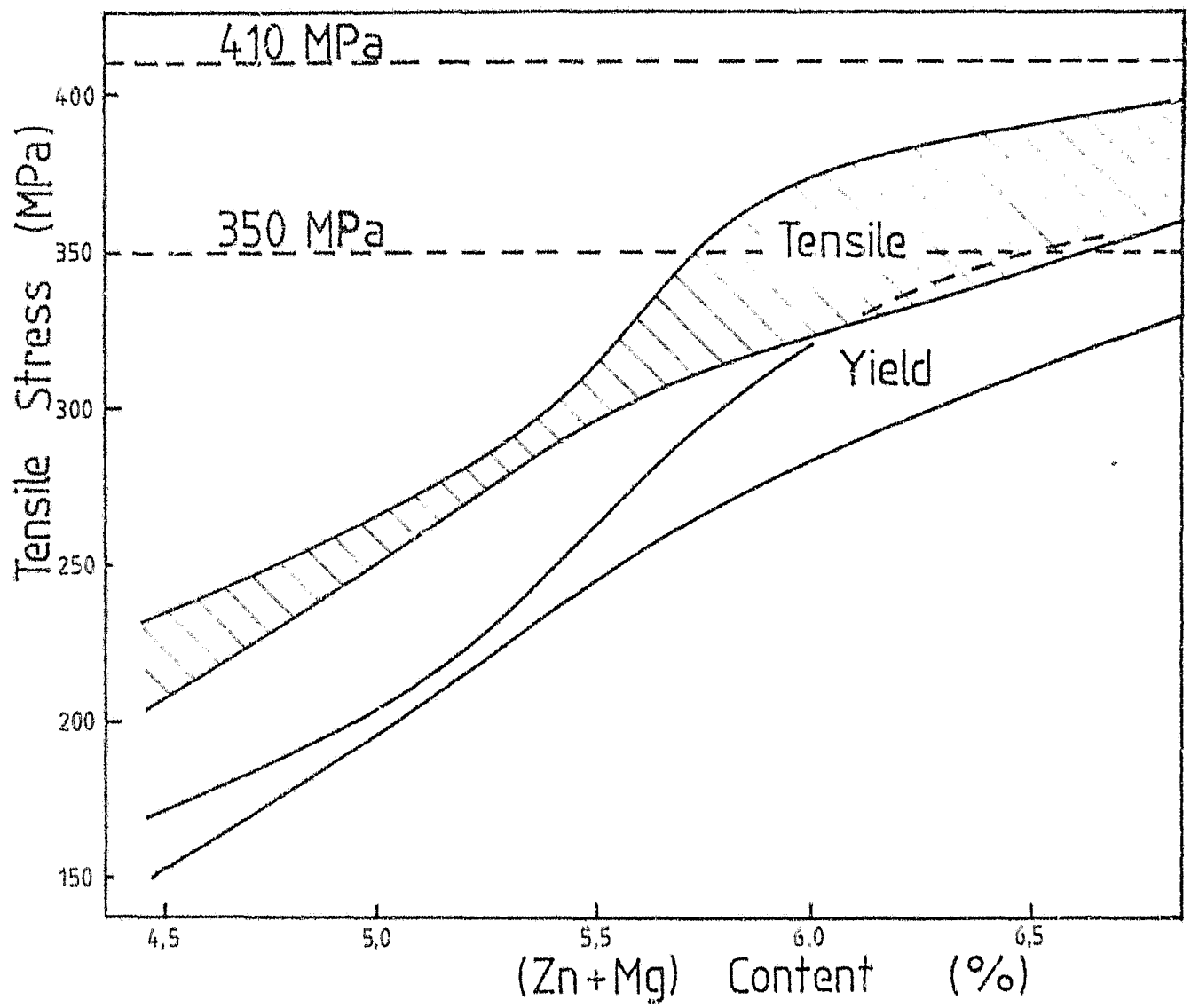


Figure 2.3 Effect of (Zn + Mg) level on mechanical properties. The horizontal dotted lines show minimum property requirements.

It has also been found that Mg contents greater than 1.5%, and increasing Zn content both lead to increased quench sensitivity of Al-Zn-Mg alloys. This effect may be explained by the solid solution saturation limit of Zn and Mg on quenching. The $MgZn_2$ - saturation limit is in the region of 6% Zn for a quench rate of 1-2 $K.s^{-1}$. With a relatively low quench rate, no further strength increase can be achieved by increasing the Zn content. Conversely, a high quench rate of 100 $K.s^{-1}$ would lead to a greater oversaturation capacity of the alloy. In principle, Cordier, et al.[10] have found that the quench sensitivity is intensified for a Zn content greater than 5% (1.5% Mg). Clearly then, an optimisation must be found between the decrease in recrystallisation on solution heat treatment and liability to quenching sensitivity on increasing the Zn content.

Another effect of an increase in the (Zn + Mg) content is the acceleration of the age-hardening kinetics. This implies that peak hardness may be achieved in a shorter period during artificial ageing. This could be explained by the greater supersaturation at higher (Zn + Mg) levels which will lead to a higher density of the hardening $MgZn_2$ precipitate phase, and hence much shorter diffusion paths.

Finally, it has also been reported that impact properties decrease as the (Zn + Mg) content increases[11]. The effect on the notched toughness in an IZOD impact test is shown in Figure 2.4. For a (Zn + Mg) content greater than 5.5%, it is also clear that the impact properties are reduced significantly by a reduction in quench rate (from water quenching to air cooling).

From these considerations, a preliminary estimate of the required Zn and Mg contents for a superior Al-Zn-Mg alloy can be made. For weldability, the (Zn + Mg) content should be limited to 7%. To guarantee minimum properties of 350 MPa (Yield Stress) and 410 MPa (Tensile Stress), the Mg content should not be less than 1.7%.

ii) Zn : Mg ratio

It has already been stated that alloy compositions with (Zn + Mg) contents greater than 6.5% (in region III of Figure 2.2) require the Zn : Mg ratio to be optimised. Ageing response is superior for alloys in this region. Therefore, the Zn : Mg ratio which controls the limit and extent of region III is an important parameter. By considering the Zn : Mg, 3 : 1 line in Figure 2.2, it can be seen that this provides the maximum strength for the least total solute content.

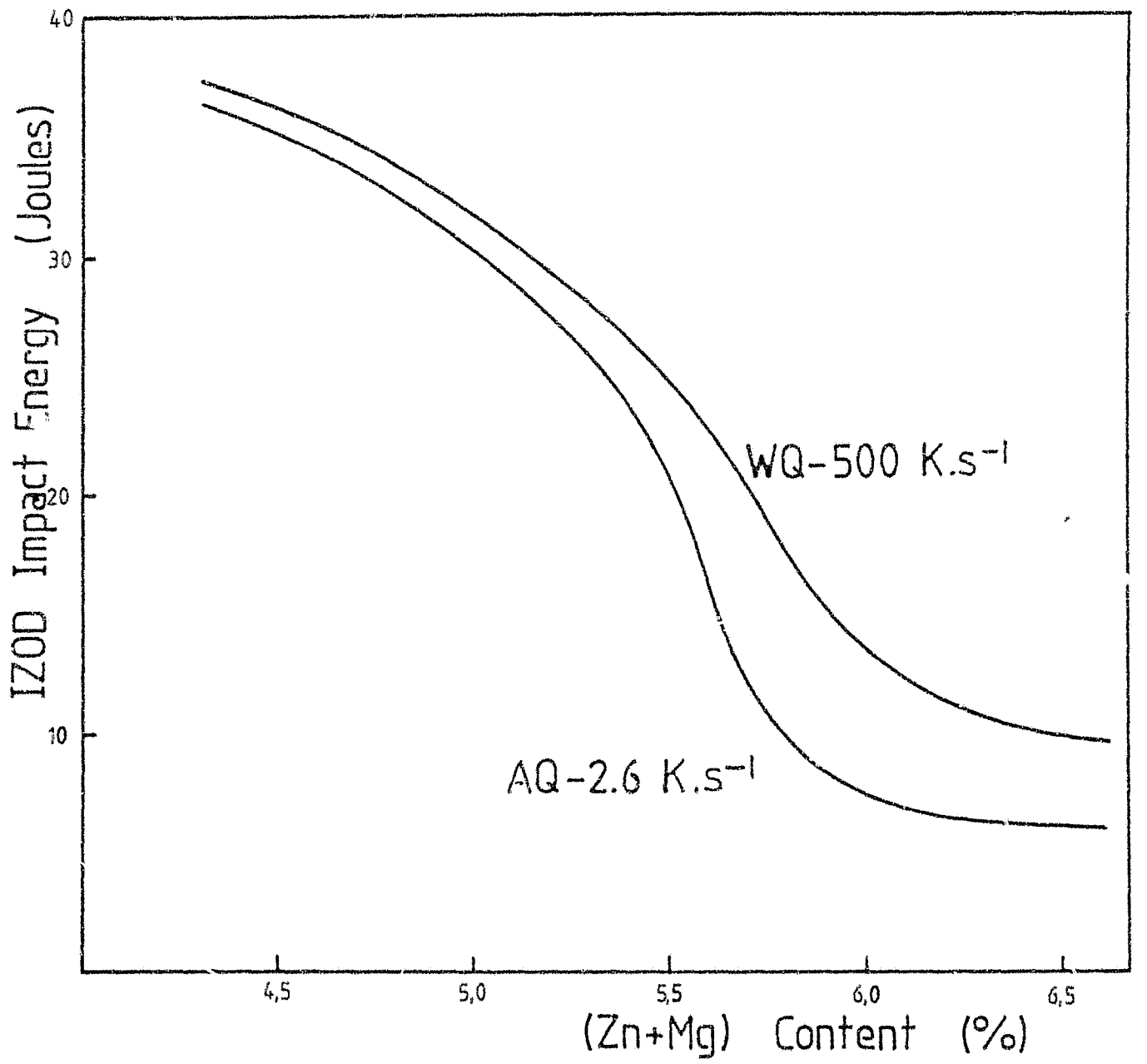


Figure 2.4 The effect of (Zn + Mg) content on notched toughness.

The effect of the Zn : Mg ratio on the susceptibility to SCC, for copper-free, weldable alloys with a (Zn + Mg) content of 8%, in the same temper condition, is shown in Figure 2.5 (from ref. 9). A similar relationship has also been observed in high strength copper-containing alloys. Experimental evidence therefore suggests that maximum resistance to SCC is obtained if the Zn : Mg ratio is between 2.7 and 2.9 [9,10,12]. It is interesting to note here that few existing commercial alloys do in fact comply with this ratio.

Having reviewed the additional requirement of a Zn : Mg ratio of 3 : 1, it is now possible to define more exactly the desired composition of a superior alloy. Given the maximum Mg content of 1.7%, the Zn content should be 5.1%.

2.2.2 Transition Element Additions

Small additions of transition elements exert a marked influence on many of the properties of Al-Zn-Mg alloys. Among the most important of these are Cr, Zr, Mn, Cu and Ti. The success of the transitions is due to their tendency to stay in supersaturated solid solution after rapid solidification in casting[13]. They then precipitate out during the homogenisation heat treatment. Precipitation is, however, drastically affected by Fe and Si impurities.

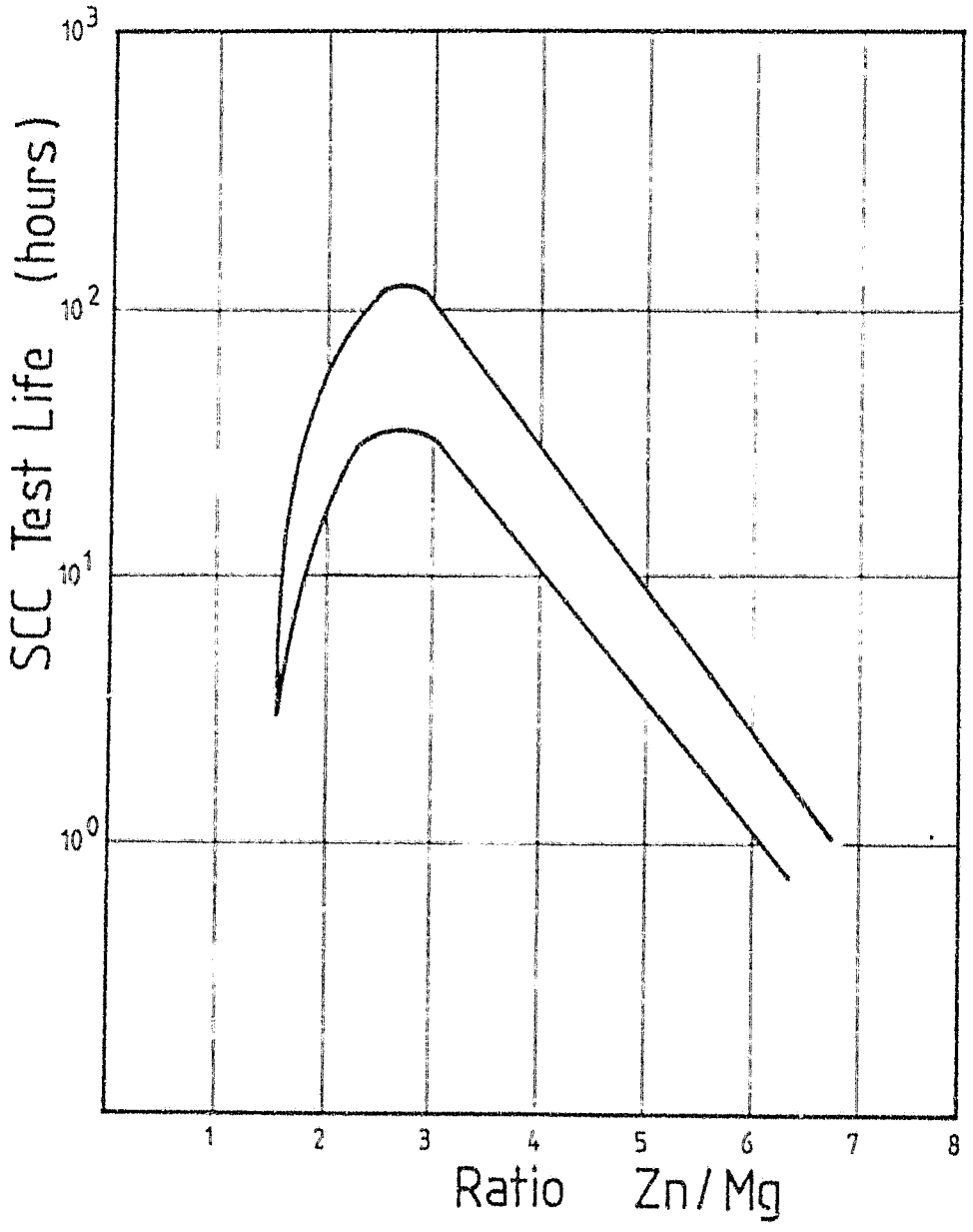


Figure 2.5 The effect of Zn : Mg ratio on SCC susceptibility of Al-Zn-Mg alloys (Zn + Mg = 8%).

The transition elements have two major effects. One is the tendency of these elements to form insoluble intermetallic particles, which pin grain boundaries and thereby stabilise the wrought grain shape. Mn and Cr are the best known examples of this class of recrystallisation inhibiting elements, although recently Zr has become prominent in this category[8]. Grain refinement can also be achieved using small additions of Ti and B.

The second effect of transition elements is to alter the second-phase precipitation kinetics. Cu delays precipitation and additions of more than 1% provide increases in both strength and SCC resistance[8,9,14,15,16]. Cr and Mn accelerate the precipitation sequence in Al-Zn-Mg alloys, in part because they precipitate during homogenisation treatment and act as nuclei for later heterogeneous precipitation of the hardening phase.

In terms of the effect on SCC, Cr initially solved many of the existing problems. However, Zr is a substitute which can offer the same SCC properties, but with improved fracture toughness[14]. In Cu-free Al-Zn-Mg alloys, small additions of Li (up to 0.6%) are also beneficial to SCC resistance[8].

It is important to realise that the strongest alloys rely on the maintenance of a fibrous structure, by the inhibition of recrystallisation. Cr, Mn and Zr are

therefore usually added to the maximum practical levels[9]. As discussed in the preceding section, to obtain the minimum mechanical property requirements (See Figure 2.3), a (Zn + Mg) level exceeding 5.5% will be necessary[10,11]. All these alloys will fall into region III or IV of Figure 2.2, where control of grain structure by the addition of transition elements is imperative for acceptable SCC resistance. The addition of these elements (particularly Cr) will, however, increase the quench sensitivity of the alloy. The effects of important minor alloying additions will now be considered individually.

i) Chromium

Cr is added in amounts up to 0.35%. The major direct effects of Cr additions are:

a) an increase in quench sensitivity;
b) an increase in resistance to recrystallisation; and
c) a decrease in the strength of the alloy.

The indirect effect of Cr additions is a substantial increase in resistance to SCC.

During homogenisation (Al, Fe, Cr, Si) and (Al, Cr) phases, ranging in size from 0.05 to 0.2 μm , are precipitated from the supersaturated solid solutions of commercial alloys. The precipitate is finely distributed throughout the matrix. This particle distribution does not increase the strength of the alloy which is determined by the hardening (Zn, Mg) phase distribution. Transmission electron microscopy (CTEM) studies have revealed that for small (0.15%) Cr additions only (Al, Fe, Cr, Si) phases are formed. At a higher chromium content (0.34%), additional (Al, Cr) phases also develop[15]. This (Al, Cr) phase is able to incorporate Mg and Zn, which reduces the age-hardening capacity of the alloy. At higher Cr concentrations this does in fact lead to a reduction in strength.

The increase in quench sensitivity is caused by the reduction of strength associated with the heterogeneous nucleation of (Mg, Zn) zones and precipitates on Cr-containing particles. This has been confirmed by Cordier, et al.[15], for the precipitation of $MgZn_2$ rods. These workers also found no evidence of segregation of Cr to, or preferential formation of Cr-phases on grain boundaries. Thus, Cr does not appear to improve SCC resistance by influencing these critical regions.

The beneficial effect must therefore be due to the inhibition of recrystallisation and the prevention of slip band formation, which may also lead to SCC. The reduction of recrystallisation reduces the number of high angle, high energy grain boundaries exposed, particularly in the longitudinal and long transverse directions. SCC will still, however, occur in the short transverse direction. The reduction of slip band formation is attributed to a spreading of the slip distribution by the Cr-containing particles.

In order to optimise the effects of Cr additions in Cu-free alloys, a balance must be found between the increased quench rate (required to maintain properties) which reduces the resistance to SCC, and the favourable recrystallisation-inhibiting effect. Experimental evidence has shown that in an Al-5Zn-1.7Mg base alloy, a 0.15% Cr addition combined with a $2K.s^{-1}$ quench rate provides superior SCC resistance, compared with the same alloy containing 0.34% Cr and quenched at the required faster rate[15]. These results have been summarised in Figure 2.6. Here, tensile properties and life spans in the edge cut SCC test[17] are shown for various quench rates after solution heat treatment.

ii) Manganese

Mn additions of up to 0.7% are normally used in commercial Al-Zn-Mg alloys. Mn produces direct effects which are in many cases similar to small Cr additions:

a) an increase in quench sensitivity;
b) an increase in the resistance to recrystallisation; but
c) an increase in strength.

Small additions (0.2%) give slight improvements in SCC, by inhibiting recrystallisation and ensuring a homogeneous dislocation structure. However, larger additions, up to 1.3% Mn, actually reduce the resistance to SCC[15].

During homogenisation, (Al, Mn, Si) phases are precipitated. These develop a coarser particle distribution than is achieved with Cr-containing phases. With small Mn additions (0.2%) the particles range in size from 0.05 to 0.5 μm . Larger additions (1,33%) produce more numerous, coarser particles, often larger than 1 μm . A major difference in the affinity between the main alloying additions (Zn and Mg) and the Mn- and Cr- rich phases becomes noticeable with additions greater than 0.2%. Unlike Cr, Mn-containing phases

do not interact with Zn or Mg and hence do not reduce the age-hardening capacity of the alloy. In fact, the separate distribution of the (Al, Mn, Si) phases also contribute to the strength, thereby leading to the observed higher values. Their coarse distribution does, however, reduce the toughness and hence formability of the alloy. This effect is intensified as the number of coarse particles increases[18].

The tensile properties and life span in the edge cut SCC test[17] are shown for a range of quench rates after solution heat treatment in Figure 2.7 (from ref. 15). The increased quench sensitivity is, as in the case of Cr, caused by heterogeneous nucleation of (Zn, Mg) phases on Mn-containing particles. Mn is less effective than Cr in the inhibition of recrystallisation due to the coarser particle distribution produced[15].

iii) Zirconium

Recently, Zr has received much attention as a potential replacement for Mn and Cr additions, in order to provide superior SCC resistance and toughness properties. Controlled additions of Zr up to 0.2% are generally made. To date, however, Zr is used mainly in combination with Cr and Mn.

Figure 2.6 The effect of quench rate on the tensile properties and SCC test life spans for:
(1) Al-5Zn-1.7 Mg,
(2) Al-5Zn-1.7 Mg + 0.15Crand
(3) Al-5Zn -1.7Mg +0.34 Cr

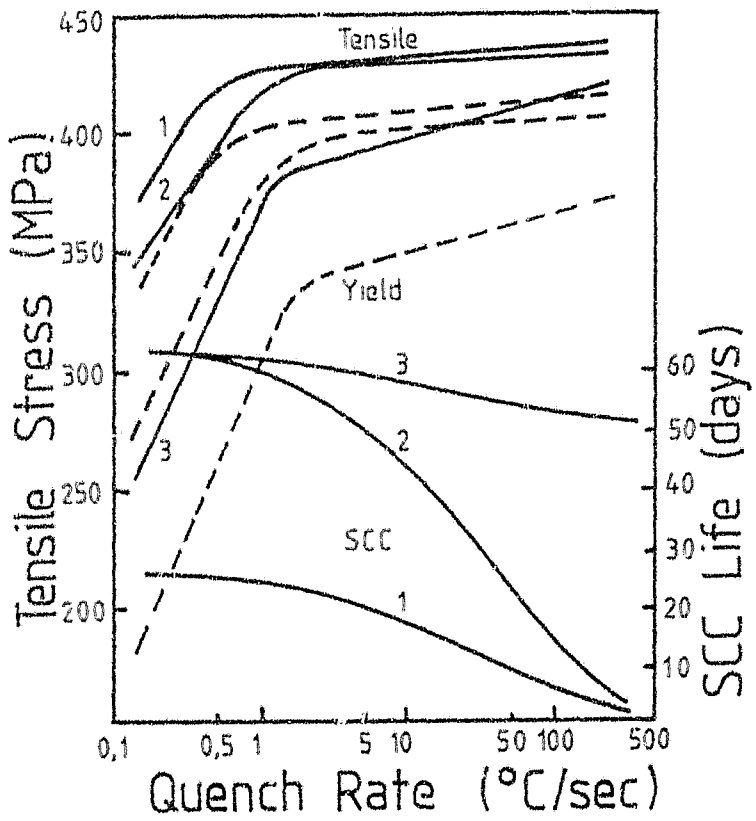
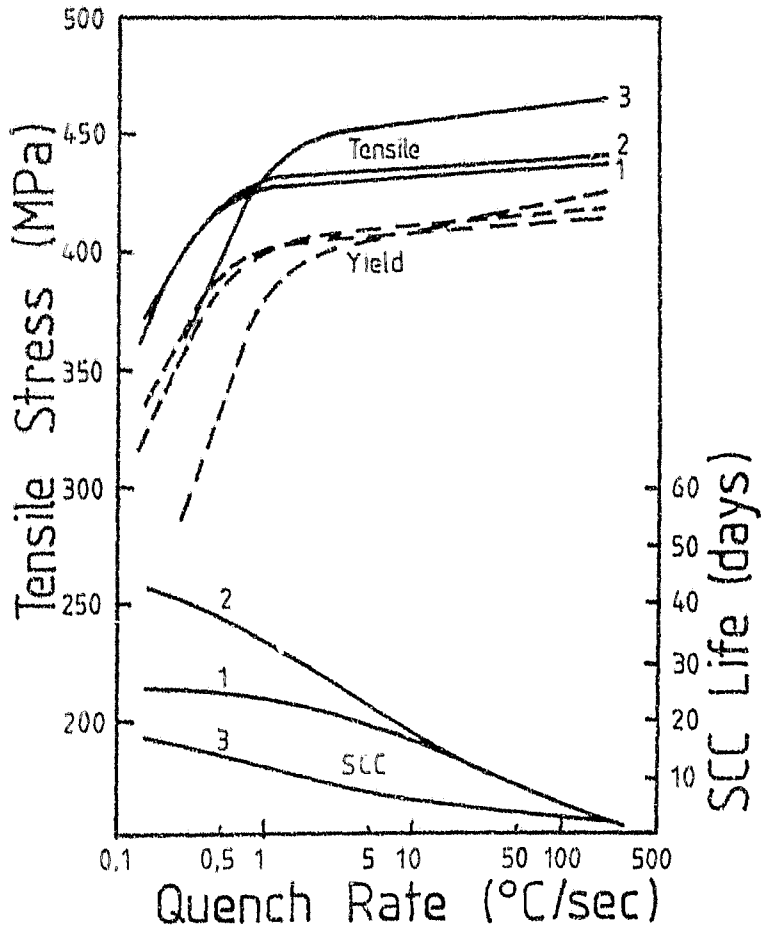


Figure 2.7 The effect of quench rate on the tensile properties and SCC test life spans for:
(1) Al - 5Zn - 1.7 Mg,
(2) Al - 5Zn - 1.7 Mg + o.2 Mn
and
(3) Al - 5Zn - 1.7Mg + 1.3Mn



Zr, like Cr and Mn, precipitates out of supersaturated solid solution during homegenisation, producing a heterogeneous distribution of intermetallic phases. The heating rate to homegenisation has a profound influence on the precipitation reactions in Al-Zn-Mg alloys containing Zr. Slow heating rates of approximately 0.014 $K.s^{-1}$ (50 $K.h^{-1}$) produce an extremely high density of metastable cubic Al_3Zr particles, which are coherent with the matrix[13]. At faster heating rates coarse equilibrium phase precipitates (tetragonal Al_3Zr) are formed directly. The direct formation of the equilibrium phase is also observed in alloys containing > 0.2% Zr. These coarse primary particles lead to a reduction in material properties. By comparing the precipitation kinetics and resultant particle distributions in high purity and commercial Al-Zn-Mg alloys, Westengen, et al.[13] have shown that the successful application of Zr depends on the modifying effects of impurities and main alloying elements on the precipitation kinetics of Zr. These, together with a slow heating rate, produce a "seeding" effect, which encourages nucleation at lower temperatures. This is extremely effective in producing a copious dispersion of fine precipitates.

Cubic Al_3Zr is fully coherent with the matrix and therefore has a low interphase boundary energy, and a low barrier to nucleation. Although some

degree of atomic matching occurs across matrix - (Mn- or Cr-) containing particle interfaces, the nucleation barrier is much higher. In consequence, the particle densities in Zr-containing alloys are approximately two orders of magnitude larger than for the other transition elements (Mn and Cr). Zr would therefore be expected to provide superior inhibition of recrystallisation[20]. In addition toughness should be improved due to the absence of coarse intermetallic particles.

An added advantage of Zr additions is that they have the least effect on quench sensitivity. Like the Mn-rich phases, the small, insoluble particles of Al_3Zr do not combine with the principal alloying additions, and do not therefore reduce the age-hardening response. It has been reported that the beneficial effects of Zr can be adversely affected by too great a Mn and Ti content[19]. Ti is therefore usually limited to 0.03 - 0.04%, although 0.04 - 0.05% has been used successfully. The effects of simultaneous Mn and Zr additions will be considered in Section (vi) on combined transition additions. For the present, controlled Zr additions of 0.15% should be considered optimum, producing exceptional grain refinement and recrystallisation inhibition, and good toughness properties.

iv) Copper

Additions of Cu to Al-Zn-Mg alloys have been found to simultaneously improve the yield strength and SCC resistance[21]. An overageing heat treatment may also be used to greatly enhance the SCC resistance without unacceptable strength penalties in these alloys[16]. Controlled Cu additions are kept below 0.3% to minimise both hot-cracking during the solidification of welds and general corrosion in service[15]. The beneficial effect of small Cu additions has been clearly demonstrated[9] and is illustrated in Figure 2.8.

No Cu precipitates are formed on homogenisation. This implies that Cu additions should have little effect on the quench sensitivity of the alloy. On ageing after solution heat treatment, a partially coherent matrix precipitate ($CuAl_2$) is formed, which increases the yield stress by 5 to 15 MPa[15].

Cu additions are known to influence the deformation behaviour and electrochemical characteristics of Al-Zn-Mg alloys. The degree of coherency of the (Zn,Mg) strengthening precipitates can be modified by Cu additions[16], which essentially delay formation of metastable precipitates[8]. On ageing, this not only increases the volume fraction of the strengthening phase, but also increases the number of precipitates. This has a marked effect on the homogeneity of the deformation process.

The beneficial effect of Cu additions on SCC resistance has been explained by Ward and Lorimer[22] in terms of a simple electro-chemical model. In aluminium alloys, Cu additions counteract the influence of Zn and tend to make the alloy, or its oxide film, less anodic.

An alternative hypothesis has been proposed by Sarker et al.[16] based on the effect Cu additions have on the deformation mode taking place during SCC. In Cu-free alloys, dislocation shearing of the strengthening precipitates occurs, resulting in inhomogeneous deformation. In the presence of Cu, however, this mode is inhibited in favour of looping mechanisms. This more homogeneous mode of deformation enhances resistance to SCC.

However, it has been shown that, even in the overaged condition (the least susceptible to SCC), little segregation of Cu occurs in the microstructural areas (the precipitate free zone (PFZ) and grain boundaries) most susceptible to SCC[15,22]. It appears, therefore, that Cu contributes directly to SCC resistance in these regions.

For weldable Al-Zn-Mg alloys, a Cu-addition of approximately 0.15% can be made in order to improve resistance to SCC and increase strength[15]. The

effects of this Cu content (at different quench rates) on the SCC life in an edge cut test[17] are shown in Figure 2.9

v) Titanium and Boron

Certain controlled transition additions are frequently made to aluminium in order to provide grain refinement. Many transition elements which exhibit peritectic reactions and form carbides with a simple cubic structure, promote grain refinement to varying degrees[23]. The most potent grain refiners are titanium, tantalum and hafnium. In commercial practice the most common grain refiner is Ti, which is added in the form of an Al-5Ti-1B "hardener". The presence of small amounts of boron in dilute Al-Ti alloys considerably enhances grain refinement.

The hardener forms $TiAl_3$ and TiB_2 particles which act both as crystallisation centres and growth restricting solute fields[23]. Electron microprobe analyses of Al-Ti-B alloys have revealed high Ti content in the intergranular regions and at the centres of the dendrites.

The amount of grain refinement obtained with a given Ti-B addition depends on the preparation and condition of the master alloy, and also on the rate

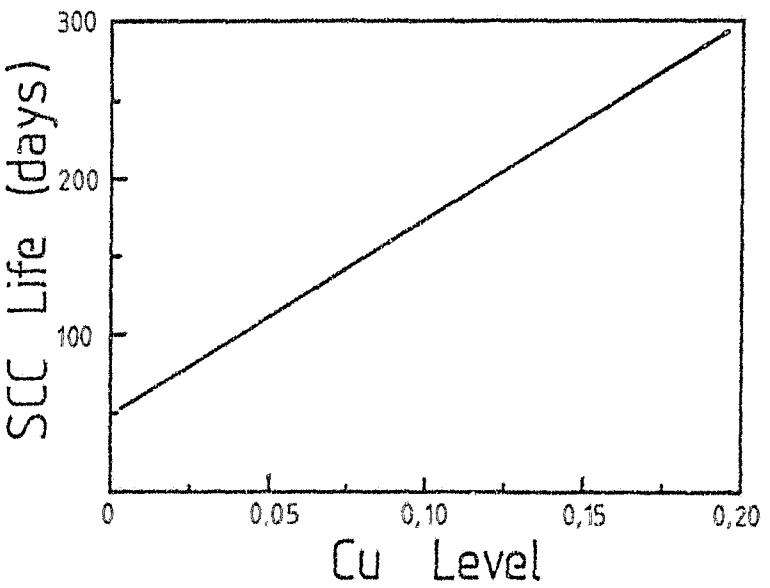


Figure 2.8 Salt spray SCC test lives for an Al -4.5 Zn - 2.5Mg alloy with minor Cu additions aged for 24 h/120°C and 2 h/180°C

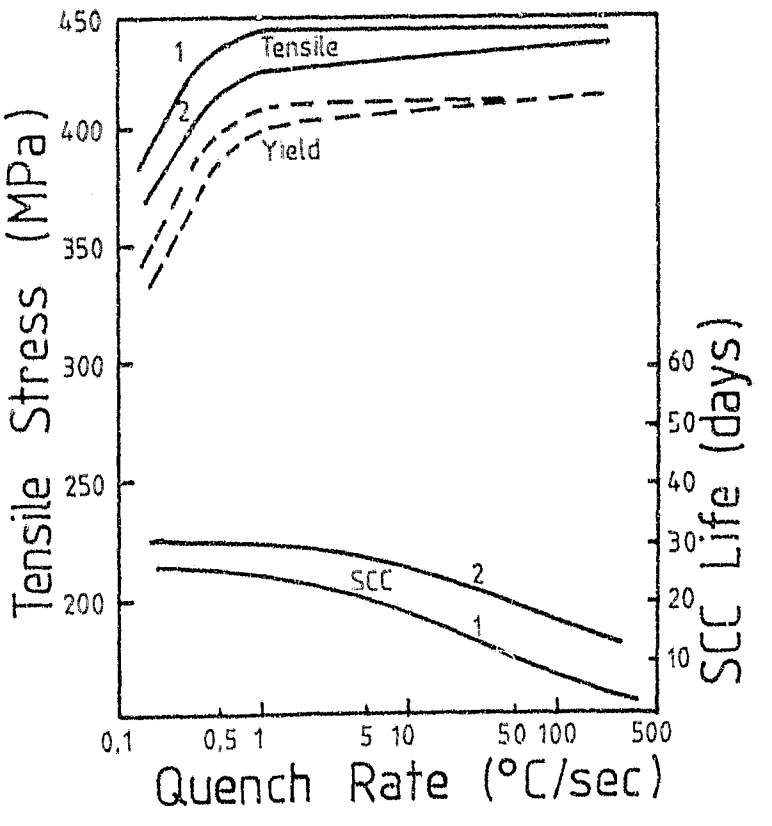


Figure 2.9 The effect of quench rate on the tensile properties and SCC test life spans for:
(1) Al - 5 Zn - 1.7 Mg, and
(2) Al - 5 Zn - 1.7 Mg + 0.15Cu

of cooling from the molten state. In normal semicontinuous direct-chill ingot production, a level of 0.004% Ti and 0.001% B, added as Al-Ti-B hardener, produces a grain diameter of 180 to 200 μm. Further additions effect a progressive reduction in grain size to a limit of 50 to 70 at Ti level of 0.02%. If additions of hardeners are made beyond this level, they merely serve to increase the solidification interval of the alloy and so extend the local solidification time in any region. As the solidification range in Al-Zn-Mg alloys is already large, any further increase should be avoided.

vi) Combined transition additions

The combined effects of a number of different transition elements do not always provide the same effect as the sum of the effects of the individual elements. The most common transitions in this category are again Cr, Mn, Zr, and Cu.

It has been shown that combined Cr and Mn additions form coarse (Al, Mn, Cr, Si) phases. This prevents Cr forming the fine precipitate dispersions which favour good resistance to SCC[15]. It is therefore generally recommended that Mn additions should be avoided, preference being given to combinations of Cr, Zr and Cu. However, it should be reiterated that the ultimate aim is the sole use of Zr additions.

Combined Cr and Cu additions give excellent resistance to SCC as the two elements have no mutual interaction. Cr forms a fine dispersion of (Al, Cr, Fe, Si) and (Al, Cr) phases and Cu remains dissolved in grain boundary regions where it improves resistance to SCC. Although insufficient publications exist in the open literature to determine the combined effects of Cr and Zr, it can generally be accepted that only limited interactions, if any, will take place. Zr additions of approximately 0.15% should be made in order to provide a recrystallisation inhibiting dispersion of particles and also to reduce weld cracking. It must, however, be remembered that if Zr is used in combined additions, a heating rate to homogenisation of not more than 0.014 $K.s^{-1}$ must be used.

Using Al-5Zn-1.7Mg as a base alloy, Cordier, et al.[15] have shown that superior SCC resistance is obtainable with transition combinations of: (0.15 - 0.20%) Zr, (0.15 - 0.25%) Cr, and (0.15 - 0.20%) Cu. (In this work, a low heating rate to homogenisation was not used and therefore the full potential of the Zr additions may not have been fully realised). The above additions have been unconditionally recommended for a high-strength and SCC resistant Al-5Zn-1.7Mg alloy. The effects of the above combined additions on tensile properties and SCC life in the edge cut test[17] as a function of quench rate are shown in figure 2.10.

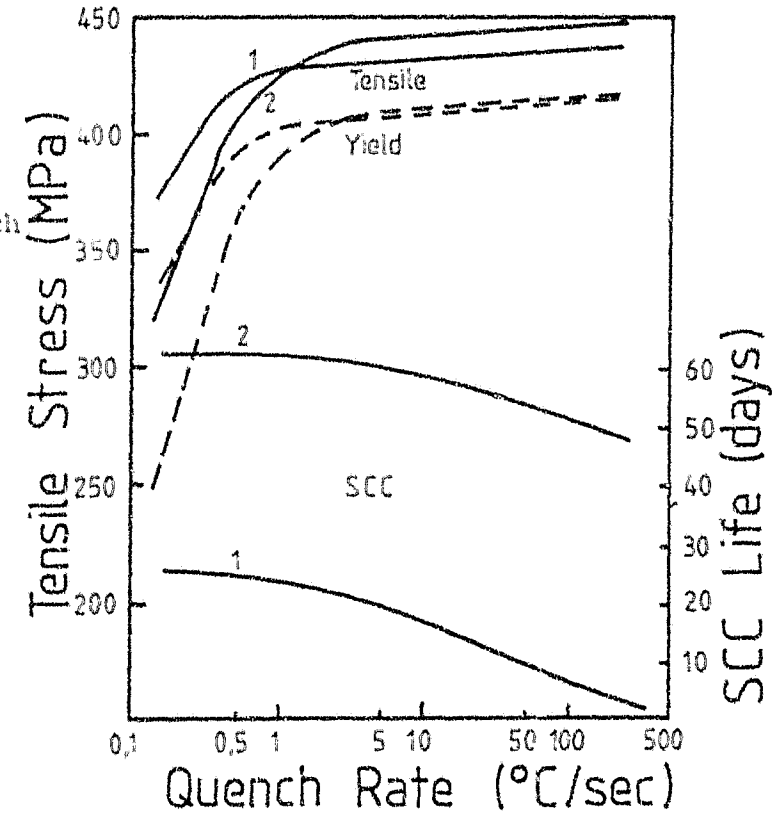


Figure 2.10 The effect of quench rate on the tensile properties and SCC test life spans for:
(1) Al - 5Zn- 1.7 Mg , and
(2) Al - 5Zn -1.7 Mg + 0.15 Cr + 0.16 Cu

2.2.3 Impurity effects

The two most important natural impurities in aluminium alloys are Fe and Si. These elements have a profound influence on the precipitation of transition elements[20]. Results of investigations on high purity experimental alloys containing transition elements cannot, therefore, be directly related to industrial alloys.

In Mn- and Cr-bearing alloys, the formation of dispersoid particles is directly affected by the impurities Fe and Si. These elements are incorporated into the precipitate crystal lattice and result in easier nucleation of those phases due to a lower nucleation barrier[13]. In Zr-containing alloys, the major influence of Fe and Si is to increase the kinetics of Al_3 Zr precipitation. In fact, the successful application of Zr additions is dependent on the catalytic action of these impurities.

Fe and Si impurities are known to reduce mechanical properties in Al-Zn-Mg alloys, particularly fracture toughness and fatigue resistance[14]. Therefore, ideally the Fe and Si contents should be as low as possible. The natural impurity limits for wrought Al-Zn-Mg alloys is approximately 0.4% for both Fe and Si. However, the highest commercially feasible purity levels are around (0.04 - 0.08%) Fe and (0.04 - 0.06%) Si[14].

2.2.4 Experimental Confirmation of some of the Major Factors

A number of experimental investigations were undertaken in order to substantiate some of the results already discussed. These studies were also intended to provide necessary baseline data required for future alloy development.

i) (Zn + Mg) Content

A range of small scale experimental alloys were cast and fabricated to determine the influence of (Zn + Mg) content on both the attainable hardness and the ageing kinetics.

The alloys were induction melted and cast under one atmosphere of argon, from commercial purity base constituents. 3kg ingots (50 x 100 x 200mm) were produced by direct casting into a mild steel mould. The alloys contained approximately 0.35% Mn as a recrystallisation inhibitor and 0.03% Ti to provide grain refinement.

After a homogenisation treatment of 10 hours at 480^{o}C, the 50mm thick ingots were hot rolled to 12mm plate using a starting temperature of 450^{o}C and a minimum finishing temperature of 350^{o}C. To achieve the total reduction, two re-heats were required during rolling.

Spectrographic compositional analyses were obtained from each alloy and these results are presented in Table II. All the alloys contained approximately 0.25% Fe, 0.12% Si and 0.25% Cu derived from the commercial purity base stock.

Table II: Experimental Alloy Compositions

ALLOY	Mn	Ti	Mg	Zn	Mg + Zn
1	0.33	0.024	0.85	3.97	4.82
2	0.35	0.040	1.14	4.08	5.22
3	0.38	0.032	0.81	4.92	5.73
4	0.35	0.028	1.63	5.44	7.07
5	0.41	0.028	2.62	5.71	8.33
6	0.36	0.025	0.79	5.81	6.60
7	0.31	0.026	1.89	6.17	8.06

A standard heat treatment schedule was applied to each alloy:

(1) a solution heat treatment (465°C/2hr, water quench);
(2) a natural age (25°C/2 weeks); and
(3) a pre-age (90°C/7 hours).

Ageing curves were then determined for a final age of 135°C for 4 - 48 hours.

A measure of the strength of the alloys was obtained from standard Vickers hardness tests (using a 20Kg load)

ii) Effect of Cr, Zr and Mn on Recrystallisation

A brief study had already been undertaken to determine the recrystallisation inhibiting effect of small additions of Cr, Zr and (Cr + Zr)[24]. In the present investigation, a further experimental alloy, containing 0.35% Mn, was prepared in order to extend the range of transition elements considered.

The compositions of these alloys (which contain similar amounts of Zn, Mg and Ti) are shown in Table III.

Table III: Experimental Alloys containing additions of Cr, Zr, (Cr + Zr) and Mn

ALLOY	Mn	Cr	Zr	Mg	Zn
8	0.01	0.19	0.01	0.80	5.30
9	0.04	0.003	0.16	0.80	5.10
10	0.04	0.19	0.18	0.80	5.50
11	0.35	0.001	0.01	0.80	5.30

A measure of the strength of the alloys was obtained from standard Vickers hardness tests (using a 20Kg load)

ii) Effect of Cr, Zr and Mn on Recrystallisation

A brief study had already been undertaken to determine the recrystallisation inhibiting effect of small additions of Cr, Zr and (Cr + Zr)[24]. In the present investigation, a further experimental alloy, containing 0.35% Mn, was prepared in order to extend the range of transition elements considered.

The compositions of these alloys (which contain similar amounts of Zn, Mg and Ti) are shown in Table III.

Table III: Experimental Alloys containing additions of Cr, Zr, (Cr + Zr) and Mn

ALLOY	Mn	Cr	Zr	Mg	Zn
8	0.01	0.19	0.01	0.80	5.30
9	0.04	0.003	0.16	0.80	5.10
10	0.04	0.19	0.18	0.80	5.50
11	0.35	0.001	0.01	0.80	5.30

The alloys were solution heat treated for 50 minutes in a salt bath at 420°C, 460°C and 500°C. The extent of recrystallisation in the as-rolled condition, and after each solution treatment was assessed for each alloy by examination under the optical microscope.

iii) Metallographic Investigation of a Representative Al-Zn-Mg Alloy

Small transition element additions and trace impurities produce many coarse intermetallic constituents in commercial alloys. A preliminary study was therefore instigated to characterise the structure of a typical alloy (Hulett's D74S). (The nominal composition of this material is given in the Appendix). The alloy was supplied by the manufacturers as 12mm plate in the standard heat-treated condition. Polished sections were etched with 40% Tucker's etchant or 9% orthophosphoric acid solution (at 70°C) for the study of macro grain structure and grain size, using optical microscopy.

The distribution of precipitates was revealed, using a Cambridge S4 scanning electron microscope (SEM), in similar samples etched in 0.5% HF or Keller's reagent. In addition, elemental distributions were determined from X-ray maps, obtained using an EDAX, energy dispersive spectrometer (EDS) attachment.

2.2.5 Experimental Results and Discussion

i) (Zn + Mg) Content

Ageing curves were determined for all the experimental alloys 1 to 7, and the results are shown in Figure 2.11. It is clear that at a final ageing temperature of 135°C the alloys do not appreciably overage even after long ageing times (48 hours).

The effect of an increase in the (Zn + Mg) content in the approximate range of 5 - 8%, leads to an increase in peak hardness (and hence tensile strength) of about 50%. This is clearly demonstrated in Figure 2.12.

The Zn : Mg ratio would also be expected to influence the hardness. The Zn and Mg contents of each alloy are represented in Figure 2.13. By comparing the peak hardness values of alloys with similar Zn contents (1 and 2; or 5 and 6) and Mg content (1,3 and 6), the relative potency of the two alloying elements could be broadly assessed. It appears that Mg is $\sim$ 40% more effective than Zn. This variation in hardness with Zn : Mg ratio also accounts for the scatter in hardness, or tensile properties, observed in Figures 2.12 and 2.3.

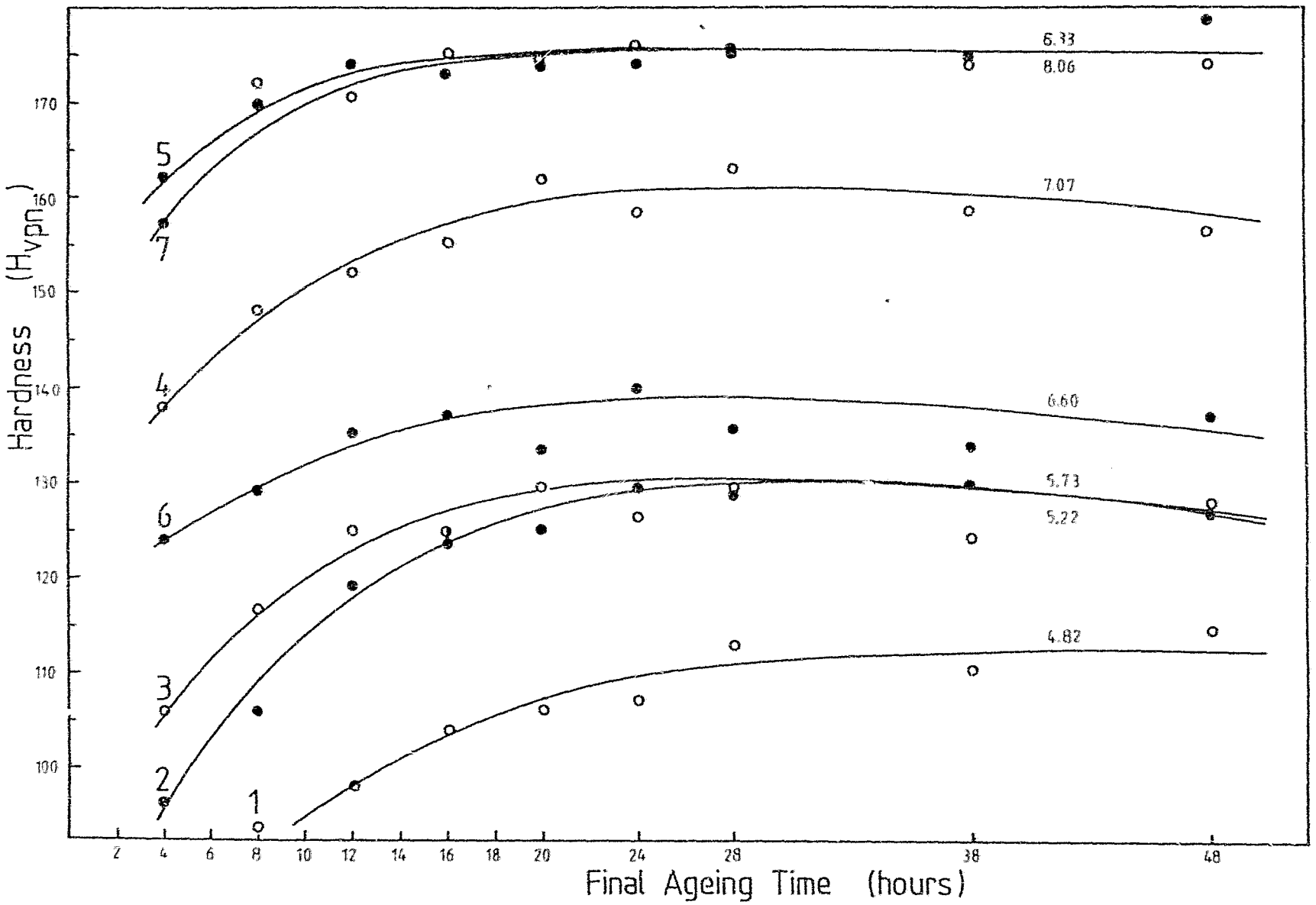


Figure 2.11 Ageing curves of the experimental alloys (1 to 7). The figures represent the combined (Zn + Mg) content.

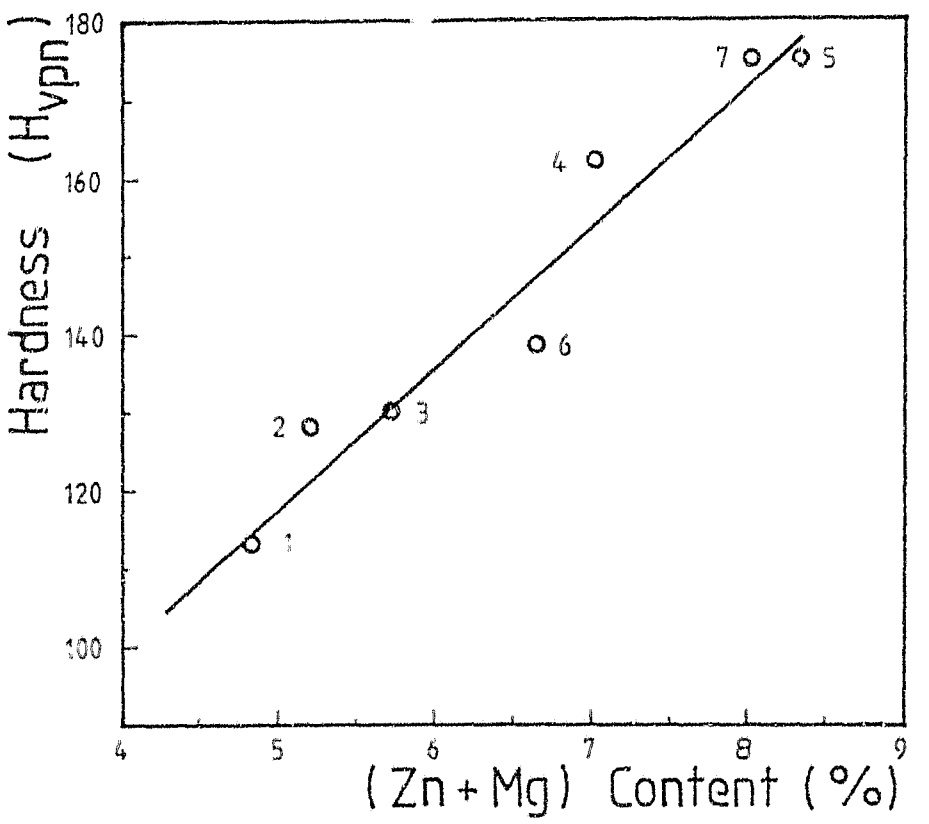


Figure 2.12 The effect of (Zn + Mg) content on hardness properties

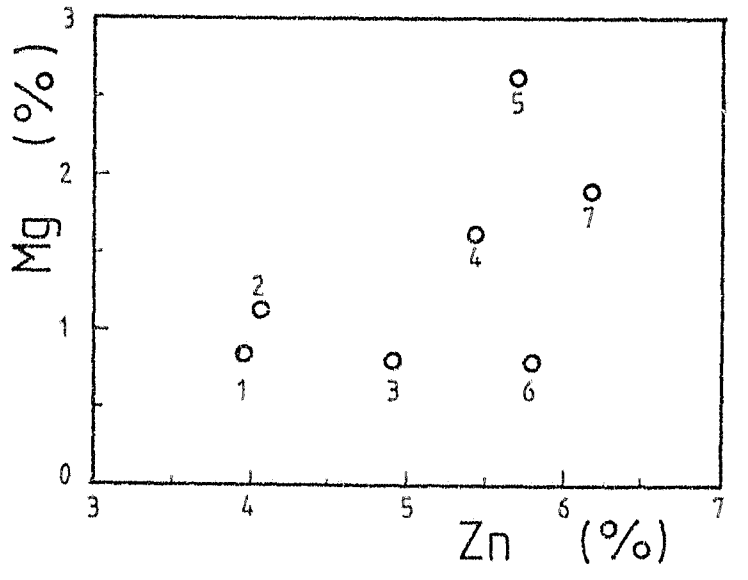


Figure 2.13 Zn and Mg contents of the experimental alloys (1 to 7)

Increasing the (Zn + Mg) content also accelerates the age-hardening kinetics. The time required to reach the peak-aged (T6) condition in the 7 experimental alloys is plotted against the (Zn + Mg) content in Figure 2.14. Within the range of alloys tested, these results do not appear to be as sensitive to the Zn : Mg ratio as were the tensile properties. An important observation is the difference in final ageing time of approximately 11 hours required to peak-age alloys 1 and 7, which is of considerable commercial importance.

ii) Effect of Cr, Zr and Mn on Recrystallisation

The relative effects of small additions of Cr, Zr, (Cr + Zr) and Mn on recrystallisation prior to, and after solution heat treatment at 3 different temperatures were determined. The extent of recrystallisation was recorded as none (0 - 10%), partial (10 - 60%) and complete (60 - 100%), and the results are shown in Table IV.

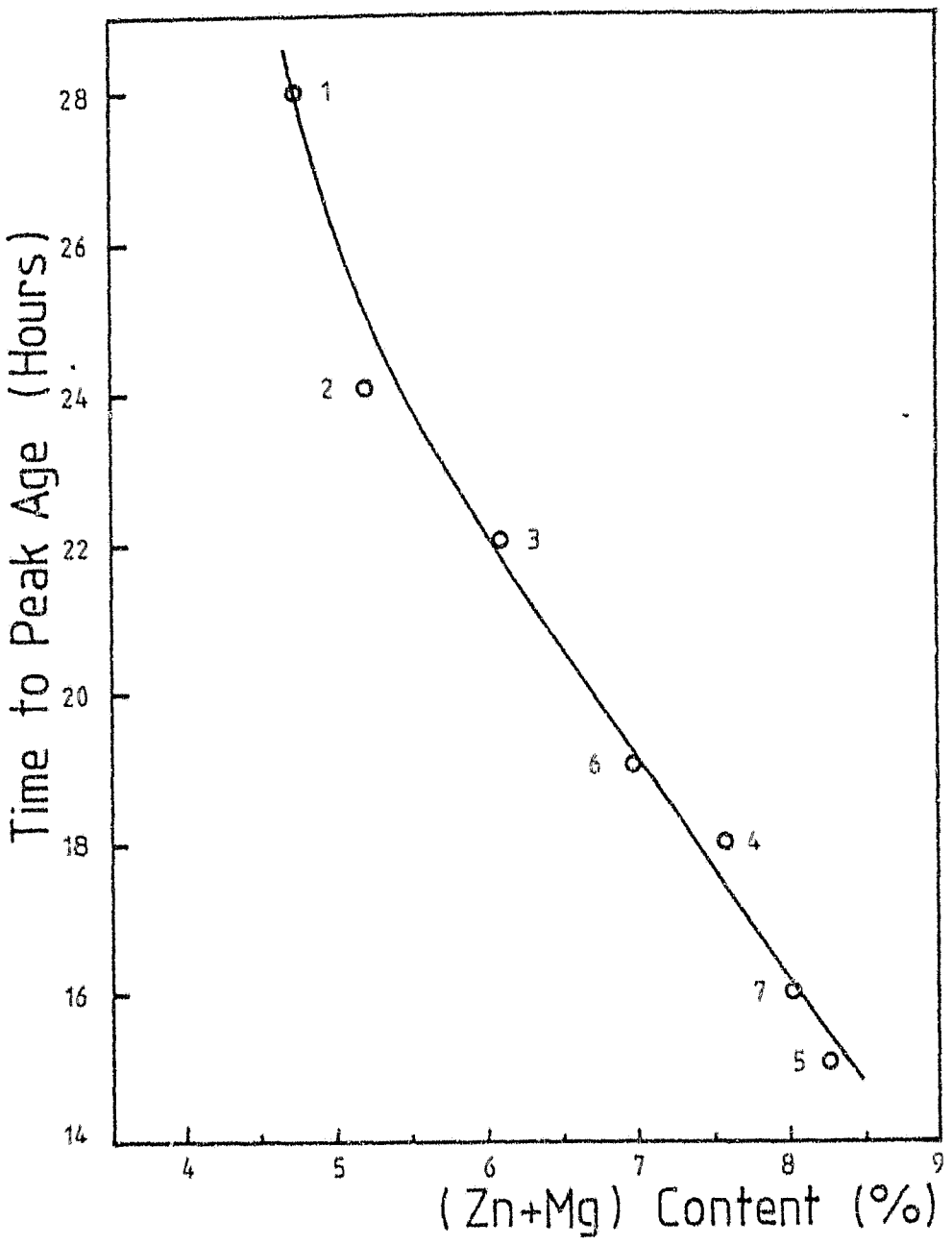


Figure 2.14 The effect of the (Zn + Mg) content on final ageing time required to peak (T6) age

Table IV: Extent of Recrystallisation

Alloy	Addition	As Rolled	Solution Heat Treatment 420°C	460°C	500°C
8	0.19 Cr	Partial	Partial	Complete	Complete
9	0.16 Zr	None	None	Partial	Partial
10	0.19 Cr + 0.18 Zr	None	None	None	Partial
11	0.35 Mn	None	None	None	Partial

From the results for alloys 8 and 9 it would appear that alloy 9 is more resistant to recrystallisation during hot working and subsequent heat treatment. As these alloys contain similar levels of Cr and Zr, respectively, it is clear that a Zr addition offers a greater resistance to recrystallisation. In the above study, the low rate of heating to homogenisation (0.014 $K.s^{-1}$) required to obtain an optimum fine Zr-precipitate dispersion was not employed. Improved inhibition of recrystallisation should therefore be expected from a Zr-addition using the required heating rate. Nevertheless, Zr still appears to be a potentially more effective addition than Cr.

The combined addition (Cr + Zr) in alloy 10 offers even greater resistance to recrystallisation.

Similar results were obtained using a single large Mn (0.35%) addition (alloy 11). The Mn-addition was evaluated as it has the least effect on SCC properties (See Figure 2.7; Section 2.2.2 (ii)). Base Al-Zn-Mg alloy compositions can therefore be assessed for susceptibility to SCC, without the complicating effects of Cr, Cu and Zr in an unrecrystallised grain structure. Such an evaluation will be reported in Chapter 4.

iii) Metallographic Investigation of a Representative Al-Zn-Mg Alloy

The characteristic coarse intermetallic precipitates found in commercial purity alloys were examined using SEM. These particles lead to reduced toughness and fatigue properties. Typical precipitates found in D74S are shown in Figures 2.15 to 2.17 (at increasing magnificatcns). The final figure clearly shows the remnants of a "Chinese script morphology". The coarse, intermetallic phases develop from components of the alloy (Fe, Mn, Si, Cu, Al and Mg) which are soluble in the liquid state but precipitate out on solidification. The aligned distribution of fragmented particles develops during hot working (rolling) of the ingot. X-ray mapping (using the EDS attachment) revealed that the particles were predominantly Fe-rich compounds. The typical

constituents of the coarse particles can be seen in the X-ray spectrum: Figure 2.18. Although Fe and Mn form the principal X-ray peaks from the precipitates, small traces of Si and Cu were also detected.

There was also frequent evidence of porosity (Figure 2.19). This is thought to nucleate on intermetallic precipitates. Support for this hypothesis is given by an Fe X-ray map of this area (Figure 2.20), which reveals high local Fe content on the cavity walls.

A fine dispersion of Ti-rich particles has also been observed (for example in the upper portion of Figure 2.21). The X-ray spectrum obtained from these particles is presented in Figure 2.22.

(A refinement of the intermetallic precipitates may be obtained by maximising the solidification rate on casting. Control of shrinkage and gas porosity (due to hydrogen) can be achieved by encouraging directional solidification (with sufficient feeding) and controlling the hydrogen content of the melt).

The hot-worked grain structure of D74S plate was examined in the optical microscope. It is clear (by comparing Figures 2.23 to 2.25) that the degree of working, (produced by hot rolling) decreases

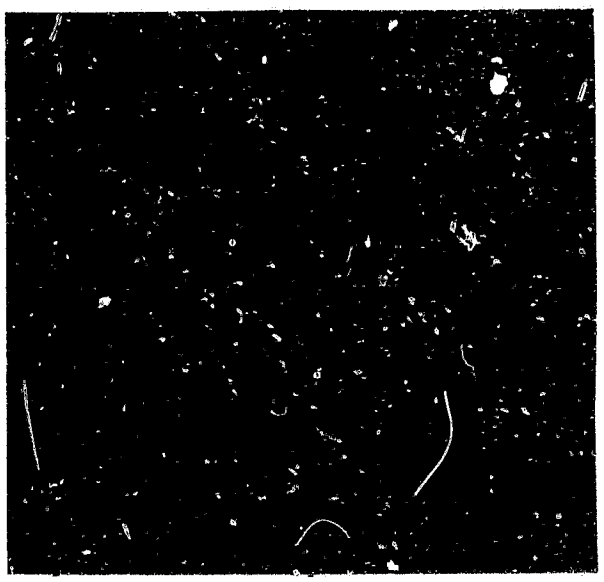


Figure 2.15 SEM micrograph showing intermetallic constituents

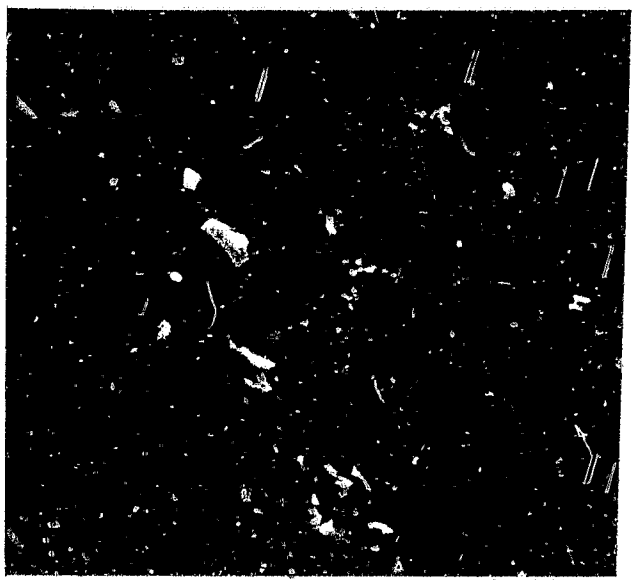


Figure 2.16 SEM micrograph showing intermetallic constituents

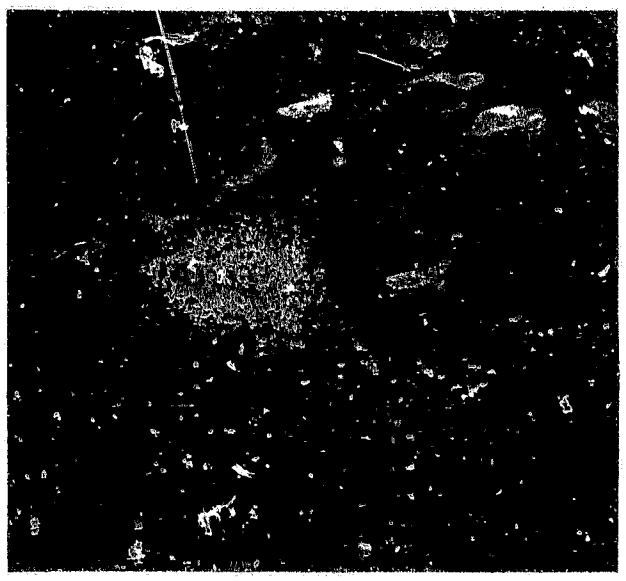


Figure 2.17 SEM micrograph showing intermetallic constituents

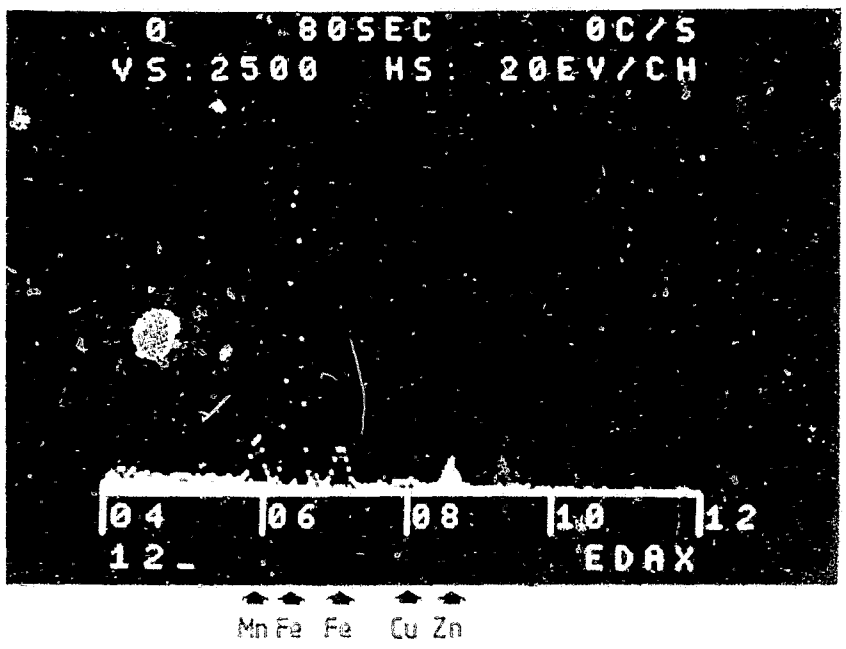


Figure 2.18 X-ray spectrum of intermetallic constituents (dotted) shown in comparison to the general background matrix (continuous white lines)

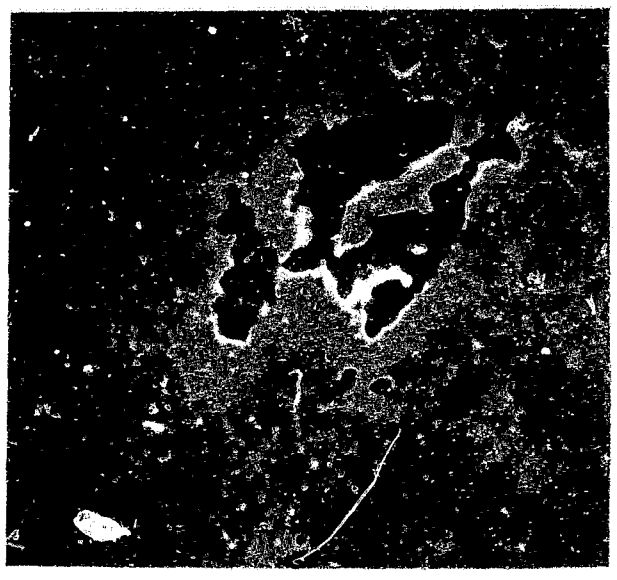


Figure 2.19 Porosity in D 74 S plate

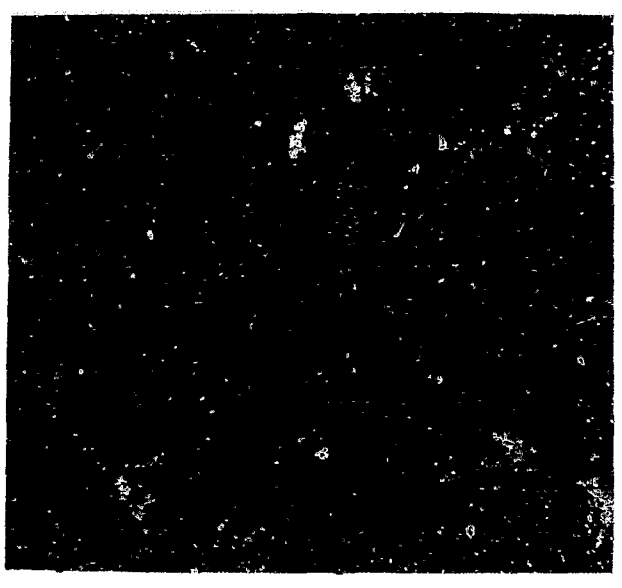


Figure 2.20 Fe-X-ray map of porosity shown in Figure 2.19

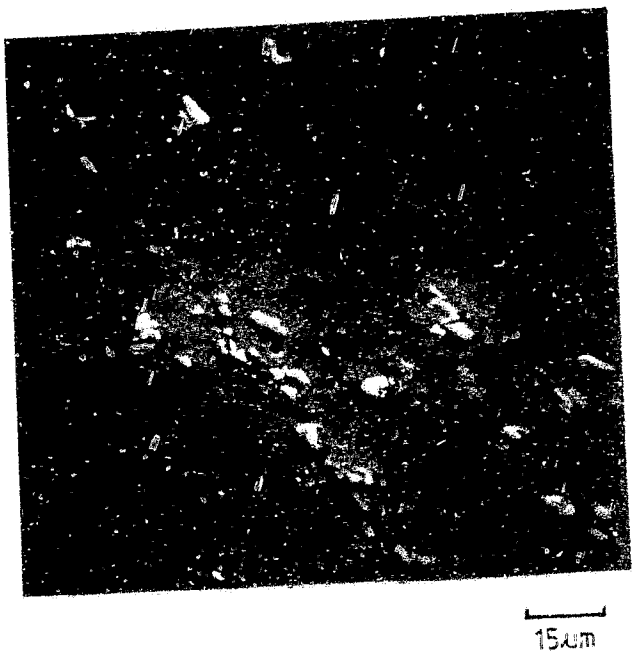


Figure 2.21 Fine Ti-rich particles visible in upper portion of micrograph

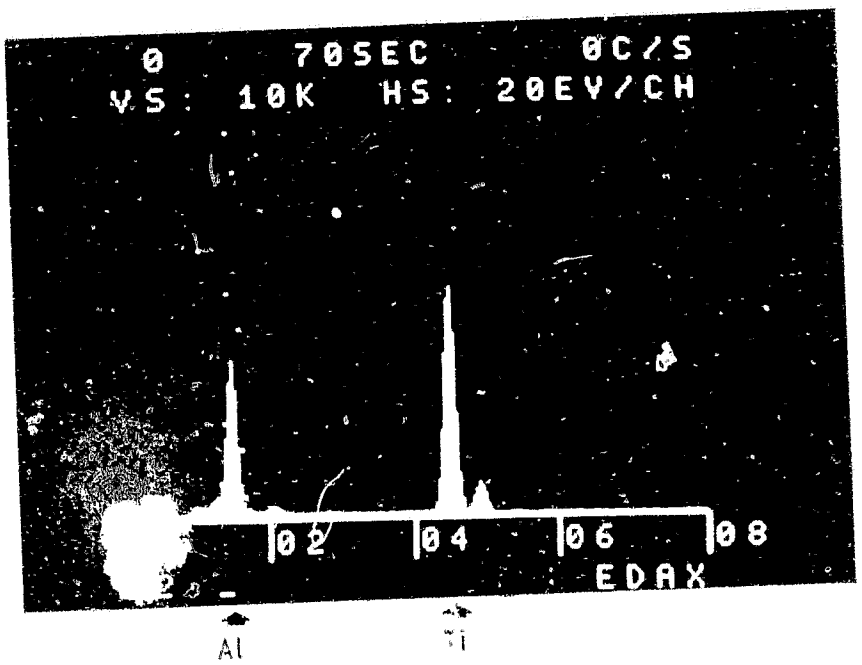


Figure 2.22 X-ray spectrum of Ti-rich particles (solid white lines) shown in comparison with general background matrix (dotted)



Figure 2.23
Macro-grain structure in transverse section near rolling surface

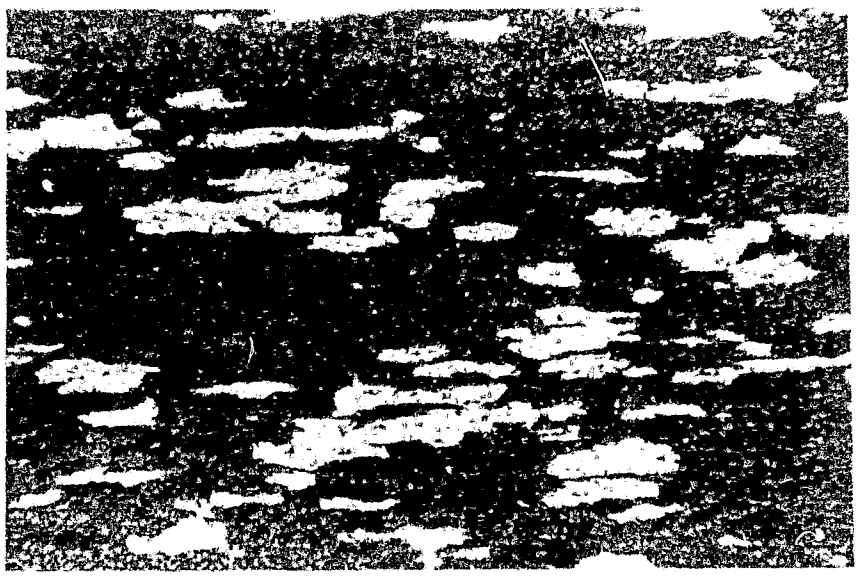


Figure 2.24
Macro-grain structure in transverse section mid way to centre



Figure 2.25
Macro-grain structure in transverse section centre of plate

markedly in the transverse section from the surface to the centre of the plate. The average measured macro-grain sizes are summarised in Table V.

Table V: Macro-grain Sizes of As-received Hot-rolled D74S Plate

Average longitudinal length:	250μm
Average long transverse width:	
1) rolled surface	80μm
2) midway to centre	90
3) centre of plate	100
Average short transverse width:	
1) rolled surface	20μm
2) midway to centre	30
3) centre of plate	50

2.2.6 Conclusions

i) Increasing the (Zn + Mg) content of Al-Zn-Mg alloys increases the hardness, and therefore tensile strength. Simple calculations suggest that Mg is approximately 40% more effective as a hardening agent than Zn.

ii) Increasing the (Zn + Mg) content also accelerates the age hardening kinetics.

iii) In an Al-5.3 Zn-0.8Mg alloy, combined additions of (0.19% Cr + 0.18% Zr) provides superior inhibition of recrystallisation than 0.19% Cr or 0.16% Zr alone. An equivalent effect can, however, be obtained using 0.35% Mn.

iv) The characteristic coarse intermetallic precipitates in D74S are predominantly Fe-rich compounds.

v) The degree of working varies through the transverse section of hot-rolled D74S plate, leading to variations in the unrecrystallised grain size.

2.3 Precipitation Sequences and Microstructure of Al-Zn-Mg Alloys

2.3.1 Decomposition of Al-Zn-Mg Supersaturated Solid Solutions

The manipulation of structure, to obtain superior properties, by thermal or thermomechanical treatments requires an understanding of the formation of the hardening dispersion of (Zn, Mg) particles in Al-Zn-Mg alloys. Many investigations have been addressed not only to the morphology and structure of precipitates, but also to their nucleation behaviour[25-29]. Nucleation

of precipitates is of special importance in Al-Zn-Mg alloys relating to the problems associated with the precipitate free zone (PFZ), and the use of a two-step ageing treatment.

The general precipitation sequence of Al-Zn-Mg alloys from a supersaturated solid solution (SSSS) is :

SSSS

↓

GP zones, spherical (~ 5nm dia). Coherent

↓

η' ($MgZn_2$) hexagonal

↓ Partially coherent

η ($MgZn_2$) hexagonal

↓

T ($Al_2Mg_3Zn_3$) b.c.c Incoherent

In commercial practice, in addition to the existing GP zones, the relatively high final ageing treatment leads to the formation of an η' (and η in the overaged condition) hardening dispersion. However, their development is influenced by the GP zones already formed during the low temperature natural- and pre-age treatments. Thus, an understanding of the initial decomposition of the solid solution is important.

In an Al-5Zn-2Mg alloy, T_{limit}, the temperature limit for GP zone formation (that is, the highest temperature at which GP zones can form) has been determined to be

125°C[26]. GP zones are formed immediately after the alloy is brought to a temperature lower than T_{limit}.

GP zone formation in a high purity Al-4.8Zn-1.2Mg alloy, aged for 24 hours between ambient temperature and 80°C, has been studied by Ungar[27]. Guinier plots of X-ray small angle scattering (XSAS) intensity distribution curves are reproduced in Figure 2.26.

In the range 20 - 60°C, the Guinier plots exhibit single straight sections (apart from low angle interparticle interference effects). Above 60°C the Guinier plots split into two straight sections indicating the presence of two groups of non-identical particles. The above findings have been confirmed by calorimetric investigations[30]. Guinier radii were also determined and these results are shown in Figure 2.27. The two different particle radii are denoted by R_{G1} and R_{G2}.

In this alloy, therefore, below 100°C a supersaturated solid solution decomposes to form GP 1 or (GP 1 + GP 2) zones. The two zones developed between 60 and 100°C have different radii and thermal stabilities. The GP 1 zones are smaller and less stable than GP 2, and the former are also produced below 60°C. Both zones are coherent with the matrix, and possess the same crystal structure.

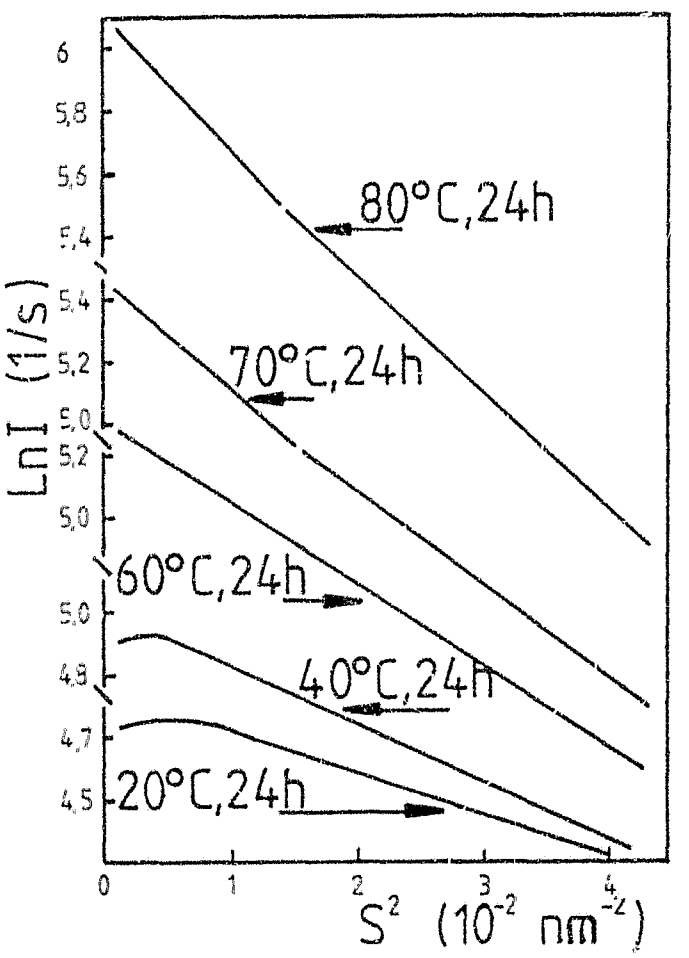


Figure 2.26 Guinier plots of samples aged for 24 h between 20°C and 80°C.

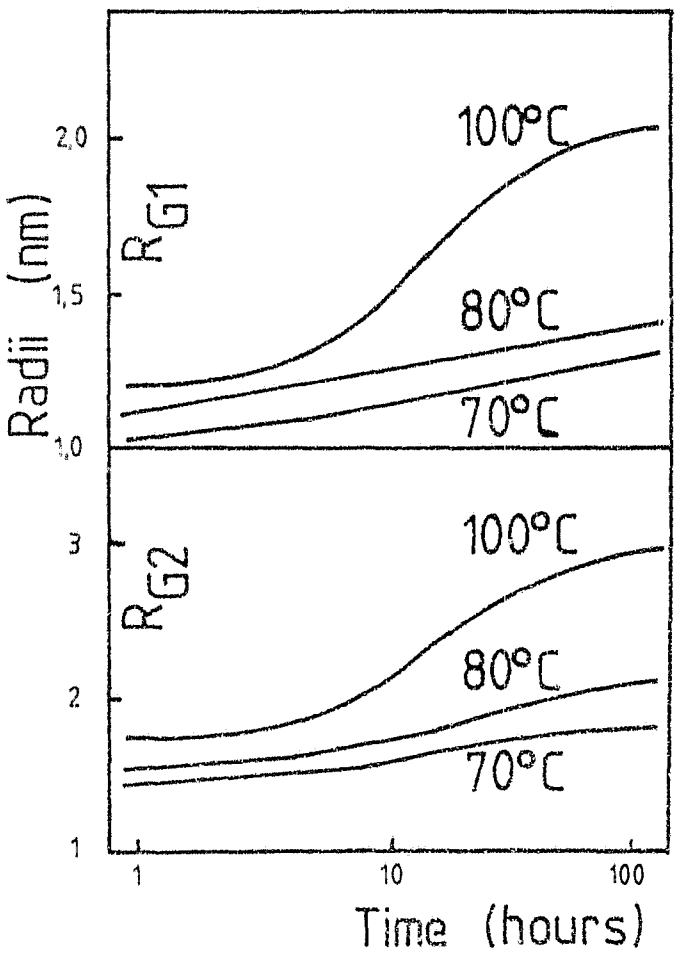


Figure 2.27 The Guinier radii, R_{G1} and R_{G2} of the two different types of G P zones as a function of ageing time at 70, 80 and 100°C

It is also clear, from Figure 2.27, that there is a rapid increase in the size of both R_{G1} and R_{G2} after 10 hours at 100°C. Ungar[27] proposed that decomposition started with the formation of GP 1 and GP 2 zones, but that the final product was a mixture of GP 2 and η' . The zone and particle formation is summarised in Figure 2.28. Three ranges of Guinier radii were specified:

$R_G < 1.3$ nm represent GP 1 zones;

$1.3 \text{ nm} \leq R_G \leq 1.9$ nm, GP 2 zones; and

$R_G > 1.9$ nm represent η' precipitates.

The determination of integral intensity ratios showed that at 70°C the formation of GP 1 and GP 2 zones takes place montonically for up to 100 hours. AT 80°C, the formation of GP 1 saturates after 14 hours, but GP 2 zones are enhanced after the same period. At 100°C, there is a transition of the zones to the GP 2 type and the formation of η' particles after 10 hours. Above 120°C, it appears that decomposition is governed only by the formation of the intermediate η' phase.

In aged structures the greatest contribution to hardening is provided by the partially coherent, intermediate phase, η' . GP zone dispersions exert the second largest effect, while the incoherent equilibrium phase, η , has very little influence on hardness[26,31].

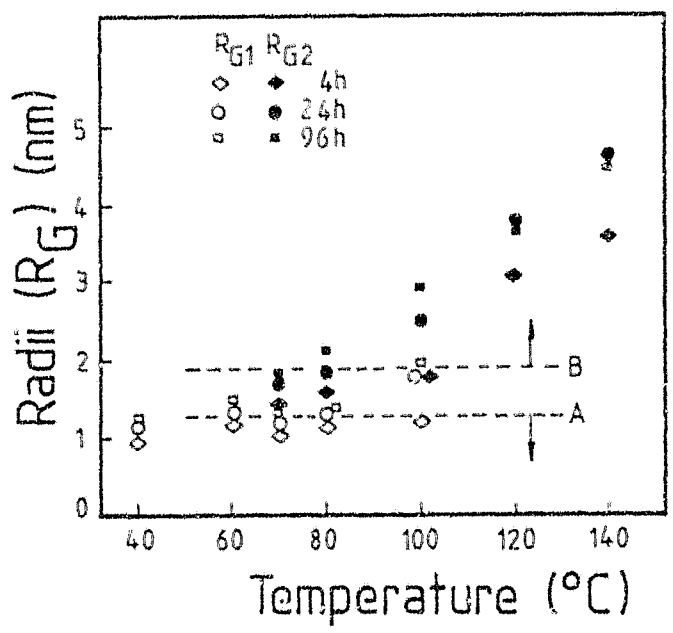


Figure 2.28 The Guinier radii as a function of temperature between 40 and 140°C at three different ageing periods. The dashed lines, A and B, separate ranges of Guinier radii corresponding to different types of particles

Peak mechancial properties are therefore achieved in alloys containing a duplex GP zone and η' -particle dispersion which is usually produced using a two-stage ageing treatment[32,33]. GP zone formation is obtained using a low temperature pre-age (below 100°C) while the η' -phase is formed in the final age at higher temperatures.

Degischer, et al.[28] have confirmed that the formation of the η' -phase is limited to ageing temperatures in the approximate range 100 to 200°C. They have suggested that GP zones form nucleation sites for the subsequent metastable η' precipitates. In addition, vacancy-rich clusters could also provide nucleation sites[34].

For longer ageing times (depending on temperature), the formation of a variety of η -particles has been observed[28]. These particles may be precipitated directly from the SSSS, or may form from existing η' particles. Depending on the type of η -phase, nucleation in distorted regions of the matrix may also occur. η particles may be considered the dominant "stable" precipitate for ageing temperatures from ambient to 200°C. The equilibrium cubic T-phase generally forms from η particles at higher ageing temperatures. However, it may be precipitated on grain boundaries at lower temperatures.

2.3.2 Microstructural Aspects of Wrought Al-Zn-Mg Alloys

Al-Zn-Mg ingots exhibit a characteristic cast grain structure, developed from heavily cored dendrites. The dendrite boundaries usually contain a constituent-particle network of soluble and insoluble phases. The scale of this structure is directly related to the solidification rate : the microstructure becoming finer as this rate increases.

During subsequent fabrication, the alloy is first homogenised and then hot worked. Homogenisation, at a relatively high temperature, serves to reduce or eliminate coring of the solid solution, increase the alloy content by dissolving constituents, and to precipitate the transition element dispersions. The plastic deformation during hot working distorts and fragments the grain structure, fracturing and redistributing the constituents. Recrystallisation is usually avoided by controlling hot working parameters and the addition of minor alloying elements. This leads to the development of a fibrous grain structure, which is less susceptible to SCC. Hot rolling produces a characteristic texture due to the alignment of grains in the direction of rolling.

The plastic strain introduced during working also influences the subsequent ageing behaviour. The high dislocation density induced in the material exerts two

major influences[35]. Firstly, the migration of vacancies to sinks (such as grain boundaries) is accelerated, thereby reducing GP zone formation. Secondly, there is a marked increase in the number of preferential nucleation sites (dislocation substructures and sub-boundaries) on which metastable or equilibrium phases can nucleate and rapidly grow during subsequent ageing.

Hot working involves deformation at temperatures above $0.5T_m$ (the absolute melting temperature). In this regime, vacancy-assisted dislocation climb leads to dynamic recovery, and a resultant polygonised substructure[36]. During the initial strain-hardening phase, dislocations accumulate in regular tangles and sub-boundaries. The latter are equiaxed and relatively stable, persisting through further steady-state deformation without change in size or wall density (in the transverse direction). (In commercial practice steady-state deformation conditions are not achieved. However, the resulting substructure is not markedly different).

In the rolling direction the grain structure is elongated. Recrystallisation is inhibited by the existing precipitate dispersion. Thus the alloy sub-structure is maintained, leading to the early heterogeneous nucleaton of hardening precipitates, without GP zone formation, on ageing. The concentration of these precipitates on sub-boundaries, rather than the development of a homogeneous dispersion, reduces the maximum attainable strength of the alloy.

major influences[35]. Firstly, the migration of vacancies to sinks (such as grain boundaries) is accelerated, thereby reducing GP zone formation. Secondly, there is a marked increase in the number of preferential nucleation sites (dislocation substructures and sub-boundaries) on which metastable or equilibrium phases can nucleate and rapidly grow during subsequent ageing.

Hot working involves deformation at temperatures above $0.5T_m$ (the absolute melting temperature). In this regime, vacancy-assisted dislocation climb leads to dynamic recovery, and a resultant polygonised substructure[36]. During the initial strain-hardening phase, dislocations accumulate in regular tangles and sub-boundaries. The latter are equiaxed and relatively stable, persisting through further steady-state deformation without change in size or wall density (in the transverse direction). (In commercial practice steady-state deformation conditions are not achieved. However, the resulting substructure is not markedly different).

In the rolling direction the grain structure is elongated. Recrystallisation is inhibited by the existing precipitate dispersion. Thus the alloy sub-structure is maintained, leading to the early heterogeneous nucleaton of hardening precipitates, without GP zone formation, on ageing. The concentration of these precipitates on sub-boundaries, rather than the development of a homogeneous dispersion, reduces the maximum attainable strength of the alloy.

The final heat-treated microstructure of Al-Zn-Mg alloys is characterised by a dense matrix precipitate of η' and η ($MgZn_2$) and coarse grain (and sub-grain) boundary precipitates with adjacent precipitate free zones (PFZ). SCC resistance and intergranular fracture are largely dependant on the grain boundary structure, grain boundary precipitates and the nature of the associated PFZ[1].

i) Grain Boundary Structure

In peak- or over-aged structures, heterogeneous precipitation on grain boundaries reduces strength and ductility. Van der Walker and Van der Sande[37] have attempted to relate the growth kinetics of boundary precipitates to the nature of low angle boundaries in high strength alloys. They found that the geometry of the dislocation configurations in these boundaries influenced both the shape and size of precipitates. In partially recovered Al-Zn-Mg alloys, two types of low-angle boundary were formed: planar and non-planar. In the former equiaxed and lath-shaped precipitates developed, while in the latter, only lath-shaped precipitates were observed.

Gronsky and Furrer[38] have also undertaken a study of heterogeneous nucleation sites and preferred growth centres with respect to boundary structure. In general grain boundaries, discrete precipitates

were observed, with a tendency to align along <110>. These grain boundary precipitates had a hemispherical cap morphology, which implies preferential growth into one adjacent grain. Low angle grain boundaries and sub-boundaries were also found to catalyse precipitation.

Random precipitation was never observed on grain boundaries. High resolution CTEM always gave indications of structural discontinuities dominating nucleation. For example, in highly ordered boundaries, extrinsic dislocations were invariably in contact with boundary precipitates; and at exact coincidence site lattice orientations, nucleation took place at sites of deviation. Thus, it was suggested that grain boundaries themselves are not heterogeneous nucleation sites, but play a role in supplying heterogeneities for precipitation.

The observed ordered arrays of precipitates implied the preference for a habit-plane relationship with one of the parent grains (in this case, the close-packed matrix plane). Suitable favourable orientations of close-packed planes can be produced by networks of ledges arising from intrinsic grain boundary dislocations. It should therefore be possible to suppress grain boundary precipitation by decreasing the mobility of dislocations in the boundary plane.

In summary, precipitate formation on grain boundaries is strongly dependant on grain boundary structure, particularly on homogeneities produced by defects. The grain boundary should not therefore be considered merely as a disordered transition region.

It should also be noted here that a fine recrystallised grain structure should be avoided. Heterogeneous precipitation on the resultant high-angle boundaries during cooling will lead to much greater quench sensitivity. The low angle sub-grain boundaries of fibrous structures will have a much smaller effect[39].

ii) Precipitate Free Zones

The nature of the PFZ and the SCC susceptibility are both influenced by heat treatment. A considerable amount of work has therefore been undertaken in attempts to link changes in SCC properties to variations in the PFZ[1,40]. The existence of such a correlation is further supported by the intergranular nature of SCC. A more detailed consideration of the PFZ is therefore warranted.

A simple model for PFZ formation, schematically illustrated by Raghavan[41], is shown in Figure 2.29. After quenching from solution heat treatment, a

characteristic vacancy profile develops adjacent to grain boundaries (which act as vacancy sinks). Assuming a critical vacancy concentration is required for the nucleation of GP zones during ageing, then a PFZ will be formed around the boundary. On further ageing it is apparent that GP zones provide nucleation sites for η' and η precipitates. The absence of GP zones in the PFZ, therefore, also precludes the formation of η' in this region.

The influence of solution temperature, quench rate and ageing temperature are shown in Figure 2.30 (from ref. 25). The precipitate free zone widths depicted in the Figure are (a) solution treated at 510°C, water quenched, aged at 135°C, (b) solution treated at 510°C, water quenched, aged at 180°C, (c) solution treated at 465°C, water quenched, aged at 180°C, and (d) solution treated at 465°C, oil quenched, aged at 180°C.

It can be seen that the width of the PFZ can be decreased by increasing the solution treatment temperature and quench rate, and by decreasing the ageing temperature. There is much conflicting evidence in the literature concerning the effects of ageing time on PFZ width. It will be demonstrated, in Section 2.4, that using a two-stage ageing treatment, the PFZ width does increase for longer ageing times.

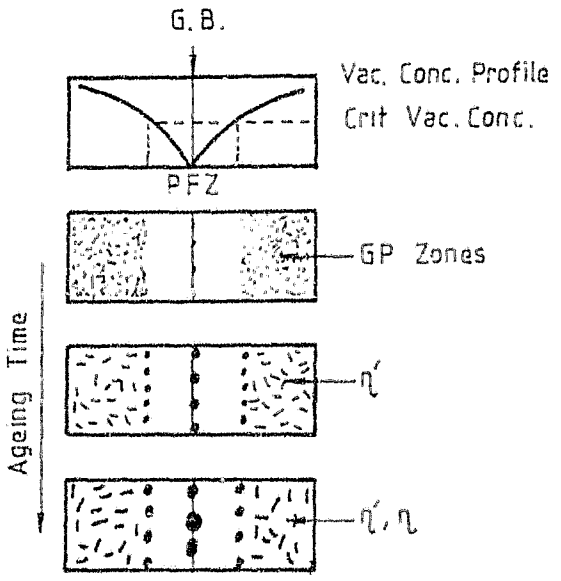


Figure 2.29 Schematic illustration of the formation of the PFZ in Al-Zn-Mg alloys

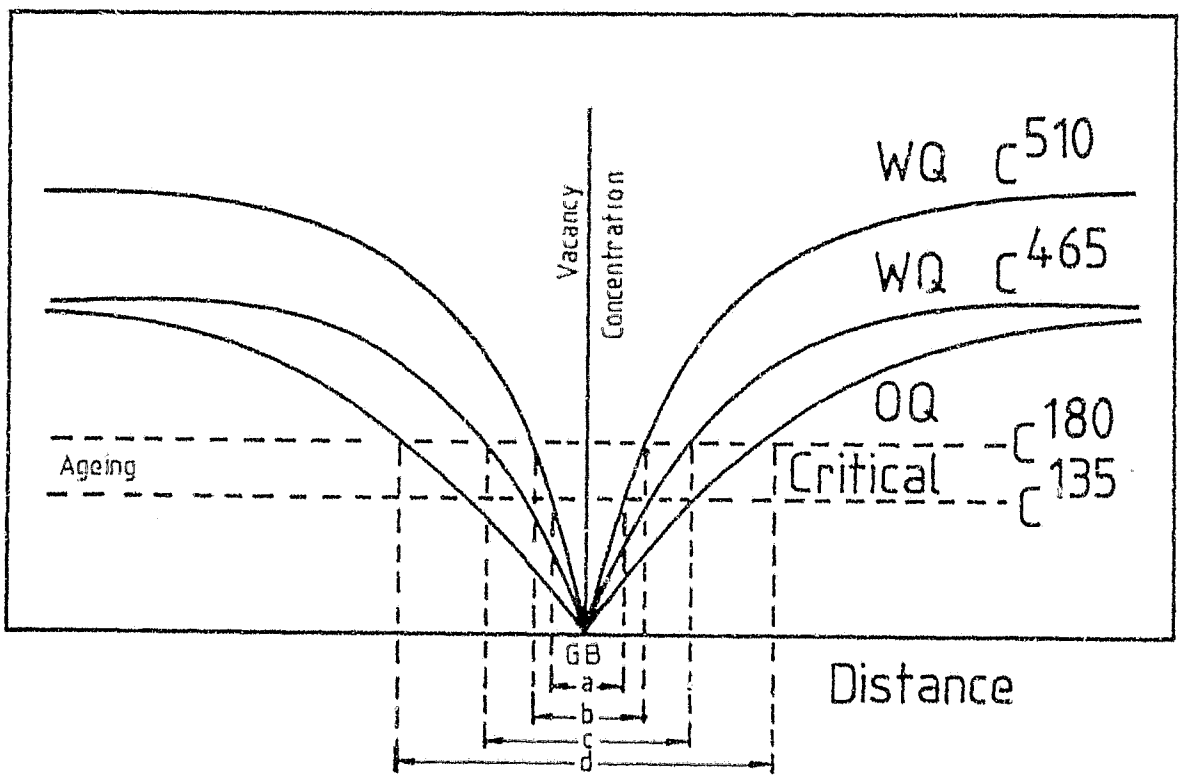


Figure 2.30 A comparison of the vacancy concentration profiles for various solution treatment, quenching and ageing conditions (see text)

It has also been shown that the PFZ is still supersaturated with respect to Zn and Mg[25,40]. This has been confirmed by applying 10% further room temperature deformation to quenched and aged alloys, and re-ageing[40]. Heterogeneous nucleation of η on the induced defects led to a reduced PFZ width. This could only occur if the zone had remained supersaturated with Zn and Mg.

iii) Solute Distribution in the PFZ

With regard to the SCC properties of Al-Zn-Mg alloys, in addition to the extent of the PFZ, the solute distribution within the PFZ is of major importance. It has been shown[41,42,43,44,45] that on ageing, Zn and Mg segregate to the grain boundaries. As the grain boundary and matrix precipitates coarsen, the solute concentrations peak in the PFZ and decrease in both the directions of the matrix and grain boundary[41] (Figure 2.31).

Only after very long ageing times (∿ 75 hours) at high ageing temperatures (∿ 200°C) does the solute concentration of the matrix become uniform across the PFZ. It should be noted that although there is initially a solute gradient running to the grain boundary, the boundary itself does not increase in solute because diffusion along the boundary is faster than matrix diffusion and the solute is therefore quickly incorporated into grain boundary precipitates.

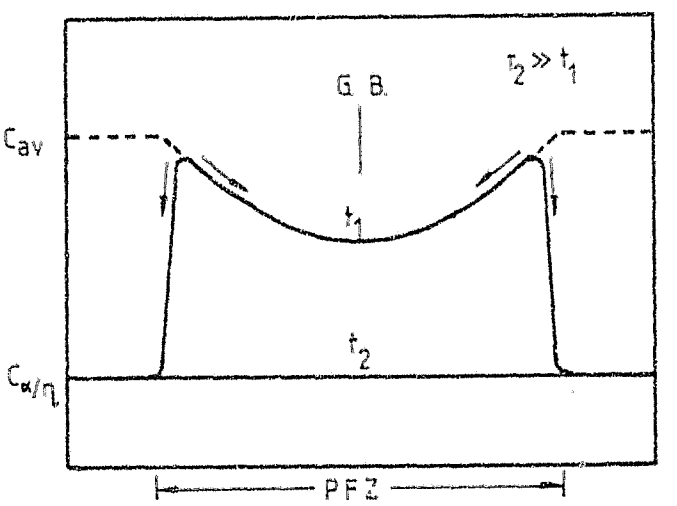


Figure 2.31 Schematic matrix solute concentration across a grain boundary for short ageing times ($t = t_1$) and long ageing times ($t = t_2$). Diffusion of solute during short ageing times is indicated by arrows. C_{av} is the average solute concentration of the alloy and $C_{\alpha/\eta}$ is the matrix concentration in equilibrium with the η precipitate

In addition to the above segregation which occurs during ageing, a further mode operates during solution heat treatment[42]. The physical basis of this segregation depends on vacancy flow during solution treatment and quenching. Anthony[46] found that:

1) reverse atom flow occurs as a consequence of vacancy flow, and
2) solute drag effects are induced by vacancies.

As the binding energies between Zn and vacancies, and particularly Mg and vacancies, are higher than kT, Mg and Zn are dragged to the grain boundaries. Assuming the solute and vacancy gradients were linear, the following equation was derived for the relative spatial extent of the two gradients

$$L_B = \left(\frac{C_V}{C_B^2 K}\right) L_V$$

where L_B and L_V are the extents of solute-enriched and vacancy-depleted regions near vacancy sinks;

C_B and C_V, the solute and vacancy concentrations; and

$$K = Z \exp. \left(\frac{B}{kT}\right)$$

In the expression for K, Z is the coordination number, and B, the solute binding energy.

It is clear that even if long range vacancy gradients develop during quenching, the solute-enriched regions near grain boundaries are still small, that is $L_B << L_V$. Embury and Nicholson[25] estimated that the extent of the solute-enriched region was approximately 3nm. This is in reasonable agreement with experimental values of 5 - 10nm.

The nucleation and growth of precipitates on grain boundaries is considerably influenced by the amount of Zn and Mg segregated to the grain boundary. According to Viswanadham, et al.[42], all the Zn is incorporated into the grain boundary precipitates, but excess Mg remains on the boundary situated between the precipitates. The amount of "free Mg" will depend on:

1) the level of solute segregation during the quench; and
2) the nucleation and initial growth rate of the precipitates, which depend on the nature of the grain boundary (as discussed in (i) above).

It was claimed that this Mg plays a role in the determination of the SCC properties of the alloy. This argument will be pursued further in Chapter 3, which deals with the mechanisms of SCC.

The aim of the following experimental sections is to describe the methodology and results of a transmission electron microscopy (CTEM) investigation of the microstructure of a representative Al-Zn-Mg alloy. The information gained was intended to provide a comparative basis for further extensive CTEM studies from which it was hoped to reveal a relationship between susceptibility to SCC and a variation of some microstructural feature.

2.3.3 Experimental Procedure

The wrought Al-Zn-Mg alloy studied was D74S, supplied by Hulett Aluminium Limited as 12mm plate. The nominal composition is given in the Appendix. This material was examined in the F (slow air-cooled after hot rolling), T6 and T7 conditions. The heat treatment of the latter two tempers were as follows:

1) solution heat treatment : (465^{o}C/2 hours, water quench);
2) natural age : (25^{o}C/2 weeks);
3) pre-age : (90^{o}C/7 hours); and
4) final age : (135^{o}C/16 hours for T6) and (160^{o}C/48 hours for T7)

Thus T6 and T7 represent the peak and overaged conditions.

Thin foils for transmission electron microscopy were prepared from 3mm diameter rods machined from heat treated plate. 0.2mm thick discs cut from these rods were mechanically ground prior to final thinning in a Struers twin-jet electropolisher. A 30% nitric acid, 70% methanol electrolyte was used at -20°C, with an applied potential of 6 - 8V.

Foil were viewed in a JEOL - 100C microscope (equipped with a single tilt goniometer stage), operating at 100kV. The microstructure and the precipitate morphology, distribution and crystal structure were studied using bright field (BF), centred dark field (CDF) and selected area diffraction (SAD) modes of operation.

2.3.4 Experimental Results

The characteristic structure of the alloy in the F condition is shown in Figure 2.32 (a, b). The main alloying additions (Zn and Mg) have to a large extent precipitated out during the slow cool. Copious precipitation of coarse η and T phases is evident both in the matrix and on grain, and sub-grain, boundaries. These figures also reveal the plate-like morphology of the particles. This can be seen more clearly at high magnifications (Figure 2.33). (It should be noted that featureless white areas appear in the BF images, due to the etching out of precipitates: a common problem in electrolytic thinning of Al alloys).

Despite the high volume fraction of precipitates, sufficient Zn and Mg must remain in solid solution to give rise to the very fine matrix particle dispersion, which can be seen in Figure 2.33. This arises from natural ageing of the material during several months storage at ambient temperatures. Given the ageing sequence discussed in Section 2.4.4, this dispersion could consist of GP zones and/or η'.

In the solution treated and artificially aged temper conditions, the deformation-induced substructure is still clearly visible (Figure 2.34 and 2.35). It can be seen that the sub-grain structure is equiaxed in the transverse section, but elongated in the direction of rolling. Heterogeneous nucleation on these sub-boundaries produces some apparently continuous layers of precipitation delineating the grains. At higher magnifications (Figures 2.36 to 2.38), however, individual boundary precipitates can be resolved. In these Figures, there is also evidence of fine precipitate formation on dislocations, both in the matrix and cell walls. PFZ's are also visible.

Further typical examples of PFZ's associated with coarse grain boundary precipitates are shown for the peak-aged and overaged conditions in Figures 2.39 and 2.40, respectively. The width of the PFZ was found to be very consistent for a given temper condition (within $\pm$ 7%). However, there was a marked increase as a result of overageing, from 38 nm (T6) to 82 nm (for the T7 temper).

The effect of overaging on the matrix precipitate distribution should also be noted by a comparison of Figures 2.39 and 2.40 (which have the same magnification). The coarse precipitates developed by overaging have lost all coherency, since there is now no evidence of any strain contrast.

These figures also reveal the hemispherical cap morphology of grain boundary precipitates, as reported by Gronsky[38], indicative of preferential growth into one grain.

The discrete nature of grain boundary precipitates and the absence of a continuous intergranular film between them can be seen by tilting boundaries through large angles in the electron microscope[38]. This effect is illustrated in Figure 2.41 (a, b). The dark boundary contrast linking the precipitates in (a) disappears on tilting through 30^{o}. Figure 2.42 shows discrete precipitates on discontinuities in a low angle boundary oriented at a high angle to the electron beam. If the same boundary were viewed parallel to the beam, it would appear to contain a continuous film of precipitate.

Several examples of precipitation on the dislocation arrays, which constitute sub-grain boundaries, have already been given. Further examples of dislocation sub-boundaries, produced by partial recovery, can be seen in Figure 2.43. The dominant boundary exhibits a typical

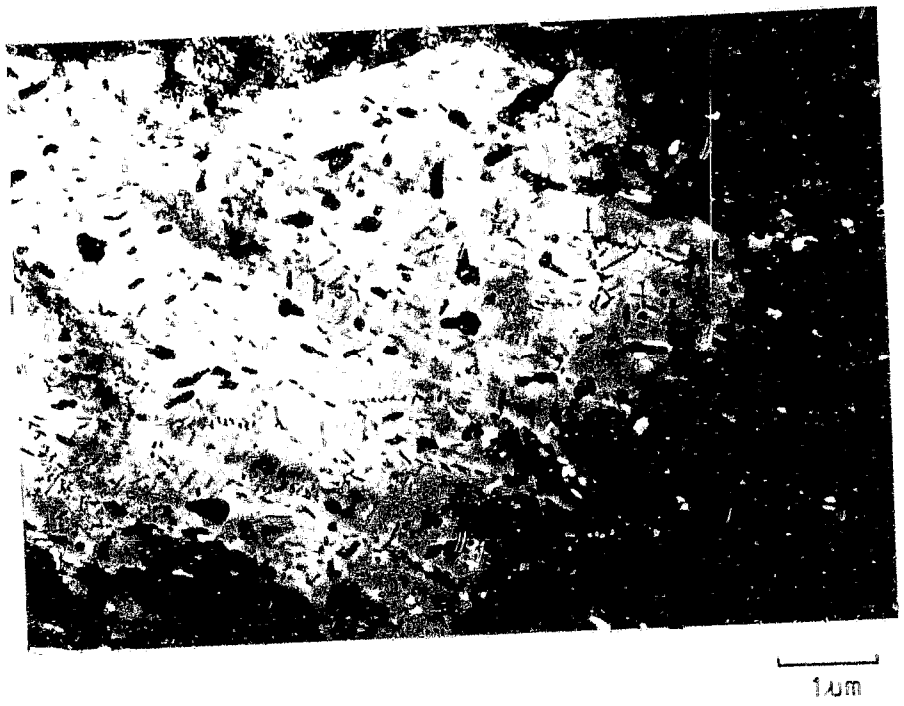
planar hexagonal dislocation array (as described by Van der Walker[37]). Precipitation on low angle boundaries is clearly evident in Figures 2.44 to 2.47.

2.3.5 Summary and Conclusions

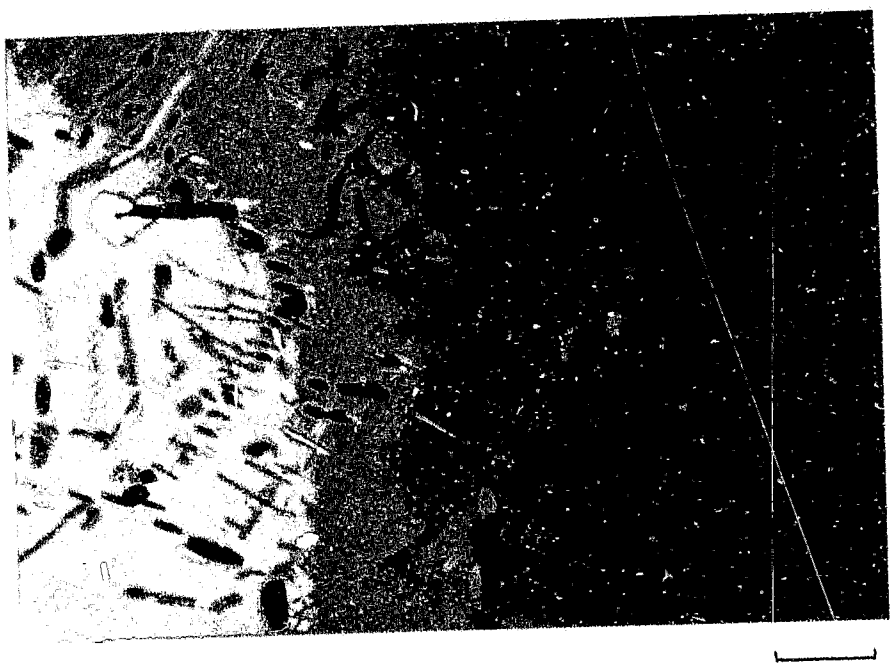
i) The decomposition of Al-Zn-Mg supersaturated solid solutions and the microstructural aspects of wrought alloys have been discussed. A structural investigation of the representative D74S alloy (in the F, T6 and T7 conditions) has been carried out using CTEM.

ii) Important microstructural features were identified. These include:

a) the deformation-induced sub-structure;
b) precipitation on dislocations in the sub-boundaries;
c) the distribution and morphology of grain boundary precipitates;
d) the PFZ (which appears to increase in width on overageing); and
e) matrix precipitation (and its coarsening with overageing).



(a)



(b)

Figure 2.32 D74S in the F condition
(BF micrographs)

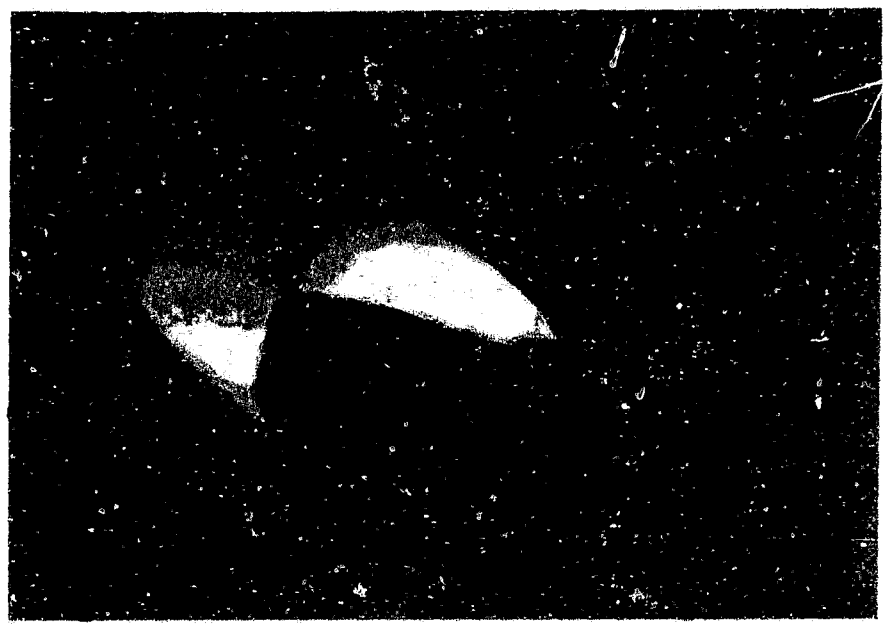


Figure 2.33 BF micrograph showing the plate-like morphology of a η particle

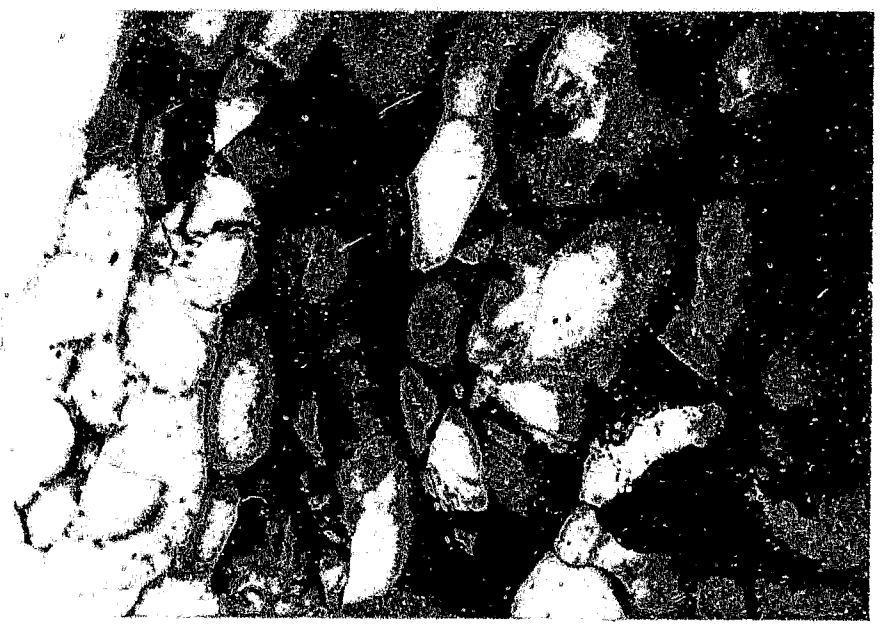


Figure 2.34 Transverse section of D74S -T6 condition (BF micrograph)



Figure 2.35 Longitudinal section of D74S -T6 condition showing elongated sub-grain structure (BF micrograph)

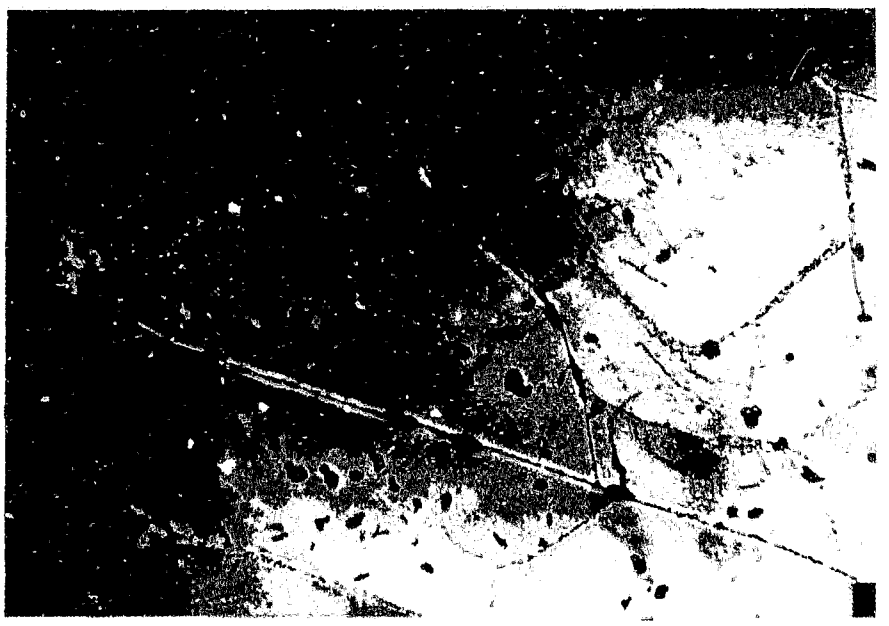


Figure 2.36 BF micrograph of D74S showing copious precipitation on grain boundaries and dislocation networks in the T6 temper.



Figure 2.37 BF micrograph showing precipitation on dislocation sub-structures in D74S - T6 temper

Figure 2.38 Morphology and distribution of grain boundary precipitates in D74S - T 6 temper (BF micrograph)



Figure 2.39 A distinct PFZ with grain boundary precipitates and copious matrix precipitation seen in D74S - T6 temper (BF micrograph)

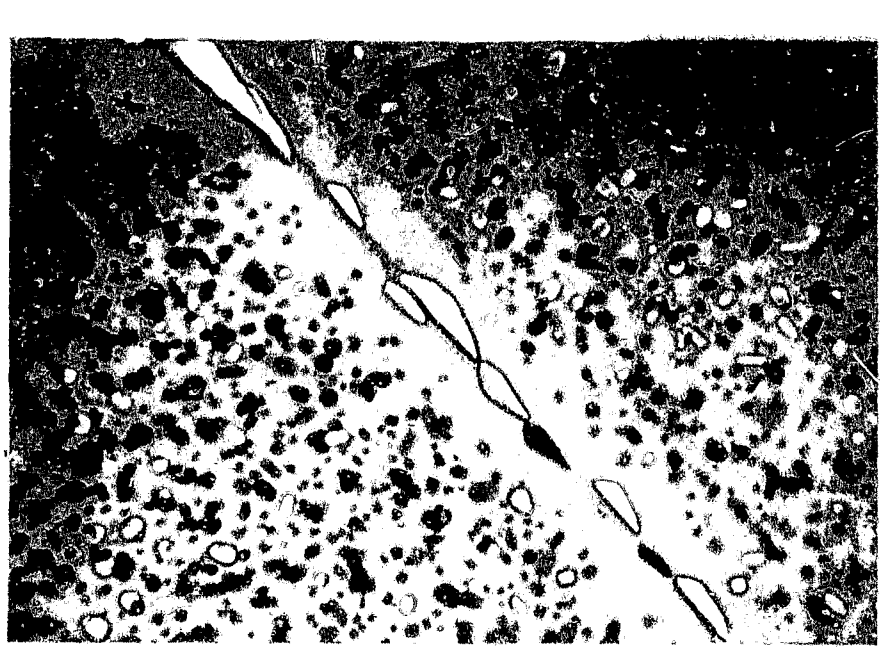
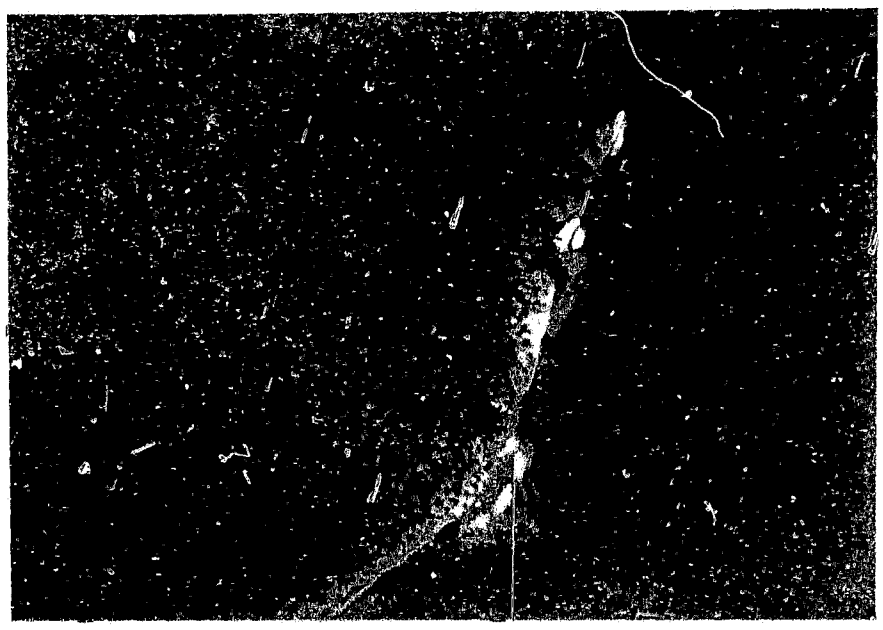
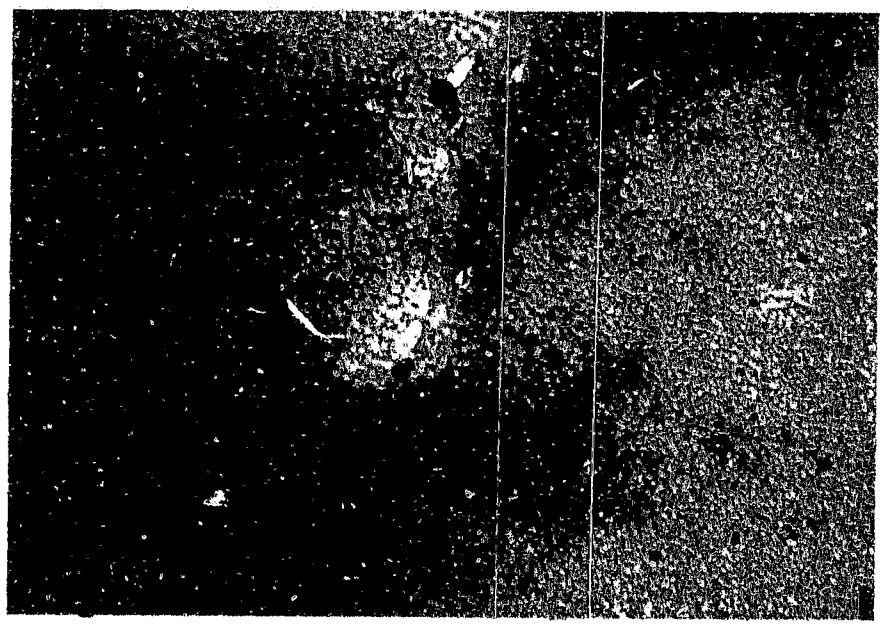


Figure 2.40 The PFZ with coarse, grain boundary and incoherent matrix precipitates in D74S - T7 temper



(a)



(b)

Figure 2.41 BF micrograph of a grain boundary with (a) zero tilt, and (b) 30° tilt in the electron microscope.

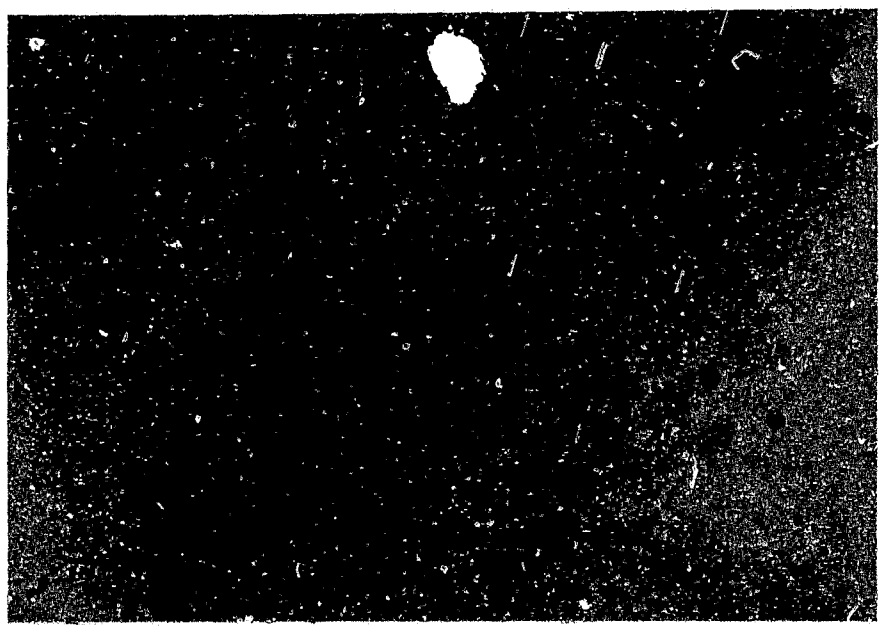


Figure 2.42 Grain boundary in D'4S at a high tilt angle.

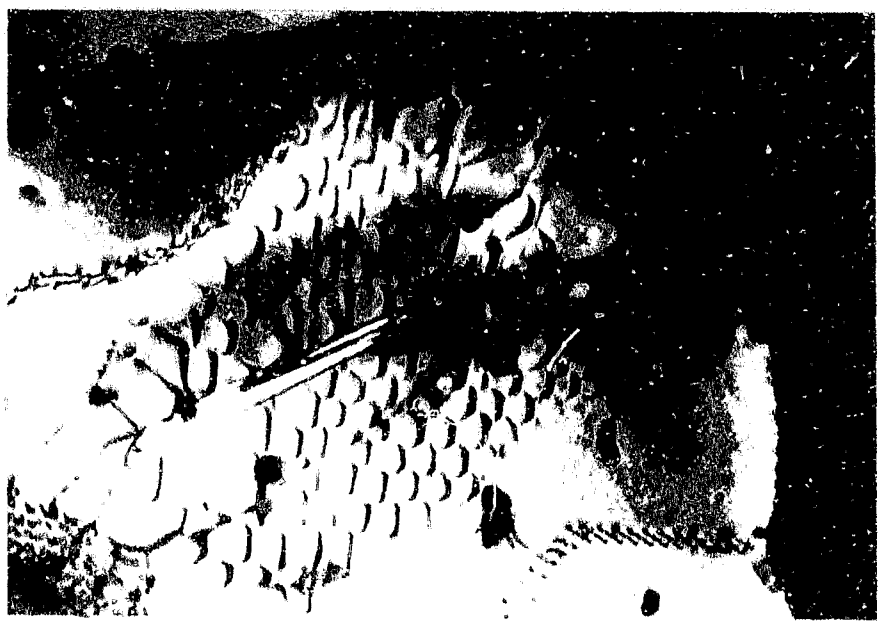


Figure 2.43 Planar hexagonal low angle boundary (BF micrograph)

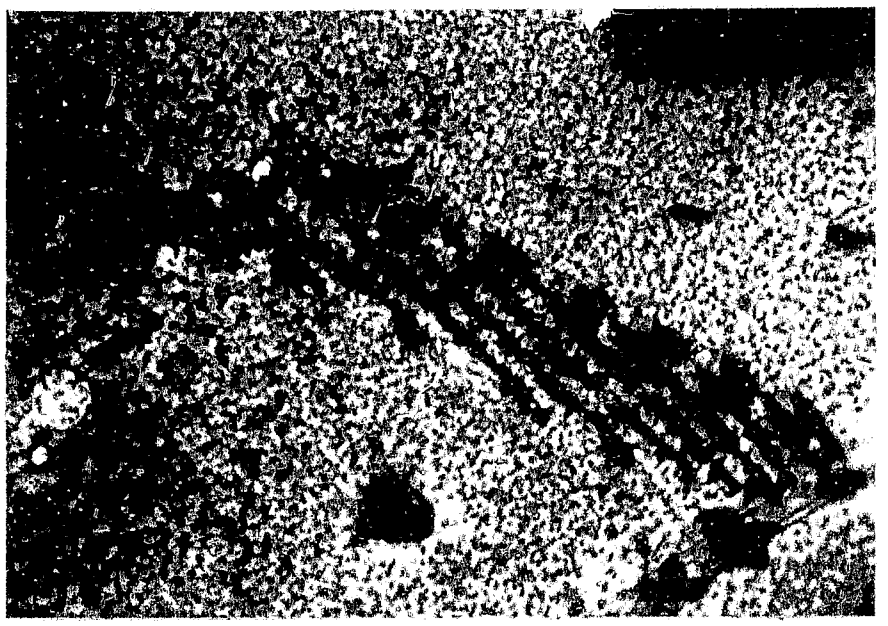


Figure 2.44 Precipitation on low angle boundaries in D74S (BF micrograph)

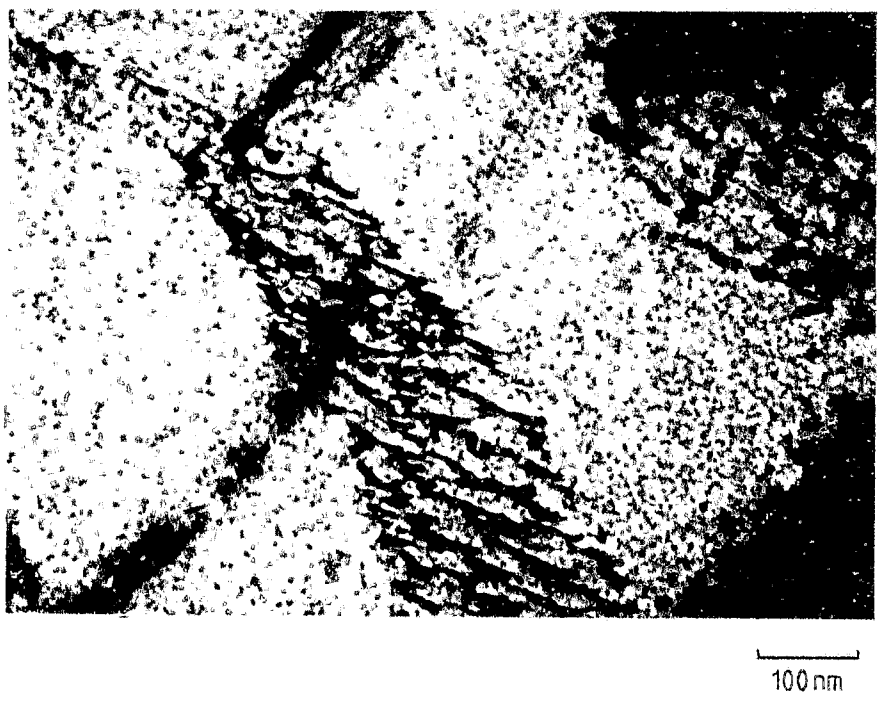


Figure 2.45 An ordered precipitate array in a low angle boundary (BF micrograph)

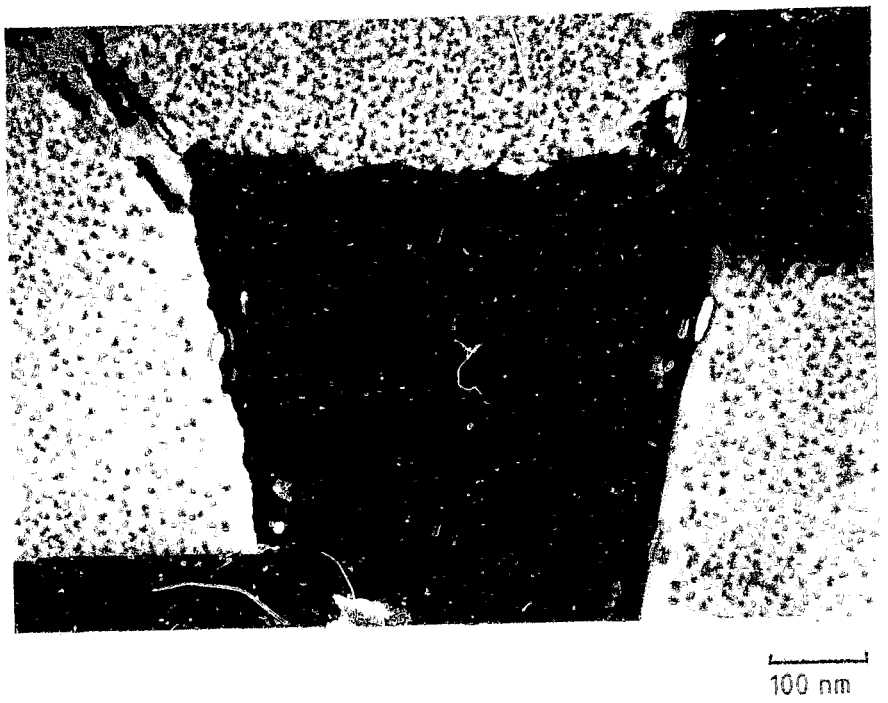


Figure 2.46 Precipitation on low angle boundaries (BF micrograph)

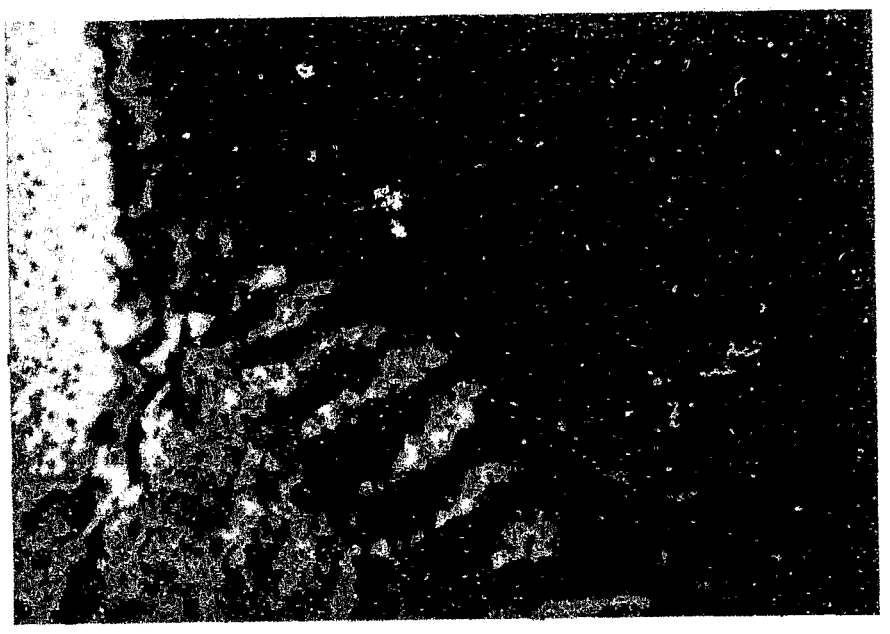


Figure 2.47 A regular array of distinct precipitates forming on the boundary seen in the centre of the above micrograph.

2.4 The Thermomechanical Treatment of Al-Zn-Mg Alloys

The properties and characteristics of wrought Al-Zn-Mg alloys are significantly influenced by the complete thermomechanical history. This section will deal with the entire heat treatment and hot working schedule applied to these alloys. This will include the thermal processes applied to ingots prior to working, during intermediate stages of fabrication, and the final precipitation hardening or ageing treatment. The major objectives of the different thermal and mechanical treatments, and their effect on properties will be discussed under the titles which appear in a typical thermomechanical treatment schedule. It is not intended to deal with complex thermomechanical treatments, which are used largely in the production of aircraft alloys. For the purposes of this development programme, production costs, rather than high strength to weight ratios, were given prececence.

2.4.1 Homogenisation and Hot Working

After solidification, the as-cast structure of Al-Zn-Mg ingots consist of a cored dendritic structure, and an interdendritic distribution of second phase or eutectic. The transition elements remain largely in solid solution. Homogenisation is primarily used to:

a) reduce segregation;

b) remove low melting point eutectics which reduce workability; and

c) to precipitate the transition element phases.

High solidification rates are generally employed in order to produce a finer dendritic cell, and intermetallic particle, size. This results in improved tensile strength and elongation[47]. There is, however, increased dendritic microsegregation, as would be predicted from the extent of departure from equilibrium conditions. The time required to reduce these segregations is dominated by the dendritic cell size and therefore the desirable effects of the higher solidification rate are not jeopardised. The homogenisation time has been found to be inversely related to the square of the dendritic arm spacing in the ingot[48]. Typical homogenisation treatments range between 10 and 12 hours at 480 to 500^{o}C.

The workability of the ingot is improved by removing non-equilibrium, low melting point eutectics which cause embrittlement, particularly, in hot rolling or forging. Solution of these eutectics during homogenisation is a prerequisite for most hot working operations.

The final important function of homogenisation is the precipitation and redistribution of the transitional elements Mn, Cr and Zr which supersaturate the ingot[49]. It should be noted that in this case heterogenisation

actually takes place, since precipitation rather than solution is involved, and hence both time and temperature are important. In the selection of the homogenisation temperature, consideration must be given to the control of grain structure, and in particular the avoidance of recrystallisation and grain growth.

The rate of heating to homogenisation (which has already been discussed in Section 2.2.2), is of crucial importance in the precipitation of the transitions, particularly Zr. In order to promote the nucleation and growth of a fine and uniform dispersion, heating rates should be kept as low as possible, preferably as low as $50K.h^{-1}$ [20,50].

The effect of homogenisation on the SCC properties is determined indirectly by the ability of the transition precipitates to prevent recrystallisation. Cordier, et al.[15] have shown that at higher temperatures (560°C for 12 hours), a significantly coarser and more widely spaced dispersion is formed in Cr- and Mn- bearing alloys. Temperatures in the range of 480 to 500°C provide the optimum dispersion. The selection of a homogenisation temperature can finally be considered to be an optimisation between two opposing effects: the resistance to SCC, and the quench sensitivity of the alloy. Higher temperatures produce a coarser dispersion and hence few nucleation sites for $MgZn_2$ precipitates during subsequent heat treatment. The quench sensitivity is therefore improved, however,

the ability of the dispersion to prevent recrystallisation is reduced and hence the resistance to SCC is lowered.

The hot working operation is required to break down the cast structure and achieve uniformity of both the grain size and the constituent size and distribution. If the ingot is hot rolled, the degree of working is not uniform throughout the plate thickness, as rolling is largely a surface effect. Uniformity of work can be increased by increasing the reduction per pass or by pre-forging the ingot before rolling.

2.4.2 Solution Heat Treatment

The main function of a solution heat treatment (SHT) is to obtain complete solution of the major alloying elements. The precipitation strengthening achieved on ageing increases with Mg and Zn in supersaturated solid solution. To this end, the highest temperature in the single phase equilibrium solid solution range of the particular alloy would seem to be required. However, two major constraints exist on the use of high SHT temperatures. Firstly, temperatures above the solidus temperature must not be used as this leads to melting of intergranular networks of eutectic. This in turn results in a reduction of strength and ductility. The second constraint is the avoidance of recrystallisation of the hot-worked structure which is influenced by both the SHT temperature and time. A coarse recrystallised grain structure leads to inferior mechancial properties and SCC resistance.

The minimum temperature required for complete SHT of cold-rolled Al-Zn-Mg sheet has been investigated[51] and the results are shown in Figure 2.48. Generally, a higher SHT temperature leads to a slightly higher tensile strength but has little effect on toughness.

The effect of SHT on susceptibility to SCC has received much attention. It has been reported that resistance to SCC is improved with lower temperatures and shorter holding times[40,52]. Commercially, SHT temperatures and times are kept as low as possible to avoid recrystallisation. A typical commercial SHT for Al-Zn-Mg plate is 465^{o}C for approximately 1 to 2 hours.

It has already been mentioned (in Section 2.3.2) that segregation and the resultant solute distribution in the vicinity of grain boundaries are considered important in determining SCC susceptibility. A study has been made of solute segregations to grain boundaries by Joshi, et al.[43], for aluminium 7075 alloy as a function of SHT temperature and ageing procedure (using Auger electron spectroscopy). It was found that for the same SHT temperature the concentration of Zn and Mg at grain boundaries is greatest for the peak aged (stress corrosion susceptible) condition and less in the over aged condition which is relatively immune to SCC. For the same peak aged condition, the Zn, Mg and Cu contents of grain boundaries are shown in Figure 2.49, for different SHT temperatures.

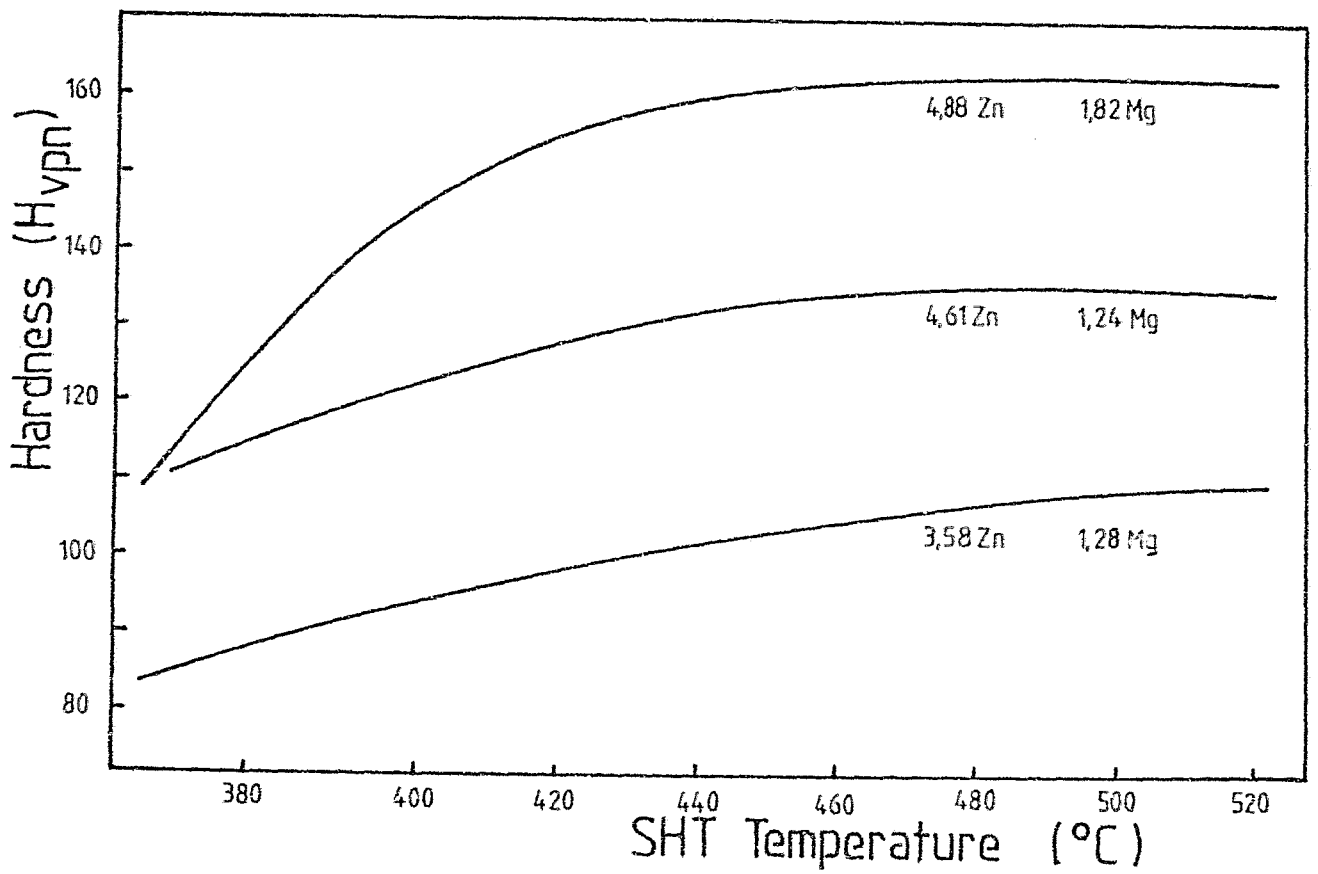


Figure 2.48 The effect of solution heat treatment temperature on the hardness of three Al-Zn-Mg alloys. The S H T time is 5 minutes.

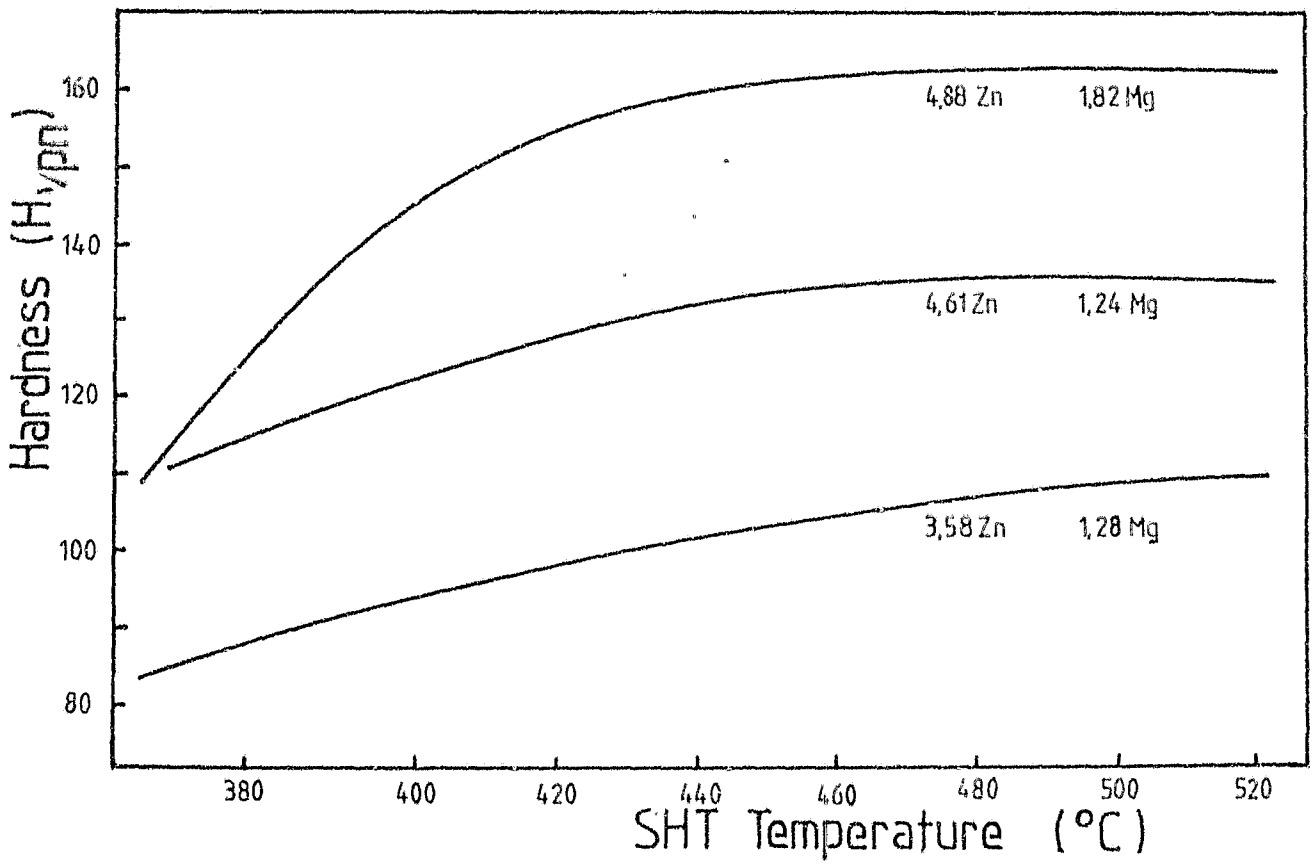


Figure 2.48 The effect of solution heat treatment temperature on the hardness of three Al-Zn-Mg alloys. The S H T time is 5 minutes.

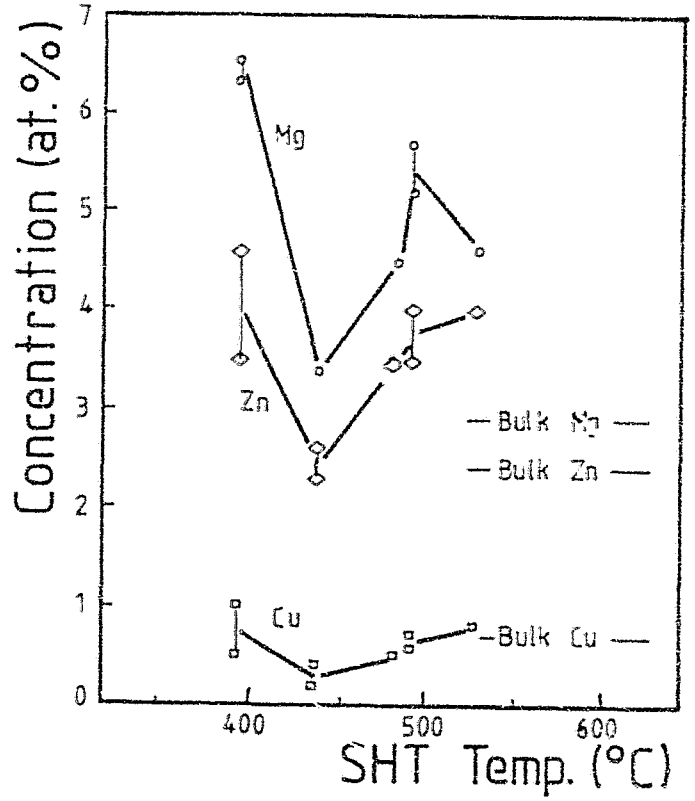


Figure 2.49 Variation of Zn, Mg and Cu atomic concentrations on the fracture surface (intergranular) of aluminium 7075 alloy with the temperature of S H T

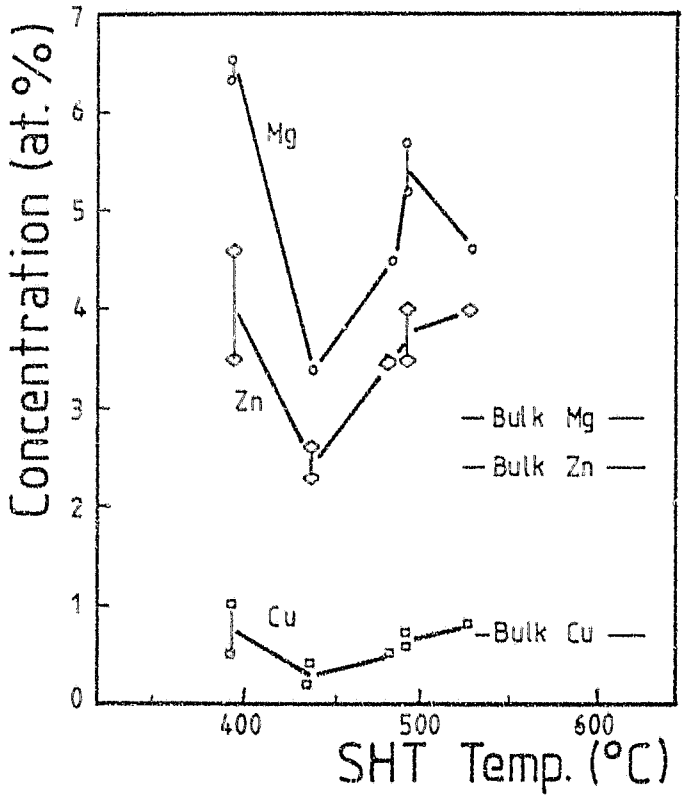


Figure 2.49 Variation of Zn, Mg and Cu atomic concentrations on the fracture surface (intergranular) of aluminium 7075 alloy with the temperature of S H T

All these elements exhibit a minimum grain boundary concentration at 438°C. This effect was explained in terms of the equilibrium and non-equilibrium modes of segregation. The equilibrium segregation of solute to grain boundaries occurs at the SHT temperature and is retained through the quench to ambient temperature; since there is insufficient time for diffusion. As the solution temperature increases, the diffusitivity of the solute increases and segregation decreases. The non-equilibrium mode of segregation involves the solute drag effect; solute-vacancy pairs moving to vacancy sinks during quenching and further ageing (discussed in Section 2.3.2 (iii)). As the solution temperature increases so the vacancy concentration increases and a greater flux of solute-vacancy pairs migrate to grain boundaries resulting in solute enrichment. In Al-Zn-Mg alloys the binding energies for Zn, Mg, Cu and Si with vacancies are all greater than the thermal energy kT, and hence they may all be dragged to grain boundaries. The minimum observed in Figure 2.49 is due to the combined action of the above two modes.

2.4.3 Quench Rate

The quench rate after solution treatment is often considered as the most critical step in the heat treatment operation. It is an important parameter in the control of mechanical and corrosion properties. The quench rate not only determines the amount of solute retained in solid solution, and hence the hardening capacity of the alloy, but also maintains a high vacancy concentration, which assists in subsequent zone formation.

There is also a critical cooling range for precipitation hardenable alloys, determined by the nucleation of diffusion-controlled solid state reactions. The principal parameters are the degree of supersaturation and rate of diffusion[2].

These factors vary oppositely with temperature, producing a maximum precipitation rate during cooling. Precipitation during the critical temperature range may be avoided by inhibiting nucleation through a sufficiently rapid cooling rate. The critical cooling range for Al-Zn-Mg alloys, depending on actual composition, is approximately 350 to 200^{o}C.

The rate of cooling may have a marked effect on the residual stresses and distortion produced in an alloy. High quench rates are therefore avoided as the residual stress increases with increasing quench rate[49]. This in turn leads to a decrease in the resistance to SCC. Impact properties, on the other hand, decrease markedly with reduction in quench rate from 500K.s^{-1} to 2.65K.s^{-1} [11]. The reduction in the fracture stress of grain boundaries arises due to:

1) the relative strength of grains increasing; and
2) the increase in grain boundary precipitation with reducing quench rate (grain boundaries of slow quenched material having greater numbers of coarse embrittling precipitates).

There is also a critical cooling range for precipitation hardenable alloys, determined by the nucleation of diffusion-controlled solid state reactions. The principal parameters are the degree of supersaturation and rate of diffusion[2].

These factors vary oppositely with temperature, producing a maximum precipitation rate during cooling. Precipitation during the critical temperature range may be avoided by inhibiting nucleation through a sufficiently rapid cooling rate. The critical cooling range for Al-Zn-Mg alloys, depending on actual composition, is approximately 350 to 200^{o}C.

The rate of cooling may have a marked effect on the residual stresses and distortion produced in an alloy. High quench rates are therefore avoided as the residual stress increases with increasing quench rate[49]. This in turn leads to a decrease in the resistance to SCC. Impact properties, on the other hand, decrease markedly with reduction in quench rate from 500K.s^{-1} to 2.65K.s^{-1} [11]. The reduction in the fracture stress of grain boundaries arises due to:

1) the relative strength of grains increasing; and
2) the increase in grain boundary precipitation with reducing quench rate (grain boundaries of slow quenched material having greater numbers of coarse embrittling precipitates).

It should therefore be possible to improve fracture properties by promoting transgranular fracture through the reduction of preferential grain boundary precipitates.

The effect of quench rate on tensile and SCC properties is shown in Figure 2.50 for a weldable Al-4.8Zn-1.1Mg alloy with minor additions of Mn, Cr and Zr[9]. The improvement in resistance to SCC with decreasing quench rate below $10K.s^{-1}$ is clearly evident. It should be noted, however, that in non-weldable Cu-containing alloys the effect of quench rate on susceptibility to SCC is reversed. In these alloys rapid cooling is known to produce increased resistance to both intergranular corrosion and to SCC[8,53].

The PFZ width and solute segregation at grain boundaries are dramatically altered by changes in quench rates. Both these microstructural features have been reported to affect susceptibility to SCC. The effect of quench rate on PFZ zone width has already been discussed (Section 2.3.2), although there is still controversy concerning the influence of this width on SCC properties[40]. Shastry and Judd[54] have shown that a major part of the solute enrichment of grain boundaries occurs during quenching itself, mainly while cooling in the high temperature range, where both the solute and vacancy diffusivities are relatively high. During slow quenching, or final ageing, solute depletion of the

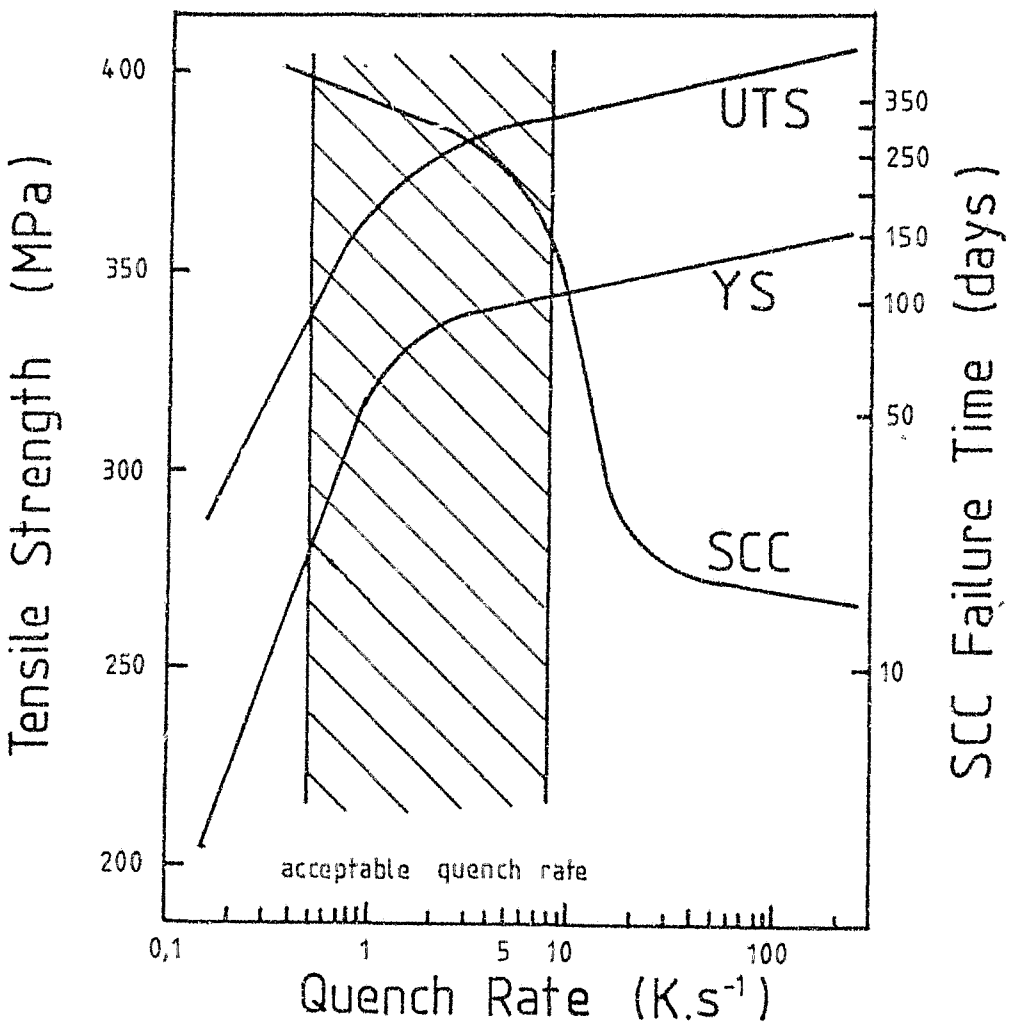


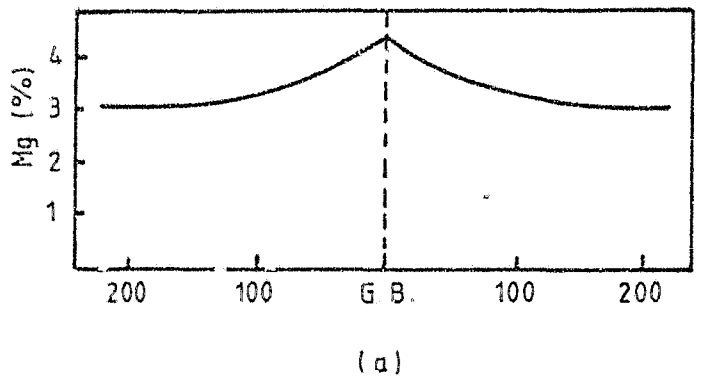
Figure 2.50 The effect of quench rate from S H T on strength and SCC resistance of an Al-4.8 Zn - 1.1 Mg + Mn, Cr, Zr alloy.

grain boundaries results in a solute concentration profile at the grain boundary. This is associated with an increase in the resistance to SCC. The depletion of solute arises due to diffusion of the solute to growing grain boundary precipitates. This effect of quench rate on the Mg concentration profile at grain boundaries of an Al-5.9Zn-3.2Mg alloy has been determined by Doig and Edington[44] and is schematically illustrated in Figure 2.51.

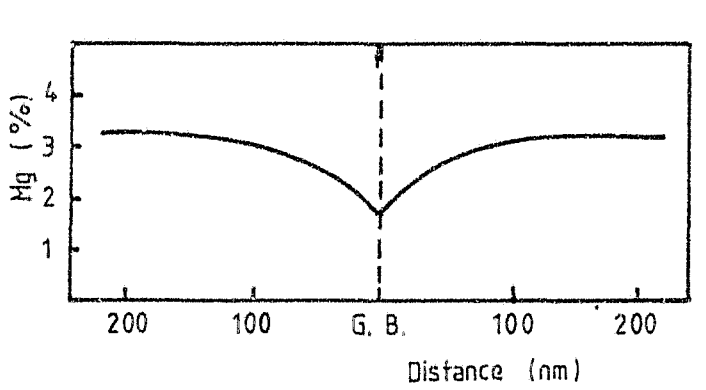
Specialised techniques have been developed to improve SCC properties. Relatively simple quench interruption techniques have been shown to decrease the SCC susceptibility[45]. It was proposed that the improved resistance to SCC was associated with the development of a distinct solute concentration profile at the grain boundaries after only 5 minutes at 300°C.

2.4.4 Natural and Artificial Ageing

Age-hardening is the final stage in the heat treatment of Al-Zn-Mg alloys. Both the precipitate dispersion and structure influence mechanical and stress corrosion properties and a stringent control of the ageing procedures is therefore required. In Section 2.3.1 it was shown that the precipitation sequence depends on the ageing temperature, since different GP zones may be formed. To summarise for an Al-4.8Zn-1.2Mg alloy[27]



(a)



(b)

Figure 7.51 Mg composition profile at grain boundaries solution heat treated at 500°C, and (a) quenched into iced brine, or (b) oil-quenched (for precipitate free regions).

SSSS $\underset{\text{age}}{\text{RT - 60}^{\circ}\text{C}}$ GP 1

$\underset{\text{age}}{60^{\circ}\text{C-100}^{\circ}\text{C}}$ GP 1, GP 2

GP 1 zones are unstable above 80°C and slowly dissolve between 80°C to 120°C.

In order to achieve optimum properties, Al-Zn-Mg alloys are usually given a natural, pre-age and final-ageing heat treatment.

It has been determined[55] that the age-hardening of dilute Al-Zn-Mg alloys was inhibited when they had a stable sub-structure, and were aged immediately after quenching from SHT. This effect, which is intensified in slow quenched materials, may be eliminated by a natural ageing interval of one week or more (at ambient temperatures) between quenching and elevated temperature ageing. No discernible microstructural changes accompany the natural ageing and the improved mechanical properties are attributable solely to the formation of zones. The natural age is used to develop a GP 1 zone dispersion, and thereby increase the number of nucleation sites for subsequent phases.

However, the effectiveness of natural ageing is dependent on composition[55]. As the solute content increases, the alloys become more quench sensitive due

to heterogeneous nucleation of coarse precipitates on dislocation sub-structures. In the presence of this dispersion, the effect of GP 1 zones is reduced. In addition, increasing the solute content will also increase the supersaturation. Therefore, the ambient temperature interval necessary for the development of a homogeneous zone dispersion in the matrix will be reduced due to a reduced homogeneous nucleation barrier with increasing supersaturation. Increased Mg content has a greater influence on both these effects than does Zn.

The effects of the natural and pre-age treatments are particularly marked in alloys containing 1 - 2% Mg and 4 - 5% Zn. The intermediate- or pre-age is used to stabilise GP 1 zones and increase GP 2 formation. At a pre-ageing temperature of approximately 80°C, GP 2 formation has been reported to increase between 10 and 100 hours, whereas the number of GP 1 zones stays reasonably constant[27]. As GP 2 formation increases (through longer times at 60 - 100°C) the effects of reversion (during final ageing) are decreased, and as the pre-age temperature approaches 100°C only GP 2 zones are formed. In commercial practice a pre-age of 90°C is often used.

On final ageing the reversion of GP 1 zones produces solute-rich regions which form nuclei for precipitates. In addition, GP 2 zones can transform directly to η' in-situ. A higher pre-age temperature

promotes a faster final age, which may result in overageing. The optimum hardness is achieved by a fine dispersion of η' particles. A final ageing temperature approaching 200°C would produce equilibrium η and T-phase particles which would reduce mechanical properties[55,56,57]. Commercially in order to peak age, a final ageing temperature of 135°C is typically used. The time required to achieve optimum hardness depends upon the major alloying additions and reference should be made to Section 2.2.1.

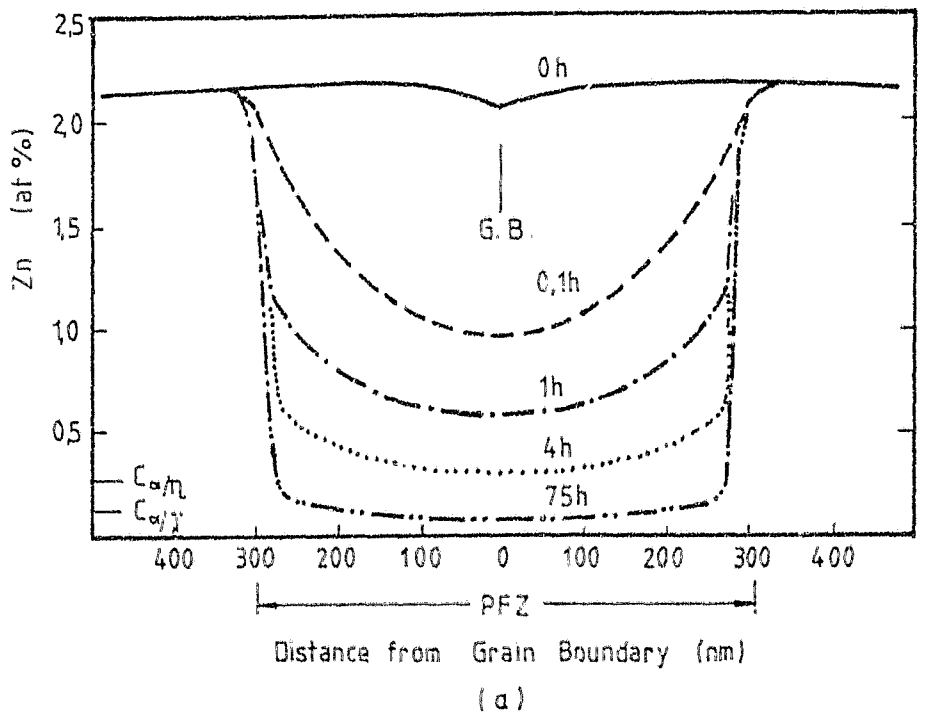
A number of important microstructural changes take place during ageing which may influence the SCC properties. The most important of these are:

1) the development of grain boundary solute concentration profiles;
2) the increase in PFZ width with ageing; and
3) the increase in size and spacing of grain boundary precipitates.

Al-Zn-Mg alloys are highly susceptible to SCC in their maximum strength (T6) conditions. These alloys have generally depended on an overageing treatment to reduce susceptibility to SCC, but at the expense of strength. Higher ageing temperatures therefore lead to improved SCC resistance.

The microstructural changes which accompany overageing and may influence SCC properties have already been listed During ageing, a solute concentration profile develops at the grain boundary due to diffusion of solute along the boundary and incorporation into grain boundary precipitates, which then coarsen. The effect of ageing on the Zn and Mg concentration profiles at grain boundaries has been determined by Raghavan[41] and is shown in Figure 2.52. It is apparent that the solute profiles increase with increasing ageing time. The formation of a distinct solute concentration profile has been associated with a decrease in susceptibility to SCC[45].

The two changes (listed (1) and (3) above) are both therefore dependent on diffusion of solute. An increase in the PFZ width (2) is not observed when the supersaturated solid solution decomposes on ageing directly to stable equilibrium phases. However, particularly when natural and pre-ageing treatments are used, metastable phases are formed close to the grain boundary. These are re-dissolved with final ageing at higher temperatures and produce an increase in PFZ width, (see Section 2.4.6).



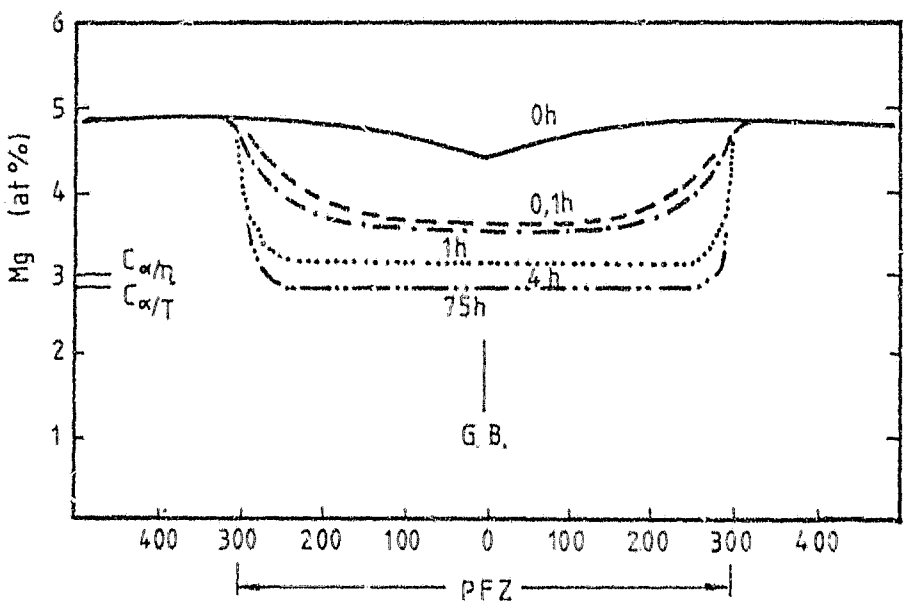


Figure 2.52 Al-5.2 Zn - 4.1 Mg alloy, solution heat treated at 465°C for 1 hour, air cooled to ambient temperature and aged at 200°C for 0·1, 1, 4 and 75 hours. (a) Zn concentration profile across a grain boundary region containing no precipitates, and (b) Mg concentration profile. $C_{\alpha/\eta}$ and $C_{\alpha/T}$ are concentrations of the matrix in equilibrium with η and T phases, respectively.

2.4.5 Experimental Aim and Procedure

The representative Al-Zn-Mg alloy, D74S, was chosen in order to determine the microstructural and mechanical property dependence on quench rate and ageing treatment.

Six 12mm plate sections of D74S (chemical composition given in the Appendix: page 205) were quenched using the quench media listed in Table VI, after solution heat treatment at 465^{o}C for 2 hours.

Table VI: Quench Medium with average quench rate

Specimen	Quench Medium	Average Quench Rate
1	Cold water quench	174.8 $K.s^{-1}$
2	Water spray	61.0
3	Boiling water quench	5.7
4	Forced air	1.6
5	Still air	0.27
6	Furnace cool	0.009

The average quench rate was accurately determined by inserting a stainless steel sheath, J-type thermocouple into a 3mm diameter hole drilled 2cm deep into the side of the plate. Good thermal contact was maintained

between the sheath and the plate during the entire quenching operation. The change in temperature was monitored during quenching by displaying the output voltage of the thermocouple on a chart recorder. The average quench rate was calculated from the resulting temperature versus time plot over the range 400 to 200°C.

The six specimens were then peak aged through the following heat treatment schedule:

natural age	:	RT/2 weeks
pre-age	:	90°C/7 hours
final age	:	135°C/16 hours

Thin foils for CTEM study were prepared using the method described in Section 2.3.3. Vickers hardness tests were performed on cut sections which were fine ground (to 1000 grit). Standard tensile test pieces were also machined from the plate. Sufficient material remained from each plate for the preparation of SCC test specimens (see Section 3.4).

The ageing characteristics and microstructural changes, particularly the change in PFZ width, were examined after a number of final ageing times at 135 and 160°C. Nine plate sections were given the following heat treatment schedule:

1) solution heat treatment: (465°C/2 hours, water quench);

2) natural age : (4 weeks with 135°C final age); or (2 weeks with 160°C final age);

3) pre age : (90°C/7 hours);

4) final age : (see Table VII).

Table VII: Final Ageing Temperatures and Times

Specimen	Final Ageing Temperature	Final Ageing Time
1	135°C	6 hours
2		12 hours
3		16 hours
4		48 hours
1	160°C	2 hours
2		4 hours
3		8 hours
4		12 hours
5		48 hours

Again, thin foils were prepared for CTEM investigation, Vickers hardness tests conducted and specimens machined for subsequent SCC testing.

Finally, evidence of solute differences between grain boundaries (in regions free of precipitates) and the matrix was sought. This was attempted using a fine electron probe and an EDS attachment in the JEOL-100C electron microscope, operating in the scanning transmission (STEM) mode. Material in the T6 condition was examined.

2.4.6 Experimental Results and Discussion

The influence of quench rate after SHT on the tensile and hardness properties of D74S is shown for a logarithmic quench rate in Figure 2.53. The range of quench rates employed varied between 174 $K.s^{-1}$ and 0.009 $K.s^{-1}$.

A sharp decrease in strength was observed at quench rates lower than 1 $K.s^{-1}$. This is clearly evident in the hardness versus linear quench rate plot (Figure 2.54). This effect may be explained in terms of the kinetics of precipitation from a supersaturated solid solution. High quench rates do not allow sufficient incubation times at elevated temperatures for the formation of stable nuclei. Hence the precipitation reaction is inhibited. Slower quench rates effectively

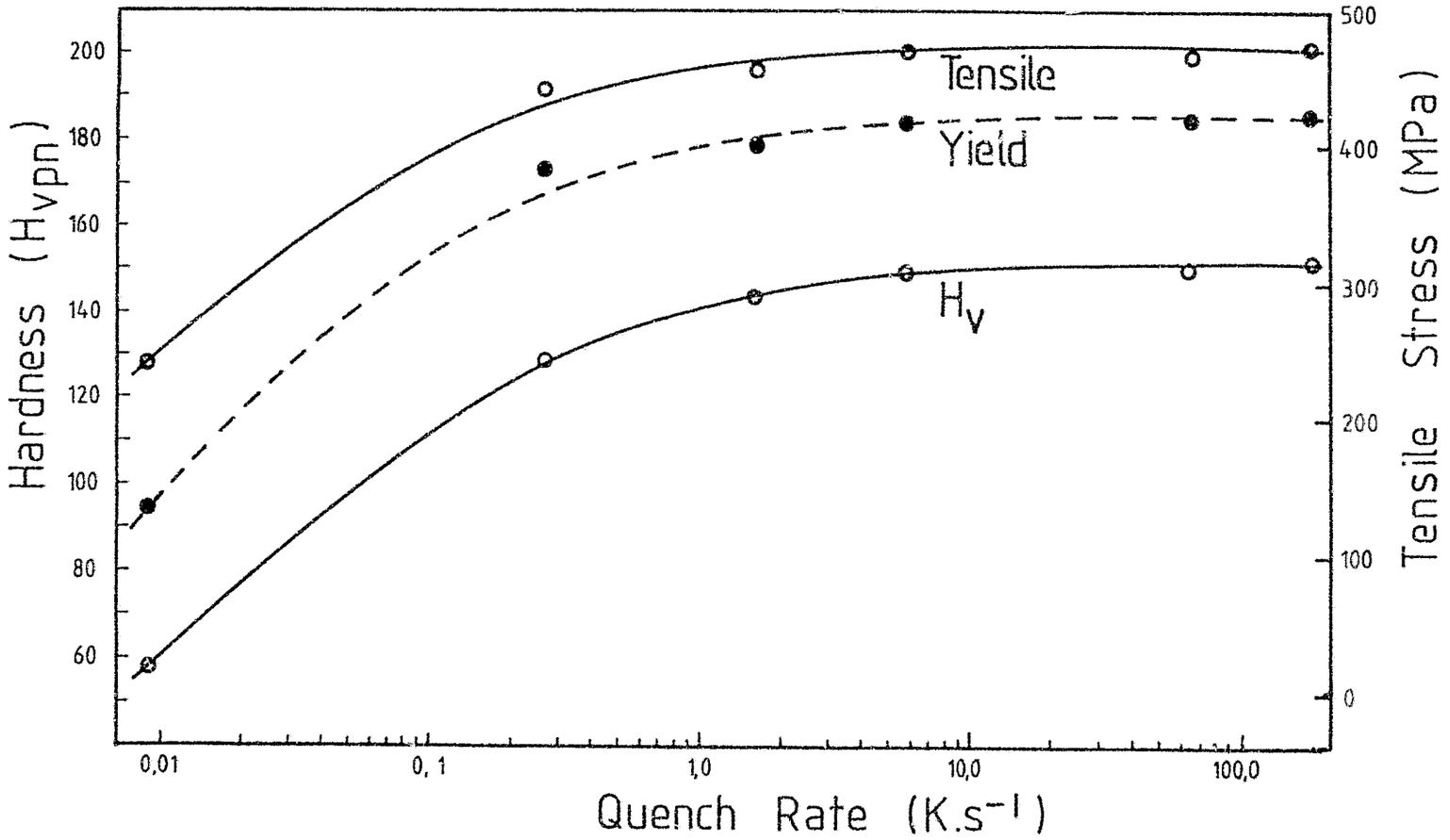


Figure 2.53 Hardness and tensile property dependence on quench rate for D 74 S.

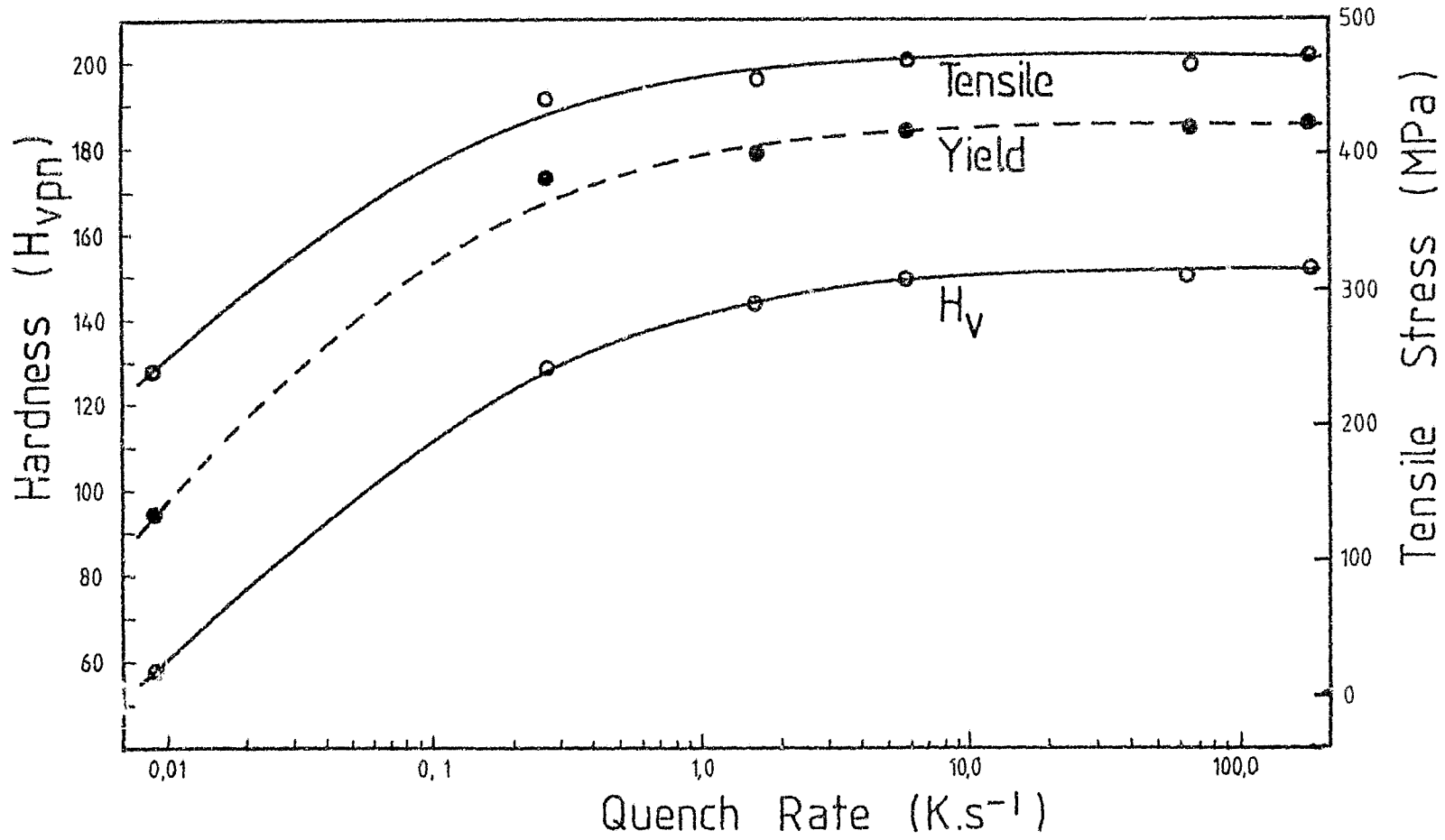


Figure 2.53 Hardness and tensile property dependence on quench rate for D 74 S.

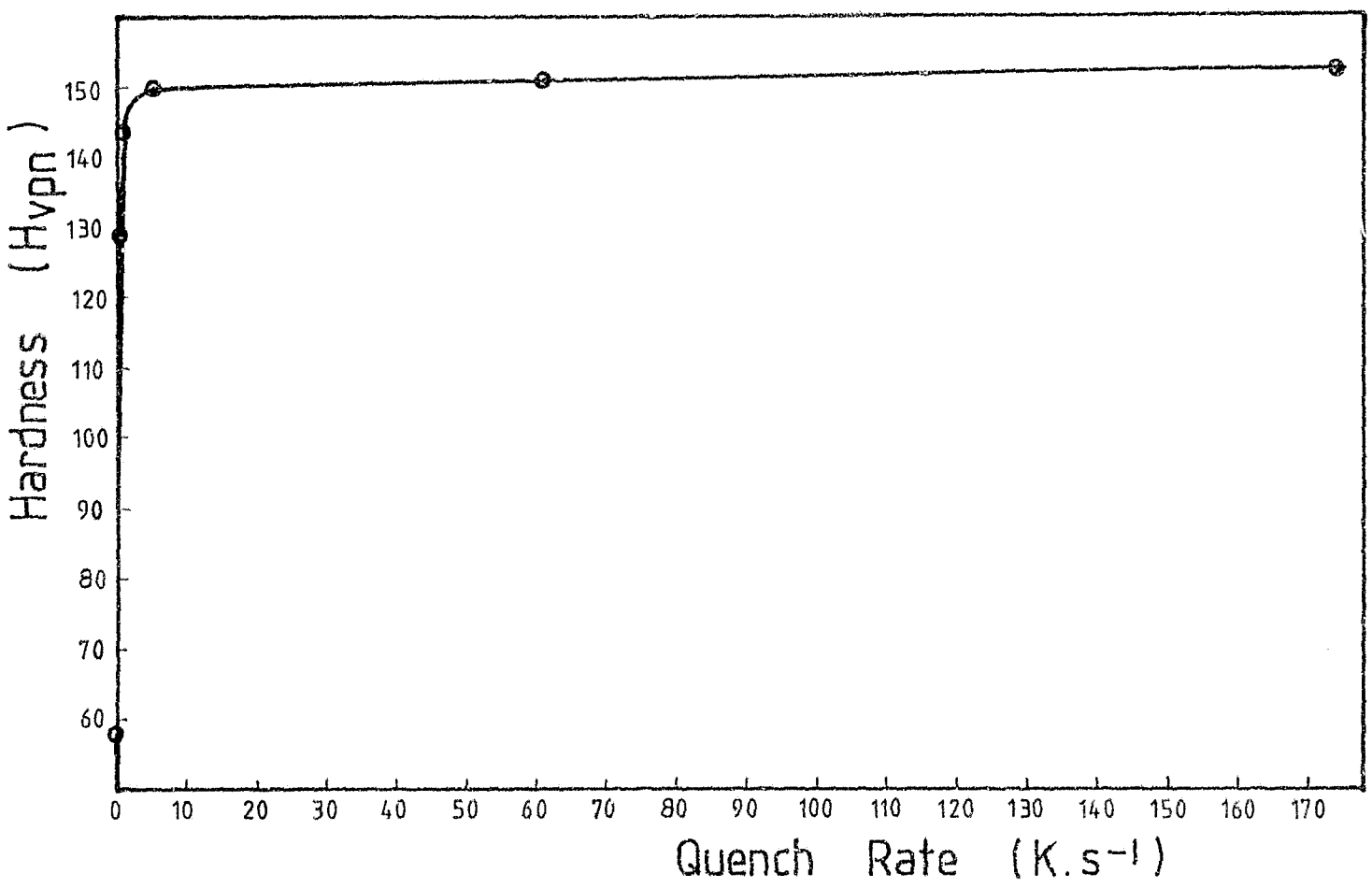


Figure 2.54 Decrease in hardness shown with a linear quench rate axis

act as high ageing temperatures. These will not produce the optimum precipitate dispersion for peak mechanical properties. On final ageing, the precipitates formed during quenching act as nuclei for further growth and lead to a coarse precipitate distribution.

Results of the CTEM investigations are shown in Figure 2.55. The variation in PFZ width with log (quench rate) is compared with the hardness values obtained. Typical micrographs showing the PFZ, matrix, and grain boundary precipitates are also included, for the first five quench rates. These clearly demonstrate a PFZ width dependence on quench rate. No PFZ was observed after furnace cooling (6) (quench rate = 0.009 $K.s^{-1}$). The microstructure of this material is similar to the F temper condition discussed in Section 2.3.4. The microstructure was characterised by copious, coarse grain boundary precipitation and an extremely coarse matrix precipitate. Its similarity to the F temper is expected as it is effectively produced in the same manner, that is, an extremely slow cool after SHT (or homogenisation in the case of the F temper).

The PFZ width was determined for each quench rate by taking the average value of at least 10 different high angle grain boundaries. (The grain boundary precipitation and PFZ width varied between high and low angle grain boundaries. However, as SCC is reported to progress mainly in high angle (high energy)

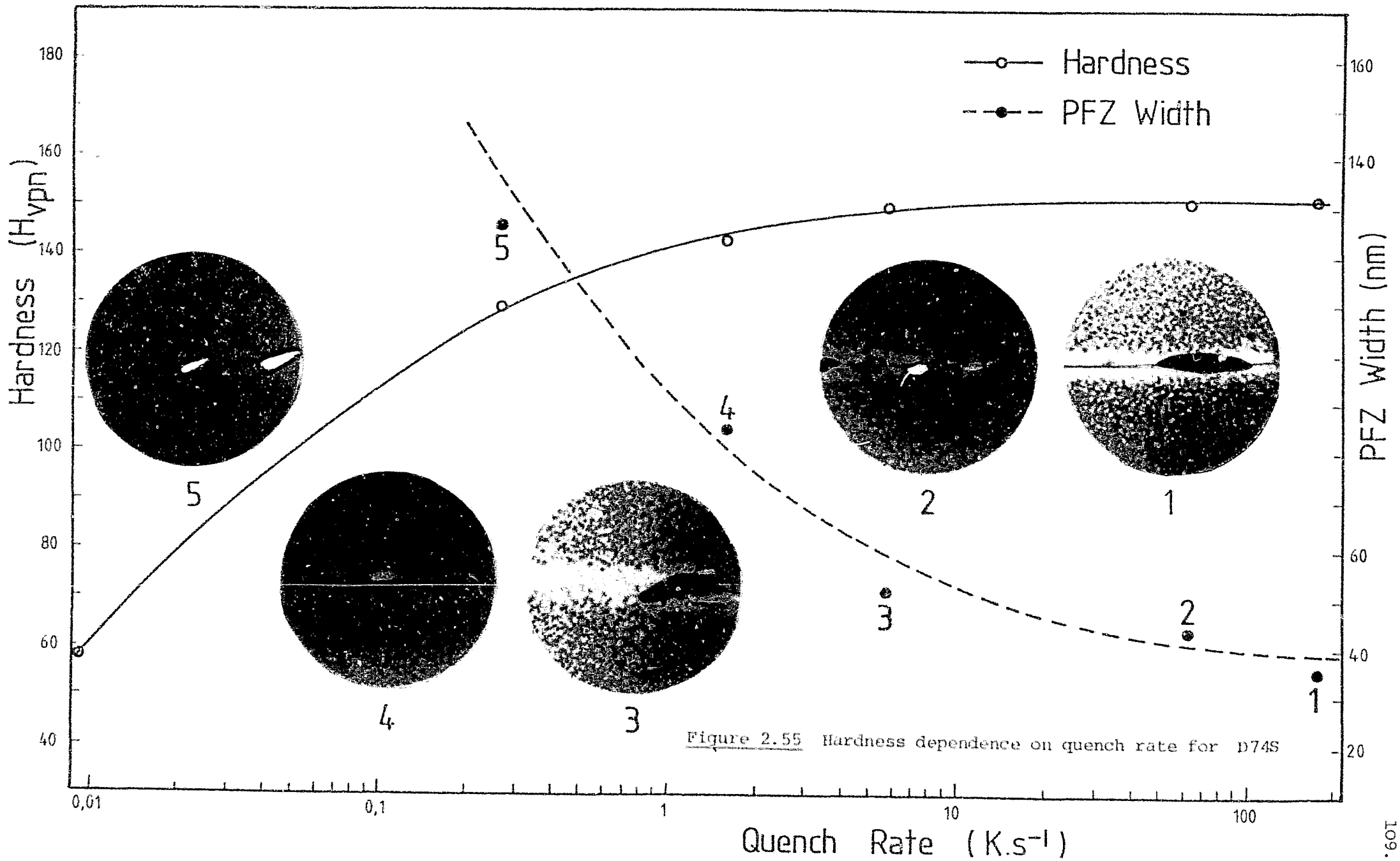


Figure 2.55 Hardness dependence on quench rate for D74S

boundaries[40], the low angle boundaries were not considered). The standard deviation from the mean ranged between 6% after rapid quenching (1) and 8% for slow cooling (5). With the quench rate plotted on a linear scale, a sharp increase in PFZ width is observed for quench rates lower than 1 $K.s^{-1}$ (Figure 2.56).

Coarsening of the matrix precipitates is clearly evident from micrographs 1 to 5 in Figure 2.55. In the first micrograph there is still evidence of residual strain contrast, implying at least semi-coherency, while the coarse precipitates (in micrograph 5) appear fully incoherent. The coarsening and reduced dispersion of the matrix precipitate with decreasing quench rate has already been explained.

The ageing characteristics of D74S (in terms of hardness variations) with 135 and 160°C final ageing temperatures, are illustrated in Figures 2.57 and 2.58, respectively. Micrographs, corresponding to each temper condition, showing typical microstructural features are also included.

The increase in PFZ width with final ageing time was determined and is represented by the dotted curves. The standard deviation from the mean was $\sim$ 5%.

A finer matrix precipitate dispersion is obtained for the lower ageing temperature (compare micrographs of the 135°C final age with those of the 160°C final age) and

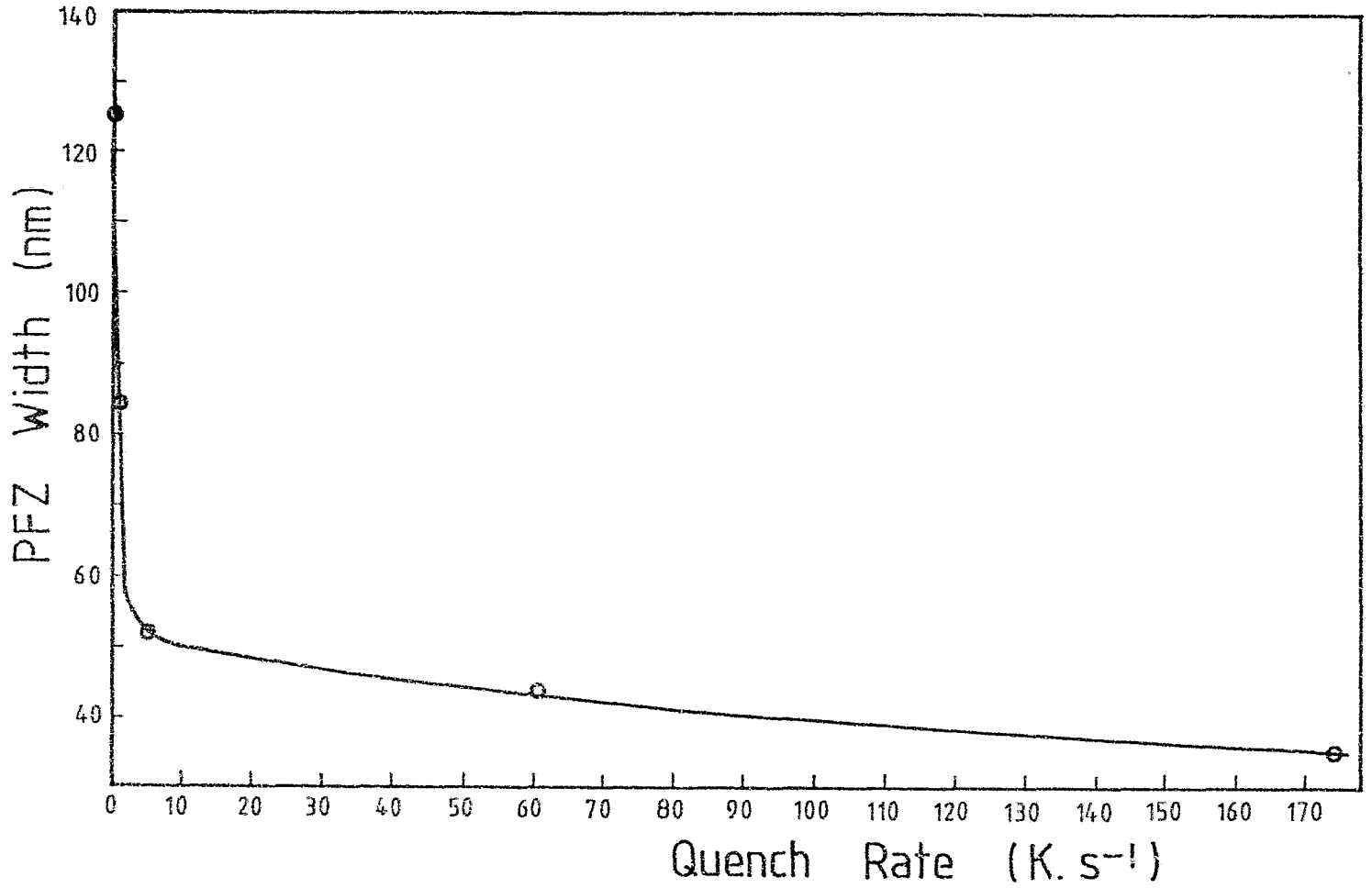


Figure 2.56 The increase in PFZ width shown with a linear quench rate axis

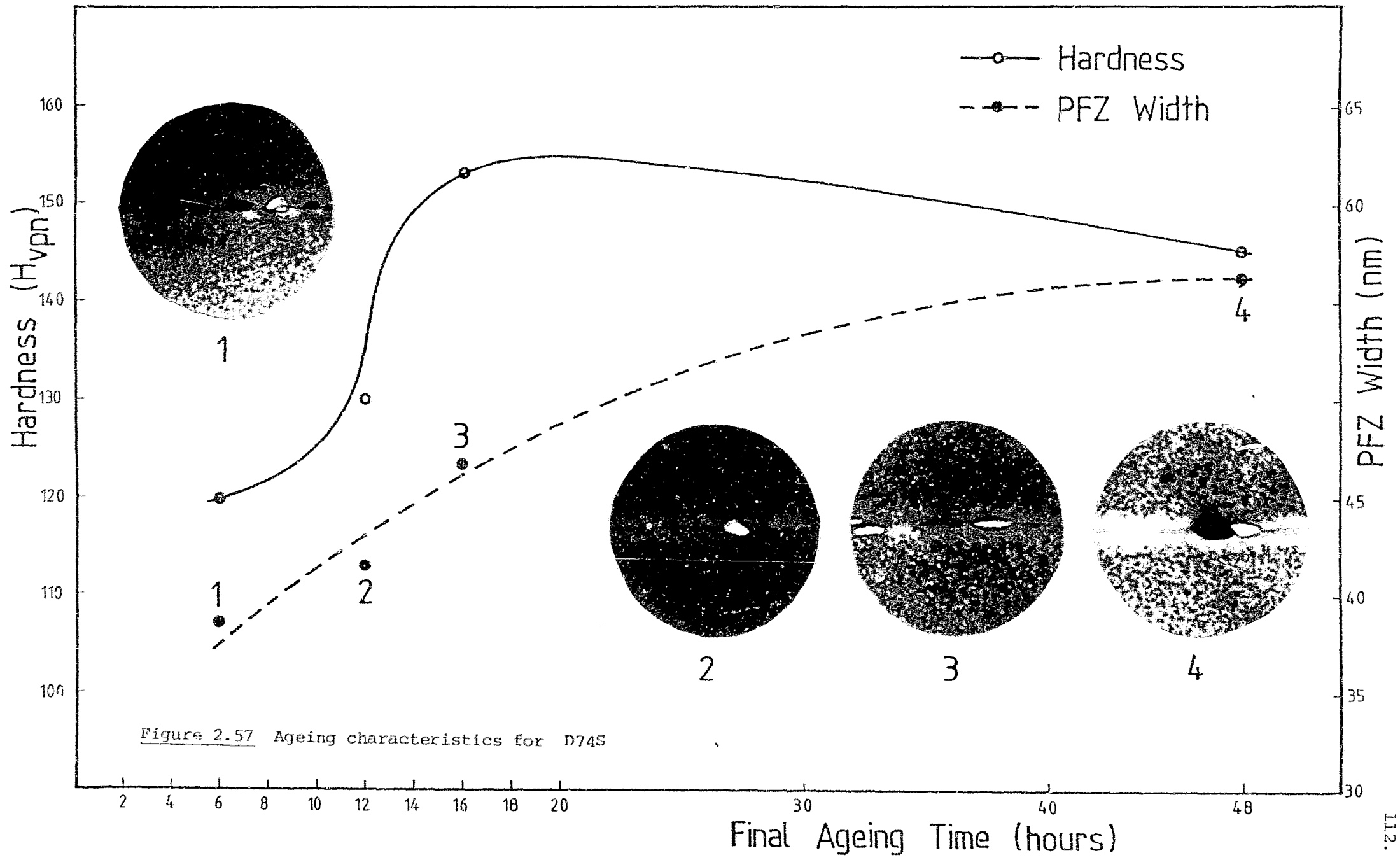


Figure 2.57 Ageing characteristics for D74S

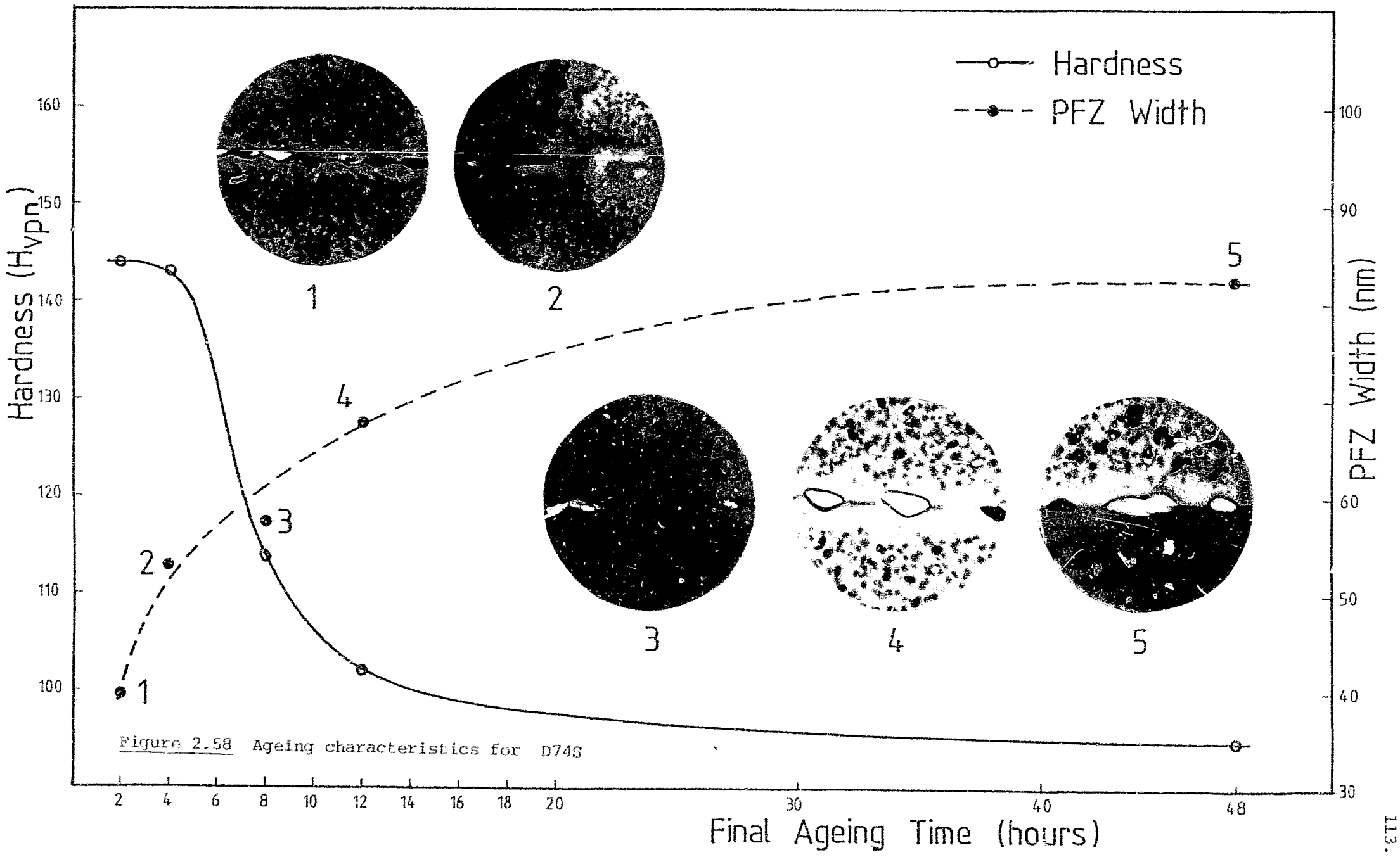


Figure 2.58 Ageing characteristics for D74S

this provided a higher peak hardress. The 135°C final age does not lead to significant coarsening of the precipitate, hence notable overageing (reduction in hardness) was not observed even after long (48 hours) final ageing times. The 160°C final age, however, does lead to significant coarsening of the matrix precipitate (micrographs 1 to 5 in Figure 2.58). This, in turn, produces a rapid overageing effect.

The three major microstructural feature changes with decreasing quench rate, increasing ageing time or temperature were:

1) a coarsening of matrix precipitates;
2) a growth in size and increased separation of the grain boundary precipitates; and
3) a monotonic increase in the PFZ width.

Sufficient material remained from all temper and quench rate conditions to undertake SCC testing. Testing procedures and the results will be discussed in the next chapter. A relationship between susceptibility to SCC and one of these microstructural features (the PFZ width) will then be investigated.

As has already been mentioned, the solute concentration profiles at grain boundaries are considered important in determining susceptibility to SCC. Attempts were therefore made to obtain information on both the Zn and Mg concentration differences between grain interiors and

grain boundary regions free of precipitates. However, due to the closeness of the energy peaks of the K_α X-rays of Al and Mg, the Mg peak is saturated by the Al peak and hence could not be resolved with the available equipment.

Operating in the STEM mode, the electron probe was first placed on the grain boundary. The X-ray spectrum of this region was obtained for a count time of 100 seconds. The probe was then placed in the matrix and the analysis repeated. The two spectra were then simultaneously viewed for comparison of the Zn peak intensities. A typical comparison representative of many spectra is shown in Figure 2.59. The continuous white spectrum represents the matrix and the dotted spectrum the grain boundary.

A decrease in the grain boundary Zn content of approximately 20 - 30% was found in the T6 condition. This result substantiates the existence of the solute profile reported in the preceding sections. Unfortunately, due to a high contamination rate in the microscope, the accuracy of the measurements were not considered sufficient to determine either the profile within the PFZ or differences in profiles in different temper conditions.

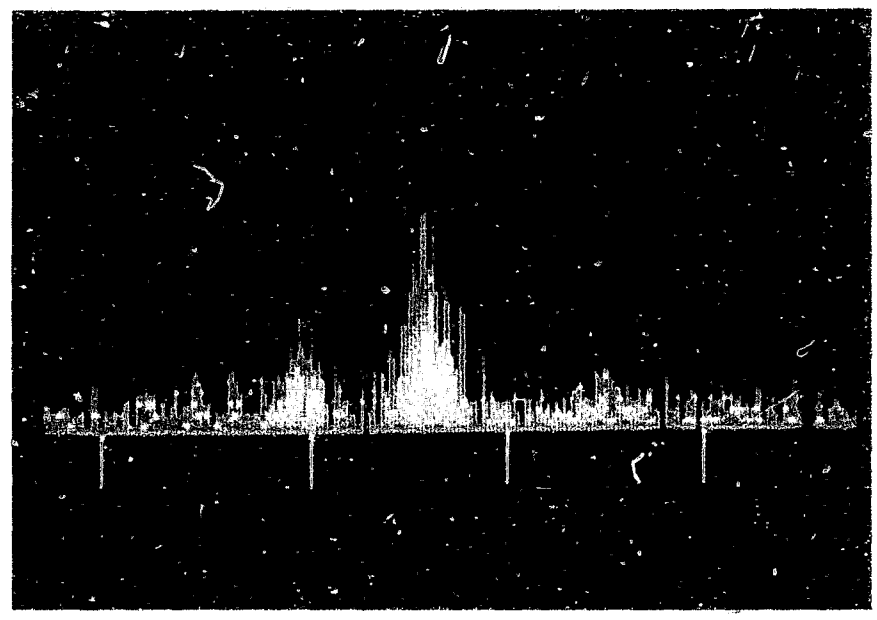


Figure 2.59 X-ray spectrum showing comparison of Zn peak intensities for grain boundary and grain interior

2.4.7 Conclusions

i) A slight decrease in strength with reduced quench rates, becoming increasingly more marked as quench rate fell below $1K.s.^{-1}$, has been observed for D74S.

ii) The following microstructural feature changes were found with decreasing quench rate:

a) a coarsening of the matrix precipitate;
b) a growth in size and increased separation of the grain boundary precipitate; and
c) an increase in the PFZ width.

Similar trends were observed with increasing ageing time or temperature.

iii) The depletion of Zn at grain boundary regions free of precipitates was found to be approximately 20 - 30% for the T6 temper.

CHAPTER 3: STRESS CORROSION CRACKING OF Al-Zn-Mg ALLOYS

3.1 Introduction

Nearly all SCC service failures of medium to high strength Al-Zn-Mg alloys up to the present have been caused by their susceptibility in the short transverse direction. Although the SCC properties in this direction are to a large extent quantitatively known, the precise mechanism of SCC is not fully understood. The many metallurgical and environmental parameters encountered in SCC susceptible service conditions complicate attempts to study this phenomenon experimentally.

In the present chapter, the current theories of SCC of Al-Zn-Mg alloys will be considered. The significance attached to microstructural features is highly relevant to the mechanisms of SCC, and will also be discussed. Compositional variations have to a large extent been discussed in detail in Chapter 2. The results presented here are primarily empirical, however, reference will be made to that Chapter where pertinent.

A major initial goal of this work was to ensure that a suitable method for rapidly assessing the susceptibility to SCC was available. This was considered important in providing comparative results between the various tempers and compositions used. A number of accelerated

SCC test methods were investigated and the results are reported. The slow strain rate test was finally selected for detailed comparative evaluations in terms of both reproducibility and reliability.

3.2 Mechanisms of SCC in Al-Zn-Mg Alloys

The synergistic action of a corrosive environment and a tensile stress, whether internal or externally applied, may produce SCC. This environmental-induced cracking is nearly always along grain boundaries and occurs at stresses usually far below those required to cause gross yielding. Some particularly important alloy/environment combinations, which are of practical importance are; high strength aluminium alloys in air, medium to high strength alloys in industrially polluted atmospheres, and finally, one of the most severe combinations, medium to high strength alloys in marine environments.

Polmear[1] has summarised a number of microstructural features which may play a role in the mechanism of SCC.

i) The PFZ. It is considered that either these zones or the grain boundaries will be anodic with respect to grain centres. Strain is also likely to be concentrated in these zones because they are relatively soft.

ii) Nature of the Matrix Precipitate. Maximum susceptibility to SCC occurs when GP zones are present, where deformation tends to be concentrated in discrete slip bands. The stress concentration generated where these bands impinge upon grain boundaries are assumed to contribute to SCC.

iii) Dispersion of Precipitate Particles in Grain Boundaries. In some alloys, SCC has been shown to occur more rapidly when particles in grain boundaries are closely spaced.

iv) Solute Concentration Profiles in the Region of Grain Boundaries. Differences in solute levels that arise between grain interiors and grain boundaries during ageing are thought to modify local electrochemical potentials.

v) Hydrogen Embrittlement. This may occur due to the rapid diffusion of hydrogen along grain boundaries.

vi) Chemisorption of the Atom Species at the Surface of Cracks. This may lower the cohesive strength of the interatomic bonds in the region ahead of an advancing crack.

Three models of SCC in Al-Zn-Mg alloys will be considered, each of which usually involves more than one of the above microstructural features. Sufficient experimental evidence has not as yet been produced to

either accept or reject categorically any one model. However, the overall process of SCC is complex and it seems probable that in any real service environment, a combination of these models will operate.

3.2.1 Hydrogen Embrittlement

SCC failures of Al-Zn-Mg alloys are ideal examples of brittle, intergranular fractures[12]. Experimental evidence accumulated over the past decade has increasingly supported the opinion that hydrogen embrittlement occurs during SCC. According to Ratke and Gruhl[58], hydrogen formed by the reaction of aluminium and the aqueous corrosive medium diffuses into grain boundaries and leads to a reduction of their rupture strength. Decohesion results in intercrystalline brittle fracture. The stress dependence of SCC is explained in terms of an equilibrium solubility of hydrogen in grain boundaries which is a function of the applied stress. Ratke offered the following experimental results to substantiate the hydrogen-embrittlement model.

1) A study of the shape of the stress corrosion cracks, in unnotched rectangular tensile specimens, revealed that the cracks were more developed in the centre than at the edge of the specimen (Figure 3.1). This is explained in terms of the solubility of hydrogen at grain boundaries under stress. In front of the embrittled zone elasticity theory

predicts the formation of a stress peak. This in turn again considerably increases the hydrogen solubility, thus orientating its direction of growth. Embrittlement is therefore promoted, the effect being strongest in the centre of the speciment where the plane state of elongation is the greatest.

2) The SCC fracture area versus measured life time exhibited a square-root/time law relationship, which suggests a diffusion process as the time-determining factor. A volume diffusion process does not operate as this would require a linear relation between the crack area and the life time. A grain boundary diffusion process was therefore suggested with an increased diffusion coefficient due to the applied stress.

3) In weak corrosive media, or in the presence of a protective coating, the SCC life times are increased. In this case the hydrogen formation represents the time-determining process.

Viswanadhan, et al.[42] concluded that there were three crucial steps which govern the SCC process:

1) generation of hydrogen;
2) entry of hydrogen through the protective surface film; and
3) concentration of hydrogen in a localised region to cause embrittlement.

The interaction of hydrogen and the microstructure of grain boundaries must therefore be understood. It is reasonable to assume that the local distribution of Zn and Mg atoms in grain boundaries influence their structure, mechanical strength and hydrogen solubility[10]. Appreciable segregation of Zn and Mg to grain boundaries in the as-quenched condition has been discussed in Chapter 2. In the overaged condition, Viswanadhan, et al.[42] have shown that all the Zn at grain boundaries has been incorporated into $MgZn_2$ precipitates. However, from Auger studies only 40% of Mg is in precipitate form. The free Mg plays a role in trapping hydrogen and providing local supersaturations, thus causing embrittlement. Hess[59] has demonstrated that the hydrogen solubility in aluminium alloys depends positively on the Mg content, negatively on Cu and Si, and is not affected by Zn.

Alani and Swann[60] have shown that hydrogen bubbles are formed at incoherent interfaces of $MgZn_2$ precipitates. As the Mg content increased, the number of gas bubbles also increased. It was proposed that Mg-H complexes were formed which release H_2 on precipitation of Mg.

Heterogeneous precipitation on grain boundaries is determined by their nature. Nucleation rates are highest on random high angle boundaries, and least on low angle boundaries. It has been found that boundaries with small misorientations are more resistant to SCC than large misorientation boundaries[40]. Better SCC properties

should therefore be possible if precipitate size and distribution on grain boundaries can be altered, without changing the bulk microstructure[42]. The role of defects in promoting grain boundary precipitation was discussed in Section 2.3.2. Gruhl[10] suggested that the use of a Zn : Mg ratio of 3 : 1 (an atomic ratio of 1 : 1) may lead to a lower level of defects in the grain boundary. It has been found that alloys with this ratio do exhibit improved SCC resistance.

Finally, in support of the hydrogen embrittlement model, numerous publications have appeared attaching increasing importance to the role of hydrogen in the mechanisms of SCC, by the observation of hydrogen precharging effects. Pathania and Tromans[61], and more particularly, Holroyd and his co-workers[62,63,64] have made substantial progress in determining the effects of hydrogen in SCC. Holroyd, et al. have shown that reversible embrittlement may be induced in Al-Zn-Mg alloys by pre-soaking in sea-water. This effect was explained in terms of the breakdown of the surface oxide film and the subsequent absorption of the hydrogen evolved. The embrittlement was found to be reversible if the material was not tested immediately after immersion. This was taken as evidence for the diffusion of hydrogen either out of the alloy (which is restricted to surface layers) or to innocuous hydrogen traps where it is prevented from further participation in embrittlement.

should therefore be possible if precipitate size and distribution on grain boundaries can be altered, without changing the bulk microstructure[42]. The role of defects in promoting grain boundary precipitation was discussed in Section 2.3.2. Gruhl[10] suggested that the use of a Zn : Mg ratio of 3 : 1 (an atomic ratio of 1 : 1) may lead to a lower level of defects in the grain boundary. It has been found that alloys with this ratio do exhibit improved SCC resistance.

Finally, in support of the hydrogen embrittlement model, numerous publications have appeared attaching increasing importance to the role of hydrogen in the mechanisms of SCC, by the observation of hydrogen precharging effects. Pathania and Tromans[61], and more particularly, Holroyd and his co-workers[62,63,64] have made substantial progress in determining the effects of hydrogen in SCC. Holroyd, et al. have shown that reversible embrittlement may be induced in Al-Zn-Mg alloys by pre-soaking in sea-water. This effect was explained in terms of the breakdown of the surface oxide film and the subsequent absorption of the hydrogen evolved. The embrittlement was found to be reversible if the material was not tested immediately after immersion. This was taken as evidence for the diffusion of hydrogen either out of the alloy (which is restricted to surface layers) or to innocuous hydrogen traps where it is prevented from further participation in embrittlement.

Resistance to SCC is known to increase when Al-Zn-Mg alloys are overaged. Holroyd, et al. also conducted SCC tests on material in this condition. At electrochemically applied anodic potentials (where hydrogen is unlikely to be involved) no decrease in susceptibility to SCC was found. However, at cathodic potentials (where hydrogen is evolved) there was a marked reduction in embrittlement. It was suggested, therefore, that the reduced embrittlement of overaged alloys found at the free corrosion potential was due to a reduction in the susceptibility to hydrogen embrittlement.

3.2.2 Anodic Dissolution

The anodic dissolution mechanism proposes that the protective oxide film on the metal surface is ruptured by continued plastic deformation at a crack tip. The exposed metal then becomes a very small and restricted anodic region[65]. Enhanced anodic dissolution of the oxide-free crack tip takes place resulting in crack extension. The results of Doig and his co-workers[44,66,67] support this model.

Solute segregation to grain boundaries is important in the anodic dissolution mechanism. The effects of heat treatment on segregation (discussed in Chapter 2) are summarised below.

i) Zn and Mg diffuse to grain boundaries during the quench, primarily due to solute-vacancy interactions.

ii) In a rapid quench this leads to solute enrichment (Figure 2.51) at the grain boundaries. In slowly cooled specimens, the solute that diffuses to the grain boundaries has sufficient time to form grain boundary precipitates. This leads to a solute depletion (Figure 2.51) at precipitate-free regions of the boundary.

iii) On final ageing the solute at the grain boundary is incorporated into grain boundary precipitates. In rapidly quenched materials, a depletion of solute is found in precipitate-free regions of the boundary. In slowly-cooled materials the existing depletion is increased (Figure 2.52).

The effects of heat treatment on susceptibility to SCC have been explained by Doig, et al.[44,66,67] in terms of the selective corrosive attack at grain boundaries which arises due to this segregation of solute. The electrode potentials of aluminium and its major alloying additions are given in Table VIII.

Table VIII: Electrode Potentials with respect to the 0.1 M calomel electrode in aqueous solutions of 53g/l NaCl and 3g/l H_2O_2 at 25°C (from Metals Handbook, Volume 1, ASM, Ohio, 1961).

Metal or Alloy	Micro-Constituent	Potential (V)
Magnesium		-1.73
	Mg_5Al_8	-1.24
Zinc		-1.10
	$MgZn_2$	-1.05
Alclad 7075		-0.99
Aluminium (99.95%)		-0.85
Copper		-0.20
Chromium		-0.49 to +0.18

Both Zn and Mg are anodic with respect to aluminium. Therefore, in typical SCC environments, (containing Cl^- ions and pH $\sim$ 8) both the grain boundary precipitates and the solute-enriched regions are anodic to the rest of the microstructure. Where enrichment of the boundary has occurred (by rapid quenching), the boundary itself will be anodic and will dissolve preferentially to produce SCC. If there is depletion of solute, either through slow quenching or overageing, then SCC proceeds by the dissolution of boundary precipitates.

Furthermore, it has been shown[66] that the initiation of SCC in an aged Al-5.9Zn-3.2Mg alloy was not related directly to the PFZ width but rather to the width of the solute depletion associated with the grain boundary precipitation. This was achieved by quench interruption techniques and varying the pre-ageing time to produce different solute profiles within PFZ's of the same width. The results were explained in terms of the anodic dissolution model.

The beneficial effects of small Cu additions on the susceptibility to SCC in Al-Zn-Mg alloys were discussed in Section 2.2.2. Substantial increases in resistance to SCC may be obtained, particularly, in the overaged (T7) temper. It has also been shown[67] that the cathodic polarisation behaviour of aluminium solid solutions in 0.1N NaCl of pH 3.5 are strongly dependent on the copper content. The solute-depleted grain boundary regions were considered as cathodic reduction regions, in which the anodic reaction of the system was balanced. The reduction in the growth rate of stress corrosion cracks in Al-Zn-Mg-Cu alloys overaged, from T6 to T7, were explained in terms of changes in the electrochemical properties of the grain boundary regions, resulting from a decrease in the local Cu concentration.

3.2.3 Stress-Relaxation Mechanism

It is doubtful whether the stress-relaxation mechanism operates as a single mechanism producing SCC. However, for clarity it will be discussed separately.

This mechanism is based on the work of Jacobs[68] who investigated the SCC of a Al-Zn-Mg-Cu alloy. The susceptibility to SCC was assumed to be due to the presence of concentrations of dislocations adjacent to undissolved particles of the intermetallic compound $MgZn_2$, which act as primary sites for SCC attack. This assumption has found further support in subsequent work[69].

The SCC susceptibility to quench rate was explained in terms of the high concentration of dislocations "frozen" into the microstructure, by a rapid quench from SHT[70]. This will produce more primary sites for preferential SCC attack. The effects of a fast quench are further compounded by the resultant residual tensile stresses. In general stresses are compressive on the surface and tensile within the material. Clearly, where partial machining of the material is undertaken, a region of tensile stress may become exposed not only to the corrosive environment, but also to further externally applied tensile forces.

The beneficial effects of overaging on resistance to SCC were accounted for by the dissipation of the concentrations of dislocations through prolonged ageing[70]. Primarily, the mechanism requires the relaxation of stress concentrations along the grain boundaries for increased resistance to SCC.

Support for this model has been provided by the investigation of a novel heat treatment technique[70,71,72], which was claimed to increase resistance to SCC without the normally associated loss in mechanical properties. This process has been termed "retrogression and reageing (RR)".

During the retrogression stage, material in the peak aged (T6) temper is heated to a sufficiently high temperature (in excess of the final ageing temperature), to cause the dissolution of the GP zone dispersion, and possibly also very fine precipitates. The time of this exposure must be insufficient to initiate the equilibrium precipitation process for this higher ageing temperature. It was also proposed that the combination of holding time and temperature allowed the dispersal of dislocation concentration by diffusion.

Subsequent reageing at the original T6 age-hardening temperature restored the original T6 microstructure and mechanical properties, in the absence of dislocation tangles. However, the validity of these results is still in question. Wallace, et al.[73] have confirmed these findings, while Swanson, et al.[74] found that the RR temper only improved initiation times for SCC. The latter demonstrated that the SCC resistance of notched specimens was no better than the conventional T6 temper.

In evaluating the applicability of these models, it must be reiterated, that in any working environment in which material is subject to SCC conditions, it is highly probable that more than one of the above mechanims will operate. Care should therefore be exercised, so that in experimental SCC testing one particular mechanism is not caused to dominate. For example, by varying the electrochemical potential it is possible to change from an anodic dissolution mechanism of SCC to hydrogen embrittlement. Aspects of SCC testing will be discussed in the following sections.

3.3 Accelerated SCC Test Methods

A number of different accelerated SCC test methods were evaluated with the aim of finding a test capable of producing a reliable indication of susceptibility to SCC. The test was required to provide a rapid assessment of different alloy compositions in different temper conditions. In addition, using these base results the performance of developed alloys could readily be compared.

It is important, when evaluating SCC tests, to consider whether the selection of test parameters used will induce one particular SCC mechanism which may not be an accurate reflection of in-service conditions. This is particularly true for applied electrochemical potentials.

A further consideration in SCC testing is what stage of the SCC process the test is actually indicating. There is a fundamental difference in the mechanisms and measurement of initiation and growth rates of SCC. Therefore, different tests may be employed to give information on the entire, or only part of, the SCC process (e.g. initiation, growth or final fracture).

Many tests already developed prove to be unrealistic, since they condemn many alloys which have acceptable service lives. Ideally, the following two points should be observed when conducting accelerated SCC tests.

1) As far as practically possible, the test should invoke the same mechanism of SCC that is likely to be encountered in service.

2) The accelerated laboratory test results should be correlated with longer-term outdoor exposures, or with any available in-service data for the alloy and its temper condition.

Many parameters exist which may be varied to give an accelerated test. These include the following:

1) the method of applying stress; either
   a) a constant total strain,
   b) a constant stress, or
   c) a constant strain rate;

2) the environment (type, concentration, pH, etc);

3) the temperature; and

4) the electrochemical potential.

A number of review articles on the theoretical aspects and methods of SCC testing already exist[65,75,76] and it is not considered necessary to discuss them in great detail here. However, the three potentially most suitable tests were evaluated experimentally, and these will be dealt with individually.

For each method, the representative Al-Zn-Mg alloy D74S (with the composition listed in the Appendix) was tested in a number of different temper conditions. In order to determine the sensitivity of the test, an attempt was made to evaluate both material highly susceptible to SCC (T6 temper) and material with a low susceptibility. The reproductibility was assessed by testing a number of specimens in the same T6 temper condition.

3.3.1 Notched Rod Load-Relaxation

The SCC susceptibility was measured from the load relaxation of a notched rod in a corrosive environment using the same method as Pathania and Tromans[61]. A schematic load versus time plot for Al-Zn-Mg alloys is shown in Figure 3.2. The defined initiation time t may

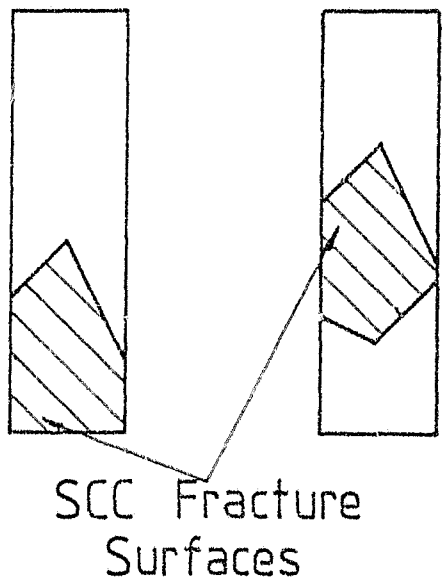


Figure 3.1 Schematic representation of the shape of the SCC fracture areas in unnotched rectangular tensile specimen.

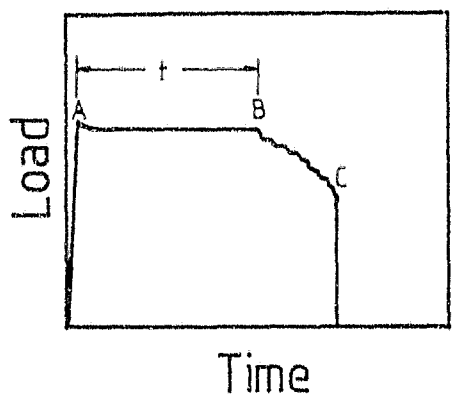


Figure 3.2 Schematic of load relaxation-time plot, showing definition of initiation time, .

be minutes or hours. Sectioning the rod before this time revealed no evidence of SCC, but in the load relaxation region (BC) cracks were observed.

i) Experimental Procedure

Several notched rods were machined in the long transverse direction from D74S 12mm plate in the F (material slow cooled after hot rolling, which has low SCC susceptibility) and T6 temper (highly SCC susceptible) conditions to the specifications given in Figure 3.3.

The rods were electropolished in a solution of 45% HNO_3, 45% H_2O and 5% HCl, by volume. Specimens were subsequently degreased ultrasonically in carbon tetrachloride for 15 minutes. Rods were placed in an environmental chamber and then fitted into a vertical Instron tensile testing machine (Figure 3.4).

The stress intensity, K_I at the notched tip is given by,

$$K_I = (0.24)\ \sigma_n\ (\pi D)^{\frac{1}{2}},$$

where D is the rod diameter and σ_n the net section stress at the notch.

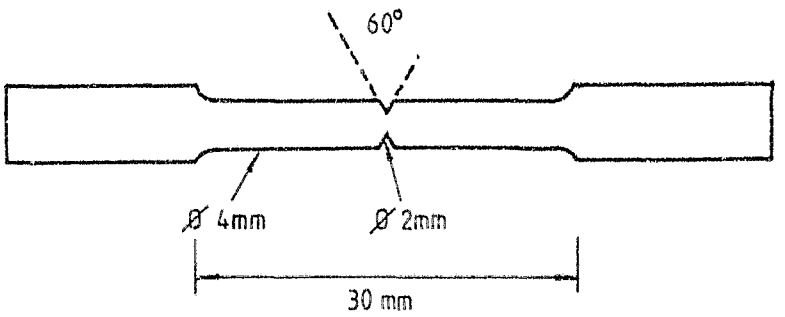


Figure 3.3 Notched rod specimen geometry

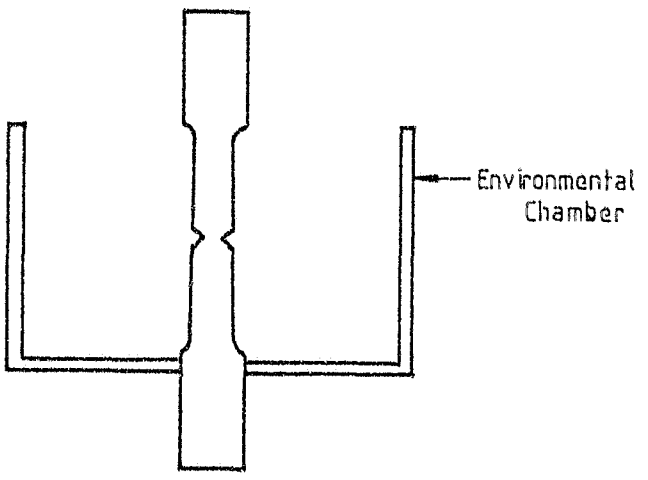


Figure 3.4 Notched rod with environmental chamber

The corrosive environment used was a 3.5 wt % NaCl and 2 wt % K_2CrO_4 aqueous solution. No temperature control was employed since preliminary tests showed that the ambient temperature did not fluctuate.

ii) Results and Discussion

No load relaxation was detected for the alloy in the F condition. Even at the highest K_I values possible and a test period of 48 hours, no SCC was initiated.

D74S specimens in the T6 temper exhibited a definite load relaxation after $\sim$ 4 hours. Difficulty was, however, experienced in reproducing the same K_I value at the notched tip for a number of different tests. This resulted in a spread of initiation times.

A further disadvantage of the notched rod load relaxation test is the complex specimen geometry, particularly of the notch, which requires precision machining.

3.3.2 Electrochemical Acceleration Technique

Following suggestions from Doig[66,67], an electrochemical acceleration technique using a smooth rod (tensile) specimen was evaluated. The experimental arrangement is illustrated schematically in Figure 3.5.

The specimen is immersed in a 1N NaCl solution with a pH of 3 (controlled by the addition of HCl). An anodic potential is supplied (approximately 800 mV s.c.e.) to produce a net anodic current from the specimen of about $1mAcm^{-2}$. Varying the potential and/or load will result in failures of the specimen in a time period of minutes to hours. Greater selectivity (however, at longer test times) are achieved with smaller current flows.

Susceptibility to SCC may be expressed in terms of time to failure or by examination of crack depth after testing for a fixed time. This latter method was rejected due to the inherent difficulties in quantitatively assessing the depth of irregular SCC cracks.

i) Experimental Procedure

The geometry of the specimens can be seen in Figure 3.5. Specimens were machined in the long transverse direction of D74S plate. The surfaces were prepared in the same way as for the notched rod load relaxation test (Section 3.3.1).

Tests were again performed on specimens in the F and T6 temper conditions. The load was applied using a simple Hounsfield tensometer.

ii) Results and Discussion

No SCC was evident in the F condition specimens even at the maximum stress ($\sim$ 95% of the 0.2% yield stress) and electrochemical potential ($\sim$ +0.5V) possible over a period of 12 hours.

Failure was, however, produced in the SCC-susceptible T6 temper specimens. Using a net anodic current flow from the specimen of approximately $1mAcm^{-2}$, the time to failure was approximately 6 hours.

The test appeared less reproducible and consistent than the notched rod load relaxation test. Factors which contribute to the inconsistency of the electrochemical test are:

1) the high initial stress required to cause failure in a reasonable time;
2) severe corrosive damage to the specimen if a lower stress is used in combination with a higher "accelerating" electrochemical potential; and
3) difficulty in reproducing the initial stress.

Although this lack of reproducibility is a problem, the major disadvantage of this test is the SCC mechanism it induces. The applied anodic potential

results in anodic dissolution of the metal and therefore dominates any other mechanism which may operate at the free corroding potential.

3.3.3 Slow Strain Rate Testing

The initial evaluation of the slow strain rate test provided the most favourable results in terms of reproducibility, reliability and sensitivity. The test will therefore be discussed in greater detail.

In essence, the slow strain rate technique compares the results of tensile tests performed in inert and corrosive environments. The specimens are strained at a slow strain rate under controlled environmental conditions. Typical strain rates range from 10^{-4} to 10^{-8} s^{-1}. Strain rates in the critical range to promote SCC maintain the delicate balance at the crack tip between deformation, dissolution, film formations and diffusion. An extensive programme of slow strain rate SCC testing of aluminium alloys has been reported[62,63,64,76-81]. Alloys in a wide variety of SCC susceptible conditions and environments have produced results fully consistent with the expected behaviour from service experience and the results of other established test methods.

In the standard form of the test, using smooth tensile specimens, the susceptibility to SCC is expressed as the ratio of the determined mechanical properties in

corrosive and inert (control) test environments. Ratios of the following parameters have been considered: proof stress, the ultimate tensile strength, the total plastic elongation, the reduction in area, the fracture energy and time to failure. The most sensitive parameters are reduction in area and fracture energy. The latter is difficult to determine accurately without computerised analyses. Hence, a reduction in area is generally used, although this does require accurate measurement. Susceptibility is then expressed as a "ductility ratio", that is, the ratio of reduction in area of the necked region of the tensile specimen tested in a corrosive environment, to that of a specimen tested in an inert environment.

i) Experimental Procedure

The slow strain rate testing procedure, used in all the subsequent SCC tests, has been standardised, as far as possible, to the method and conditions adopted by the European Aluminium Association[76,79,80,81].

a) Strain Rate

A simple Hounsfield tensometer was modified to provide the very low strain rates (in the order of 10^{-6} s^{-1}) required for the test. This was achieved by the construction of a gear and pulley system which provided a low-speed

crosshead drive to the tensometer. The crosshead speed achieved in this manner was $(1.43 \pm 0.01) \times 10^{-4}$ mm.s^{-1}. Using a tensile specimen with a gauge length of 33.13mm, the resulting initial strain rate,

$$\frac{de}{dt} = \frac{1}{\text{gauge length}} \text{ (crosshead speed)}$$

$$= 4.32 \times 10^{-6} \text{ s}^{-1}$$

This strain rate led to failure times of 4 to 7 hours in all the alloys tested.

In order to obtain tensile properties, the Hounsfield tensometer was also strain gauged, and the necessary electronics constructed to obtain a direct reading of applied load during testing. This enabled plots of load versus extension to be recorded during testing.

b) Test Cell

A test cell was constructed from perspex, with internal dimensions 45mm x 80mm x 150mm high, to contain 0.5 litres of test solution. The solution to specimen area ratio was approximately 90ml.cm^{-2}.

Control of the solution temperature was achieved using a 150W immersion heater and thermostat within the cell. The temperature was maintained at 30 $\pm$ 2°C. Clean, dry air was bubbled through the solution to provide aeration and circulation. A platinum wire coil, positioned around the test specimen, enabled the free corroding potential to be monitored. This could also be used to provide different applied electrochemical potentials. The test cell is shown in Figure 3.6.

c) Test Solution

The corrosive environment test solution used consisted of a 3% NaCl and 0.3% H_2O_2 solution in distilled water, adjusted to a pH of 3.5 using HCl. The inert environment used was polythene glycerol, which provides improved protection against embrittlement than the silica gel used in other investigations.

d) Test Specimen

Tensile specimens were machined in the long transverse direction from heat-treated 12mm hot-rolled plate. Ideally, six specimens were prepared to enable three tests to be carried out in both inert and corrosive environments for each alloy or temper. Specimens were circular in

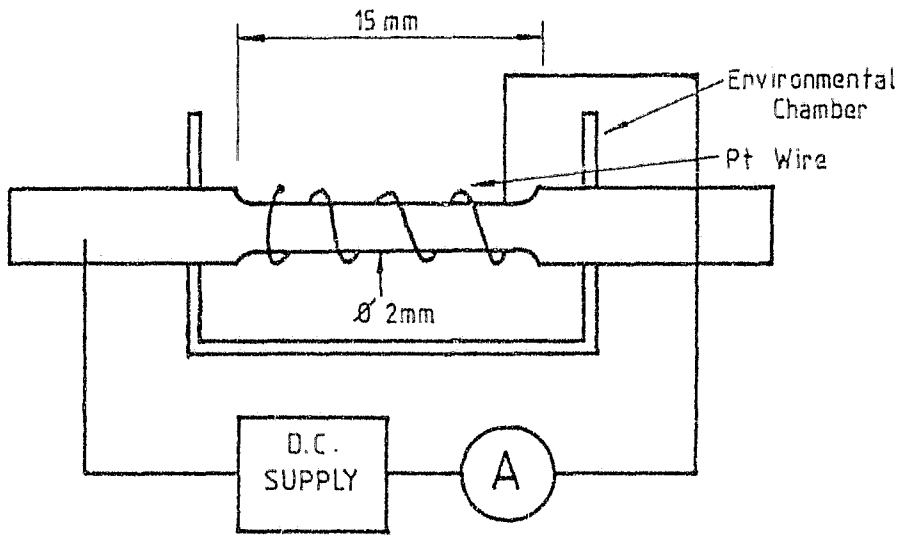


Figure 3.5 Electrochemical acceleration test: experimental arrangement

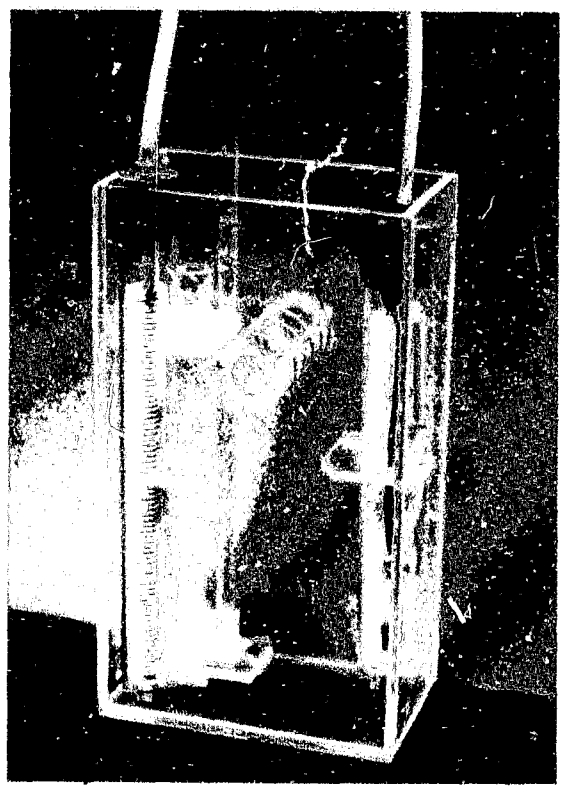


Figure 3.6 Test cell used for slow strain rate testing

section, with 7 mm diameter shanks and a wasted portion of 4 mm diameter, giving a gauge length of 33.13 mm. Final surface preparation of the gauge length involved a mechanical polish with 1000 grade emery paper using paraffin as a lubricant. The specimen diameter was then measured, taking care not to damage the surface. Degreasing was achieved by ultrasonic cleaning for 15 minutes in ethanol.

After immersion of the specimen in the corrosive environment, conditions (such as temperature, free corroding potential, etc) were allowed to stabilise for 15 minutes before loading.

e) Ductility Ratio

After fracture, the ductility ratio was expressed in terms of a chosen "ductility" parameter. Proof stress, ultimate tensile strength, elongation and time to failure were simply taken from the plot of load versus extension, recorded during the test.

Reduction in area at fracture was initially measured using a travelling microscope. The two fractured sections of the specimen were held together in a simple jig for measurement of the diameter of the necked region. A mean value was calculated using at least 3 different diameters.

Later measurements were facilitated by the use of a calibrated reduction in area gauge. Although, less accurate, the maximum error of these measurements was found to be approximately 2.5%.

After final fracture a number of specimens were prepared for SEM observation to determine the mode of failure. Fracture surfaces were viewed in a Cambridge S.4 scanning electron microscope.

This test procedure was used to determine the applicability of the slow strain rate method, not only in D74S - T6 and T7, but also in other existing alloys D54S - H2 and B51S - T6. The compositions of all these alloys are in the Appendix.

ii) Results and Discussion

Initial tests were conducted on D74S to determine whether the test was capable of distinguishing between the high susceptibility to SCC of the peak aged (T6) temper and the low susceptibility of the overaged (T7) condition. The hardness values for these tempers were 135 HV and 113 HV, respectively.

The test results showed that the reduction of area provided the most sensitive "ductility" parameter as an indication of susceptibility to SCC. The

reduction of area "ductility ratio" for the peak aged temper was 0.28, and 0.99 for the overaged temper. The test specimens after testing are shown in Figures 3.7 and 3.8. The difference in reduction of area between peak and overaged tempers, tested in the corrosive environment, is clearly visible in Figure 3.8.

Initial tests on the peak and overaged tempers clearly demonstrated the ability of the slow strain rate test to discriminate between a high susceptibility and low susceptibility condition. The test showed a 70% change in ductility ratio. Even with a maximum error of $\pm$ 3% in the reduction of area measurements (the standard deviation of 4 measurements of reduction of area is never more than 2.5%) the test would still show a 60% change in ductility ratio.

A study of the fracture surfaces produced by slow strain rate testing revealed that the morphology of fracture is influenced by the test environment. A typical ductile cup-cone type fracture (Figure 3.9 (a)) was observed in specimens tested in an inert environment. The use of a corrosive environment results in a more brittle shear fracture (Figure 3.9 (d)). At higher magnification, SEM observation of the inert specimen revealed "classic" ductility characterised by dimple formation through microvoid coalescence. (Figures 3.9 (b) and (c)). Central

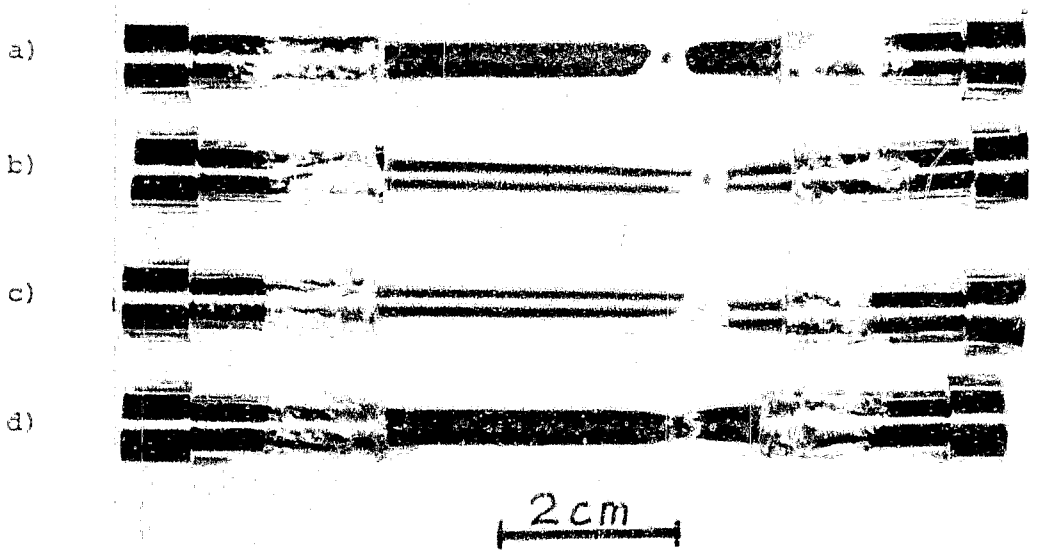


Figure 3.7 SCC test specimen. a) Peak aged-corrosive, b) peak aged-inert, c) overaged-inert, and d) overaged-corrosive.

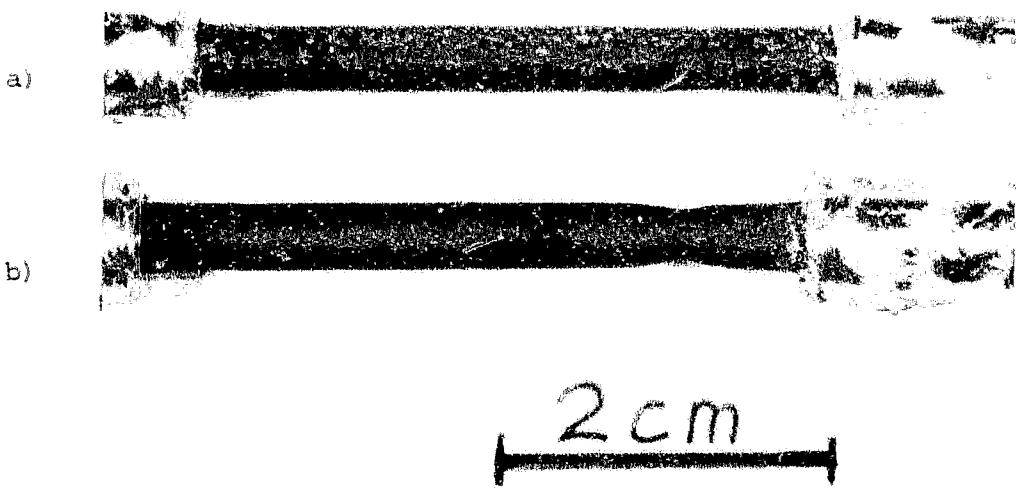


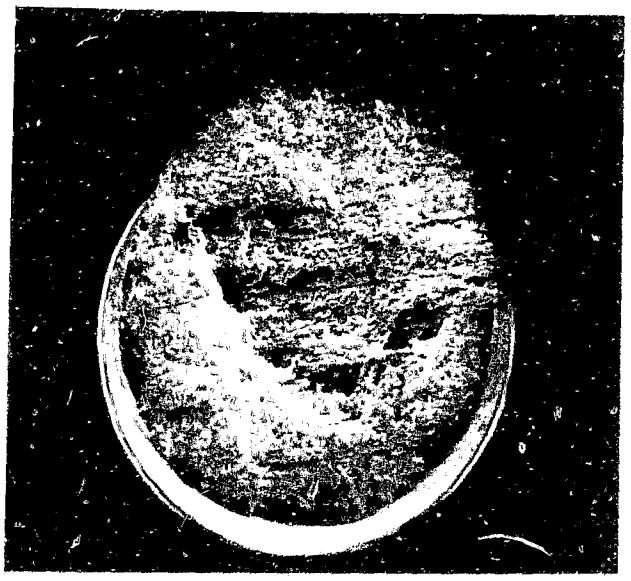
Figure 3.8 SCC test specimen. a) Peak aged, and b) overaged specimen, tested in a corrosive environment slowing difference in reduction in area.

regions of the corrosive specimen revealed essentially the same ductile mode of failure. This ductile failure mode is predominantly transgranular. A band showing effects of embrittlement was observed around th edge of the corrosive fracture surface. Although micro-ductility was evident in this band, the surface has features of a more brittle intergranular fracture (Figures 3.9 (e) and (f)). This probably reflects the tendency for cracks to follow grain boundaries resulting in a mixed mode intergranular - transgranular fracture.

Results of slow strain rate testing of D54S and B51S showed no significant difference in reduction of area between specimens tested in the inert and corrosive environments. This implies that the ductility ratio for both alloys was approximately unity.

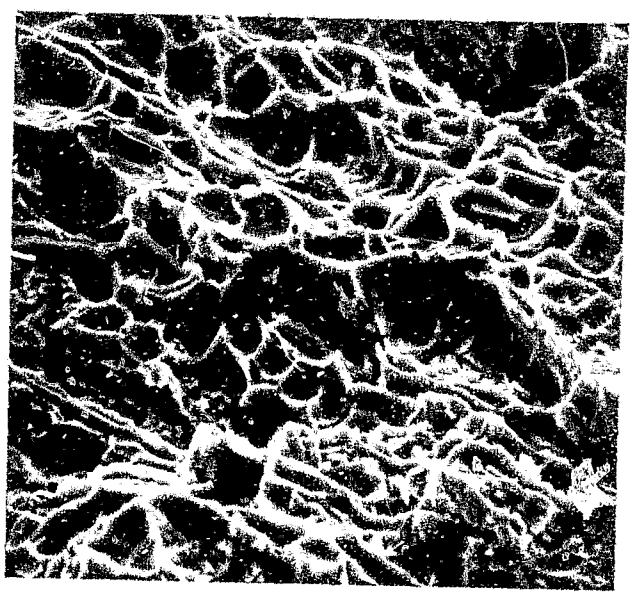
These results were expected as neither alloy is prone to SCC, except under the most severe service environments. This was demonstrated by observing the effect of electrochemical potential on the loss of ductility of D54S-H2, (Figure 3.10).

A progressive increase in the degree of embrittlement was observed with increasing or decreasing the potential from the free corroding



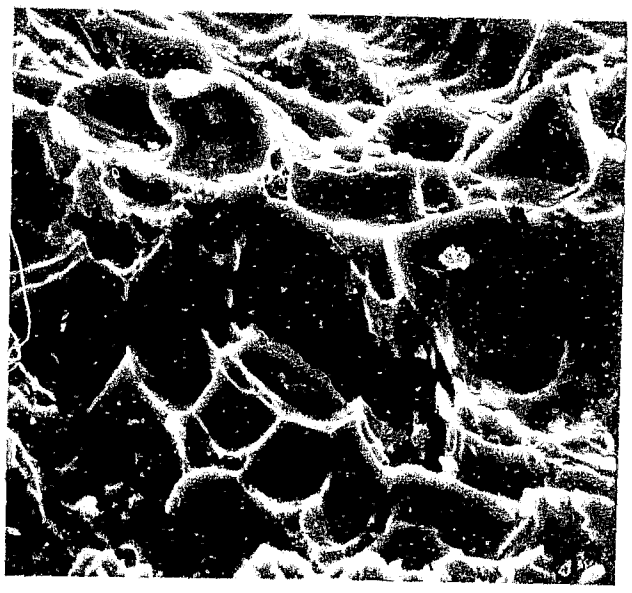
1mm

(a) Ductile cup-cone failure



20μm

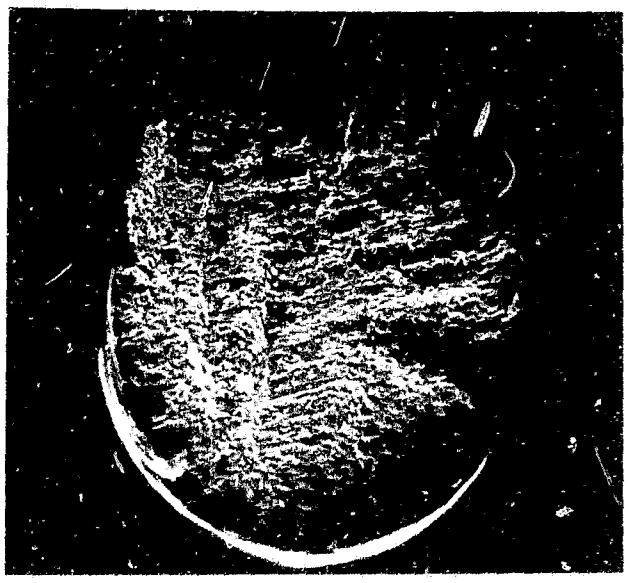
(b) Ductile transgranular fracture.



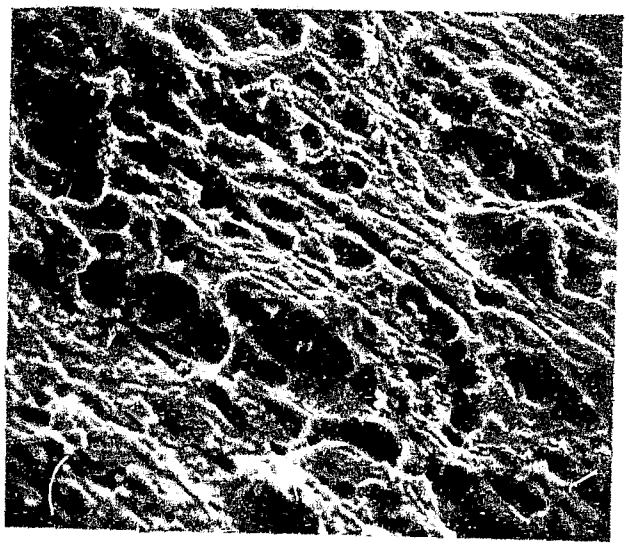
10μm

(c) Ductile transgranular fracture

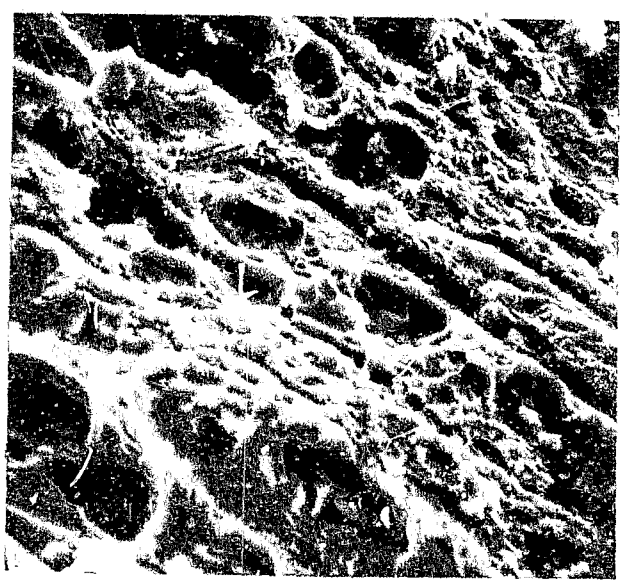
Figure 3.9 Fracture surfaces of D74S failed in the slow strain rate test: (a - c) inert environment.



(d) Shear fracture surface



(e) Mixed mode intergranular-transgranular fracture.



(f) Mixed mode.

Figure 3.9 Fracture surfaces of D74S failed in the slow strain rate test: (d - f) corrosive environment.

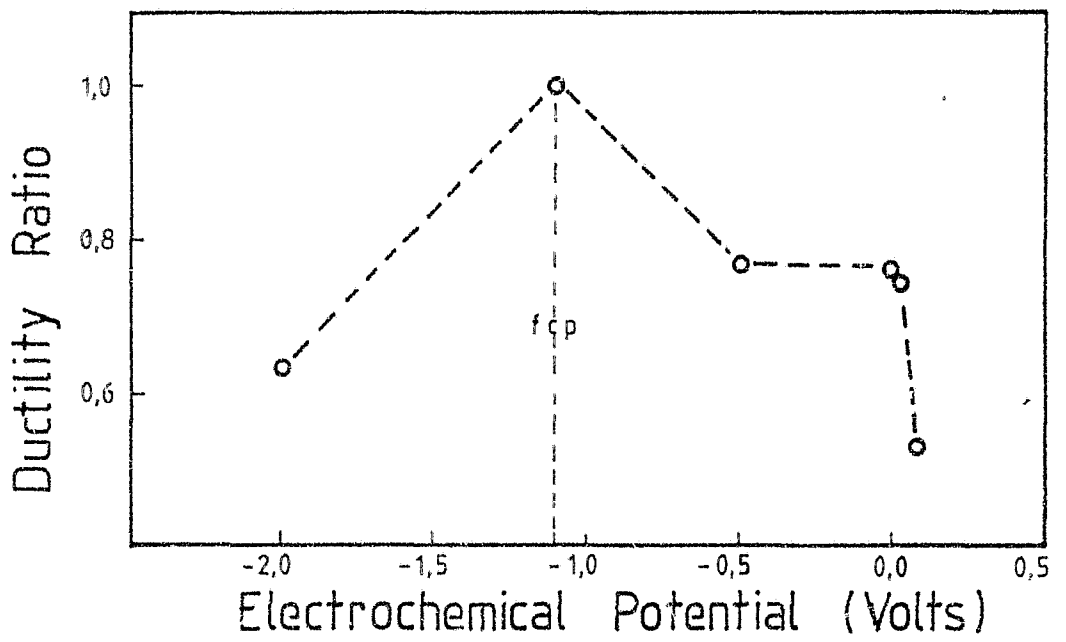


Figure 3.10 The effect of electrochemical potential on the loss of ductility as measured by loss of reduction in area.

Author Dauskardt R H
Name of thesis The development of Aluminium-Zinc-Magnesium alloys for superior stress corrosion resistance 1983

PUBLISHER:
University of the Witwatersrand, Johannesburg
©2013

LEGAL NOTICES:

Copyright Notice: All materials on the University of the Witwatersrand, Johannesburg Library website are protected by South African copyright law and may not be distributed, transmitted, displayed, or otherwise published in any format, without the prior written permission of the copyright owner.

Disclaimer and Terms of Use: Provided that you maintain all copyright and other notices contained therein, you may download material (one machine readable copy and one print copy per page) for your personal and/or educational non-commercial use only.

The University of the Witwatersrand, Johannesburg, is not responsible for any errors or omissions and excludes any and all liability for any errors in or omissions from the information on the Library website.